

Cite this: *Polym. Chem.*, 2022, **13**,  
3188

## Recent advances in self-immolative linkers and their applications in polymeric reporting systems

Alexander G. Gavriel,<sup>a</sup> Mark R. Sambrook,<sup>b</sup> Andrew T. Russell\*<sup>a</sup> and  
Wayne Hayes<sup>ID</sup>\*<sup>a</sup>

Interest in self-immolative chemistry has grown over the past decade with more research groups harnessing the versatility to control the release of a compound from a larger chemical entity, given a specific stimulus. Originally conceived in 1981 to overcome electronic or steric features which may prohibit cleavage of a prodrug linkage; today's self-immolative linkers are widely used, *inter alia*, within medicinal chemistry, analytical chemistry, and material science. The incorporation of these linkers can be found in small molecules, dendritic and polymeric systems where a controlled release profile is required. This control can be of a binary character, release or not release, or a more nuanced issue of rate of release. In this article, we build upon our previous review in 2011 discussing key literature within the self-immolative field and, in particular, a selection of more recent examples that highlight how this field has matured in the past decade, with relevant earlier literature to provide context.

Received 1st April 2022,

Accepted 17th May 2022

DOI: 10.1039/d2py00414c

rsc.li/polymers

### 1 Introduction and key concepts

Over the past two decades, the chemistry of self-immolative systems has received significant attention and the technology has developed sufficiently to permit application in areas as diverse as the pharmaceutical sector,<sup>1–3</sup> degrade-on-demand adhesives,<sup>4–6</sup> chemosensors<sup>7</sup> and the detection or disclosure of toxic compounds.<sup>8–10</sup> In 1981 seminal studies conducted by Katzenellenbogen and co-workers on prodrugs led to the term 'self-immolative connector' being proposed, and this degradable unit has subsequently been referred to in the literature as a 'self-immolative spacer' or 'self-immolative linker'.<sup>11</sup> The chemistry of self-immolative systems has been the subject of several reviews in the past decade, and indeed we published a review a decade ago on the topic of self-immolative linkers in polymeric delivery systems.<sup>12–37</sup> In this review, we will build upon our original survey<sup>12</sup> to evaluate the most recent developments in self-immolative linkers including those utilised in polymeric systems and will assess the degradation chemistries plus the different macromolecular architectures used. Important advances have also occurred in the more general area of self-reporting materials, not always incorporating a self-immolative linker, and these have been reviewed recently by Mutlu and Barner-Kowollik.<sup>38</sup>

The self-immolative linker (spacer) has been defined by Schmidt and Jullien in their 2015 review as: 'self-immolative spacers (linkers) are covalent assemblies tailored to correlate the cleavage of two chemical bonds in an inactive precursor'.<sup>21</sup> In a similar way, Corso and Gennari used the following definition in 2021: 'self-immolative (SI) spacers (linkers) are covalent constructs designed to degrade spontaneously in response to specific stimuli'.<sup>39</sup>

They have developed from traditional protecting group strategies, wherein a reactive functionality in a molecule would be protected, modifying the reactivity at that site. Following whatever synthetic manipulations are desired, the protecting group is cleaved in a selective manner to release the modified molecule. In the present context, the act of protection has been used to modify a particular property of a molecule *e.g.* colour, fluorescence, biological activity; whereas, the selectivity in deprotection has been utilised in a number of ingenious ways as a means of detecting a specific environmental factor and responding to it *e.g.* the presence of a hydrolytic enzyme or toxic molecule to release a drug or indicator molecule. The molecules prepared are often referred to as SIEs (Self-Immolative Entities) and in their classical manifestation are composed of three parts, a trigger group (a protecting group), a linker, and a reporter group (it should be noted that in Katzenellenbogen's original work these were referred to as a specifier, a self-immolative connector or link and a drug). In principle, the linker may not be necessary, whereupon the SIE becomes a two-component system of the type that predated Katzenellenbogen's work. However, the field has attracted its own lexicon of terminology and the reader should be aware of

<sup>a</sup>Department of Chemistry, University of Reading, Whiteknights, Reading, RG6 6AD, UK. E-mail: w.c.hayes@reading.ac.uk

<sup>b</sup>CBR Division, Defence Science & Technology Laboratory (Dstl), Porton Down, Salisbury, Wiltshire, SP4 0JQ, UK



synonyms used in the literature such as cargo, effector or reporter groups for the released molecules or atoms. In that case, upon a given specific stimulus (herein referred to as an activation event), the protecting group is activated so that the bond to the reporter group becomes labile and leads to its release (Scheme 1a). However, this approach is not always feasible as the covalent linkage between the trigger and reporter may be resistant to cleavage; for example, by steric bulk surrounding the scissile bond or electronic factors that enhance the stability of the bond.<sup>40,41</sup> To overcome this impairment, a linker is incorporated joining the trigger and the reporter moieties. The linker forms a scissile bond to the trigger group and a stable linkage to the reporter; however, upon activation of the trigger and subsequent cleavage, the linker–reporter coupling is rendered labile, resulting in disassembly of the now two-component system and release of the reporter (Scheme 1b). The incorporation of a linker has facilitated further developments in the field that go beyond reactivity and

embrace the ability to release multiple reporter groups, *vide infra*. Prior to our 2011 review, the field had integrated advancements from the polymer field such as dendrons and self-immolative polymers to allow for amplification of detected events (Scheme 1c and d),<sup>23,42–44</sup> this reaching impressive levels with dendritic chain reactions (Scheme 1e), potentially delivering exponential growth of the signal from the analyte.<sup>27,45</sup> The classic tripartite structure proved adaptable; for example, such that the linker moiety simultaneously functioned as a reporter group, *vide infra*. From the impressive foundations already present in 2011, many ingenious applications, new dendritic chain reactions, and exciting developments in information storage have been reported.

## 2 Classes of self-immolative elimination pathways

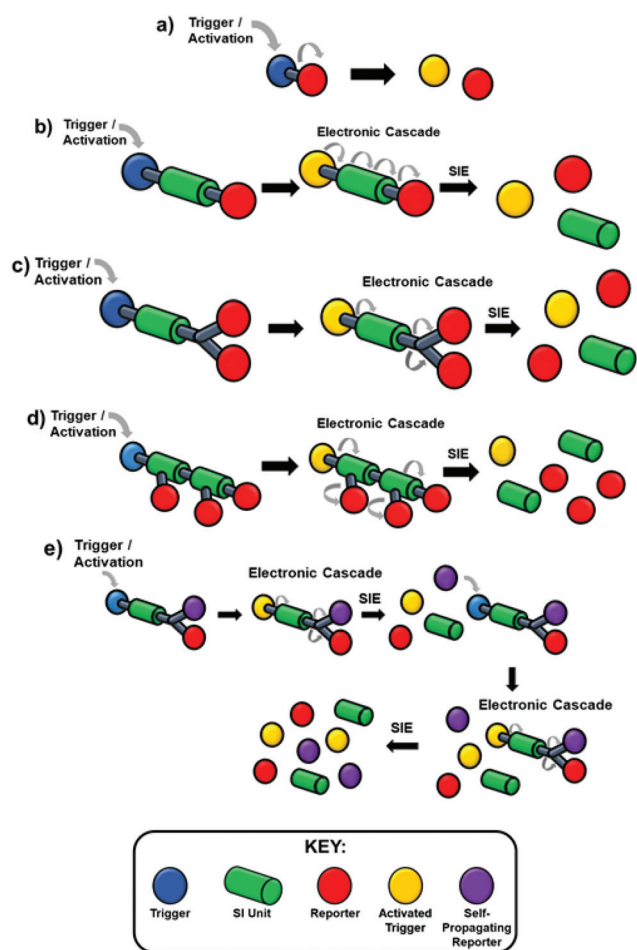
Self-immolative elimination occurs when a molecular system undergoes a spontaneous and irreversible disassembly into its constituent fragments through either an electronic cascade, *via* an elimination pathway or, alternatively, where self-immolation is achieved through a cyclisation–elimination event. Although these degradation processes differ fundamentally from each other, the pathways that drive self-immolative elimination both lead to: (i) an increase in entropy coupled with (ii) the irreversible formation of thermodynamically stable products (*e.g.* CO<sub>2</sub>). The more general area of stimuli responsive materials, where a single trigger site is not always present, has also led to important developments *e.g.* recyclable polymers,<sup>46</sup> and has been recently reviewed by Gillies.<sup>34</sup> These will only be covered for examples that include a specific trigger(s) within the structure *e.g.* an OTBS group.<sup>47</sup>

In order to aid the reader of this review, a specific colour scheme has been employed in the diagrams to highlight the individual components of self-immolative systems herein; trigger (blue), self-immolative linker (green), reporter (red).

### 2.1 Self-immolation *via* an electronic cascade process

A significant number of self-immolative systems that undergo an electronic cascade commonly feature an aromatic linker with an electron-donating substituent (such as hydroxyl, amino or thiol residues) that is in conjugation (*ortho*- or *para*-) with a leaving group in a benzylic position on the molecule. The presence of an electron-donating group is essential to lowering the energy barrier of dearomatisation within the self-immolative process (thus forming a quinone methide, azaquinone methide or thioquinone methide intermediate). In general, amine groups have been found to be the most effective at promoting rapid cleavage, post activation, though hydroxyls, particularly when deprotonated, have been found to have significant roles, such as when linked to the anomeric position of carbohydrates and when generated from C–B bonds, *vide infra*.

Katzenellenbogen's seminal account reported a model tripartite prodrug that employed the self-immolative linker



**Scheme 1** (a) Two-component system, (b) traditional non-amplified self-immolative system, (c) dendritic self-immolative system resulting in an amplified reporting event, (d) polymeric self-immolative system resulting in an amplified reporting event and depolymerisation, (e) dendritic chain reaction whereby the reporter event allows for a further trigger event.



4-aminobenzyl alcohol.<sup>11</sup> The self-immolative elimination of 4-nitroaniline (used as a model for drug compounds) from **1** was demonstrated, following hydrolysis its scissile amide bond, catalysed by trypsin, with *N*<sup>ε</sup>-Boc-Lys serving as the trigger moiety (Scheme 2). The *N*<sup>ε</sup>-Boc-Lys protected amide **1** is insufficiently electron releasing in nature ( $\sigma_p^+ = -0.6$ ) to facilitate spontaneous disassembly at a rate relevant to its use as prodrug ( $t_{1/2} \approx 40$  h in 0.05 M Bistris buffer (pH 6.9) at 25 °C). However, upon trypsin mediated hydrolysis of the amide, a strongly electron-releasing amine ( $\sigma_p^+ = -1.31$ ) is revealed and promotes self-immolation through a 1,6-elimination process. Elimination proceeds from the intermediate **2** with concomitant decarboxylation, resulting in the release of 4-nitroaniline **3**. In conjunction with release of **3**, highly reactive aza-quinone methide species **4** was presumably formed which was readily quenched by water to afford 4-aminobenzyl alcohol **5**. Thus, the presence of a nucleophile was required to complete product formation from **2** and the rate of fragmentation was likely increased by the reaction occurring in a polar protic solvent system.<sup>48,49</sup> The decomposition of **2** could also be described as solvolysis (or solvolytic cleavage).

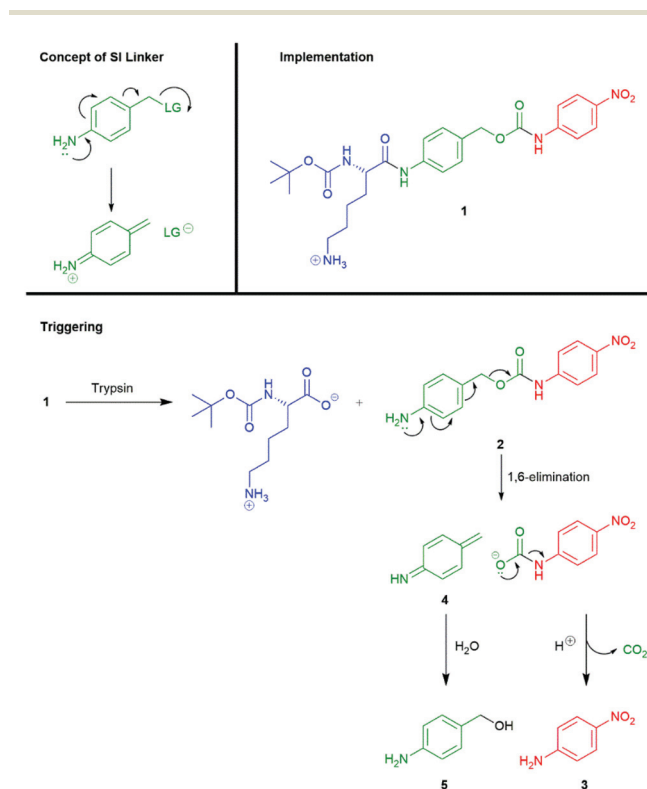
An interesting point, raised in a footnote to the paper, concerns the fate of **4** when alternative nucleophiles are present; for example, in the case of formation of **4** in a cell, the possibility of quenching of **4** by glutathione was considered. This raises a very important point regarding the fate of such reactive intermediates, generated from the linkers, that is worthy of

consideration in the application of a SIE system; some examples of recapture of the reporter group has been observed by Hay, Du and Li, and Phillips.<sup>50–52</sup> In addition, reversible reactions of the reactive intermediates from self-immolative processes with DNA bases have reported by Fakhari and Rokita.<sup>53</sup> These observations and reports highlight an important aspect of use of self-immolative systems in biological environments – there is a need to understand the biocompatibility and toxicity of such reactive intermediates before these highly innovative, degradable materials can be translated into ‘real-world’ applications. Established tumour imaging applications; for example, by chemiluminescence, have been carried out in animals without significant side effects being reported (*vide infra*), though this aspect was not the focus of the studies. In the treatment of cancer, selective cell death is desirable and release of reactive intermediates at the target site may not be an issue and possibly beneficial. By contrast, off-site release may be problematical but, to date, detailed findings of such studies have yet to be published.

Since Katzenellenbogen’s ground breaking report,<sup>11</sup> numerous groups have utilised successfully this type of benzylic spacer including some recent examples from Byun *et al.*, Anami *et al.*, Wei and Safina *et al.*, Gennari and Piarulli.<sup>54–58</sup> It has also been demonstrated that the hydroxyl and thiol analogues, 4-hydroxybenzyl alcohol and 4-mercaptobenzyl alcohol, respectively, also undergo 1,6-elimination upon cleavage of a triggering moiety attached to the ring heteroatom.<sup>59,60</sup> In a study by Senter on mercaptobenzyl alcohols, following rapid disulfide reduction, the *para*-derivative **6** fragmented with a  $t_{1/2}$  value of 10 minutes, as compared to a  $t_{1/2}$  of 72 minutes for the *ortho*-derivative **7**, to release mitomycin C (Scheme 3). The *meta*-derivative **8** proved stable toward release.<sup>59</sup> That the rates of fragmentation increased with a change in pH from 6, to 7.2 to 8.0 supports the role of deprotonated thiol (thiophenol  $pK_a$  6.6).

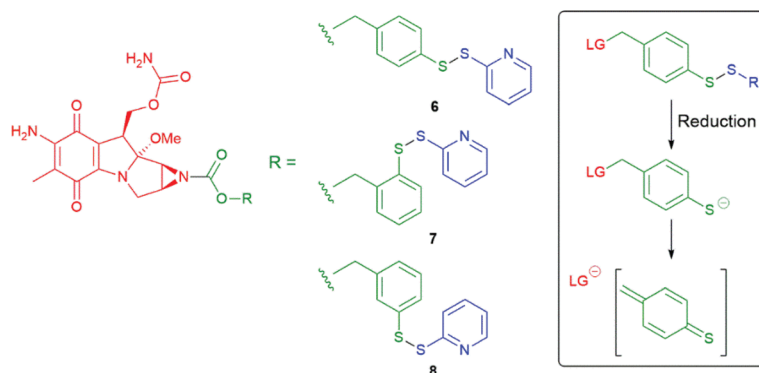
Shabat and co-workers have reported previously kinetic studies with aminobenzylalcohol linkers that undergo single *para*/1,6- or *ortho*/1,4-elimination and observed 1,6-elimination to be more slightly rapid than 1,4-elimination, in agreement with Senter’s observations on thiobenzyl alcohol linkers.<sup>61</sup> As a result of the increased electronegativity of oxygen with respect to nitrogen, hydroxybenzyl alcohol-based linkers undergo disassembly at relatively reduced rates, although these can be enhanced through the incorporation of additional ring substituents or the use of mild basic conditions to effect deprotonation.<sup>49,62–65</sup>

In addition, Shabat and co-workers evaluated a pyridine core-based AB and AB<sub>2</sub> self-immolative dendron (AB<sub>n</sub>, where A and B represent an electron-donating group and suitable leaving groups, respectively, and n correlates to the number of leaving groups present).<sup>66</sup> Under physiological conditions, the AB system constructed from a pyridine core, a reporter, and an enzyme (penicillin-G-amidase, (PGA)) sensitive trigger unit underwent 1,4-elimination more rapidly than its parent system featuring a benzene core. Furthermore, the pyridine core-based AB<sub>2</sub> dendron was also found to release its two reporter



**Scheme 2** Trypsin mediated release of 4-nitroaniline through self-immolative elimination of a 4-aminobenzylalcohol linker.<sup>11</sup>



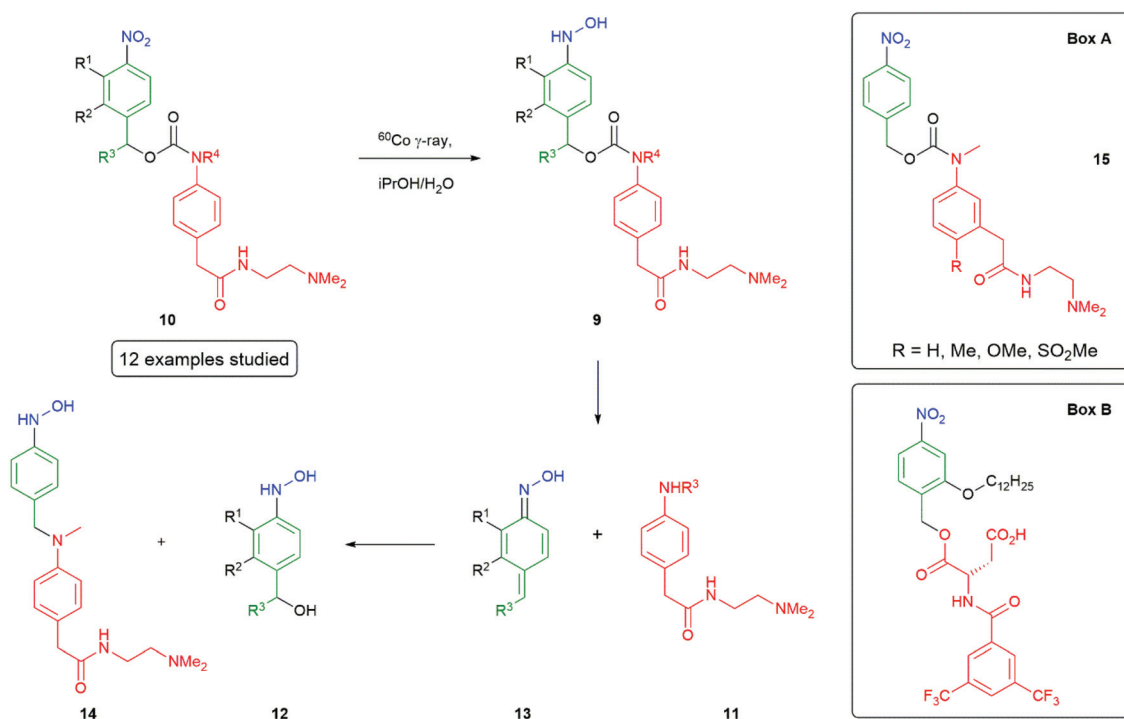


Scheme 3 Prodrugs 6–8 for mitomycin C with release triggered by reductive cleavage of a disulfide bond.<sup>59</sup>

units upon activation through 1,6- and 1,4-pyridinone-methide elimination reactions and faster than the analogous benzene system. To promote the elimination the conjugate base must be formed; given the  $pK_a$  of 3-hydroxypyridine (8.7) vs. phenol (10.0) under aqueous conditions, a larger concentration of the conjugate base is expected in the pyridine system in comparison to the benzene system. This difference in  $pK_a$  serves to explain the variation in the rates of elimination, though it introduces the potential for variance in aromatic resonance energy to affect rates of elimination *vide infra*.

Hay *et al.*<sup>50,67</sup> have investigated the influence of ring substituents on the rate of 1,6-elimination of *para*-hydroxylamino-benzyl alcohol linkers **9**, following radiolytic reduction of the

corresponding nitro compound **10** to release aniline **11** (Scheme 4). Twelve analogues were analysed and revealed that the presence of electron-donating groups were found to enhance the rate; whereas, electron-withdrawing groups serve to decrease the rate of elimination. The highest effect on self-immolative elimination rate occurs when electron-donating or withdrawing groups were *ortho* to the benzylic leaving group ( $R^2$  in **9** rather than  $R^1$ ), permitting conjugation with the developing cation formed during departure of the reporter group. Indeed, data on the electron-donating substituents *e.g.* OMe could be fitted to the equation  $\log(Mt_{1/2}) = 0.57\sigma + 1.30$ , where  $Mt_{1/2}$  is the maximum half-life and  $\sigma$  represents  $\sigma_p$  for 2-substituents and  $\sigma_m$  for 3-substituents.



Scheme 4 Reductively triggered self-immolative compounds showing the effects of ring substituents on the rate of fragmentation and recapture of the reporter group.<sup>50,68</sup>



An increase of elimination rate was also observed when a methyl group was substituted at R<sup>3</sup> to create a secondary carbon, consistent with its ability to stabilise a developing positive charge. As noted above, Hay also reported that the extent of release of the reporter group can be compromised by recombination of the reporter group with a precursor to **12**, probably the azaquinone methide intermediate **13**: a detailed analysis being given for **14**. This was found to be pH dependent with greater formation of the reporter group at pH 3 and more recombination at pH 7.4.<sup>50</sup> The observation of a reduced fragmentation rate (factor of 2) upon methylation at R<sup>4</sup> suggested the leaving group structure may also be important. A study of the four related compounds **15** (Box A) showed different extents of release of reporter group, at the end of the reduction process, dependent upon its structure though a clear connection to pK<sub>a</sub> of the reporter group remained elusive. Hamachi has reported an interesting application of nitroreductase to trigger a signal-amplifiable, self-assembling <sup>19</sup>F NMR-MRI probe, based on the self-immolative molecule shown in Box B.<sup>68</sup> Cleverly, this molecule utilises a hydrophobic *ortho*-alkoxy group that simultaneously facilitates its self-assembly into an NMR silent aggregate (mean diameter of 100 nm by DLS), prior to self-immolation, and increases the rate of that self-immolation, following reduction of the nitro group.

The generation of an aniline by reduction, to initiate 1,6-elimination, has also been examined from the diazo functional group. This has proved of value in drug release in the colon by action of azo reductase *e.g.* for controlled release of Tofacitinib for the treatment of ulcerative colitis.<sup>69,70</sup>

Senter *et al.* have also flagged the importance of the leaving group during an investigation into release of a reporter group linked through an alcohol moiety and have shown the effect on self-immolative ability, elimination rates, and conjugate stability.<sup>71</sup> In this study, 4-aminobenzyl ether-based conjugates

were studied with the *N*-protected dipeptide trigger group, benzoyloxycarbonylvaline-citrulline (*Z*-val-cit). *Z*-val-cit was conjugated with the amino group of aminobenzyl ether derivatives of 1-naphthol **16** and *N*-acetylnoephedrine **17** (Scheme 5). The amide bond in these derivatives was sensitive to hydrolysis by the protease enzyme Cathepsin B. Upon treatment with Cathepsin B, the peptide bond of conjugate **16** was hydrolysed and release of 1-naphthol occurred through 1,6-elimination from intermediate **18**. Under identical reaction conditions, the conjugate **17** featuring *N*-acetylnoephedrine was also subject to hydrolysis of the amide bond to yield the corresponding aniline **19**, but 1,6-elimination of *N*-acetylnoephedrine did not occur. The failure of **19** to undergo 1,6-elimination was attributed to a higher pK<sub>a</sub> of the reporter moiety. Stirling has noted the nucleofugality of leaving groups cannot always be correlated to the pK<sub>a</sub> of their conjugate acid.<sup>72</sup> However, in the context of β-elimination reactions with an E1c<sub>B</sub> character, Stirling assigns the leaving group rankings (*via* a logarithmic scale) of PhO<sup>−</sup> (8.9) and MeO<sup>−</sup> (6.1), consistent with the above observations. Germane to the upcoming discussion, Stirling notes that ‘small variations of structure within a series of leaving groups of the same type, *e.g.* aryloxy, do, however, show a correlation with pK<sub>a</sub>’.

Based upon these studies, the phenolic anticancer drugs etoposide and combretastatin were synthesised with ether **20–21** and carbonate **22–23** linkages to the *Z*-Val-Cit-*p*-amido-benzyl self-immolative unit, forming the corresponding tripartite prodrugs (Fig. 1). The phenolic ethers **20–21** proved to be stable in aqueous buffers as well as in human serum, and self-immolative fragmentation occurred only upon treatment with Cathepsin B. In contrast, the carbonates **22** and **23** were found to be unstable in aqueous buffers as well as in human serum. This study highlights that the design of a self-immolative system should consider the possibility of release by other than the desired mechanism. Similar studies were reported by



**Scheme 5** Variation of the self-immolative ability of the 4-aminobenzyl ether linker when coupled to either naphtholic or alcoholic reporter groups.<sup>71</sup>



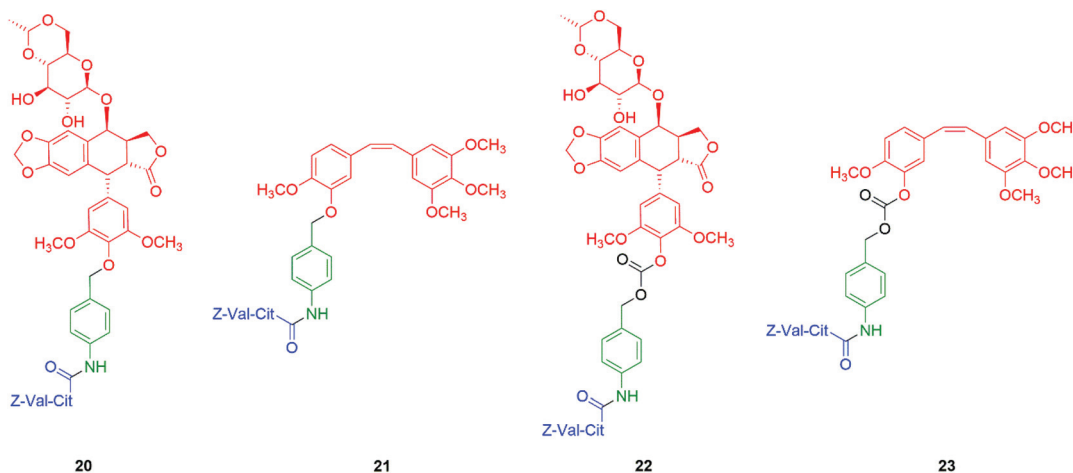


Fig. 1 Self-immolative tripartite prodrugs of anticancer agents etoposide and combretastatin A-4 described by Senter *et al.* in their ether (20–21) and carbonate (22–23) forms, respectively.<sup>71</sup>

Burke and co-workers,<sup>73</sup> and Leu and co-workers<sup>74</sup> who described the self-immolative ability of glucuronide hydroxybenzyl ether prodrugs of 10-hydroxycamptothecin.<sup>74–76</sup> Recently, Zhang, Pillow and co-workers have investigated the self-immolation of 4-aminobenzylalcohol linkers with phenol-based drugs as reporter groups in antibody drug conjugates.<sup>77</sup> They concluded that a case-by-case evaluation was necessary to determine their likely effectiveness. Related to these studies have been the application of self-immolative linkers in protein activity assays that take advantage of the highly reactive (aza) quinone methide<sup>78</sup> and quinone methide species.<sup>79</sup>

Building upon these observations, Phillips and co-workers have reported protected 4-aminobenzylalcohol linkers such as 24, substituted by electron donating groups, that allow tunable release of phenols with  $pK_a$  values  $\leq 11.5$ , directly connected to the benzylic carbon and under neutral conditions (Fig. 2).<sup>49</sup> A particularly reactive conformation, that simultaneously allowed facile interaction of the methoxy lone pairs with the aromatic  $\pi$ -system and, by conjugation, the  $\sigma^*$  orbital of the departing C–O bond, was shown to be favoured. Of general sig-

nificance to SIE triggered decomposition, the effect of solvent polarity was explicitly considered by variation of the ratio of two solvents, MeCN:H<sub>2</sub>O; an increased rate of release was observed with increased polarity. That the fragmentation of many prodrugs has utilised enzymatic reactions in water could leave this point less easily recognised.

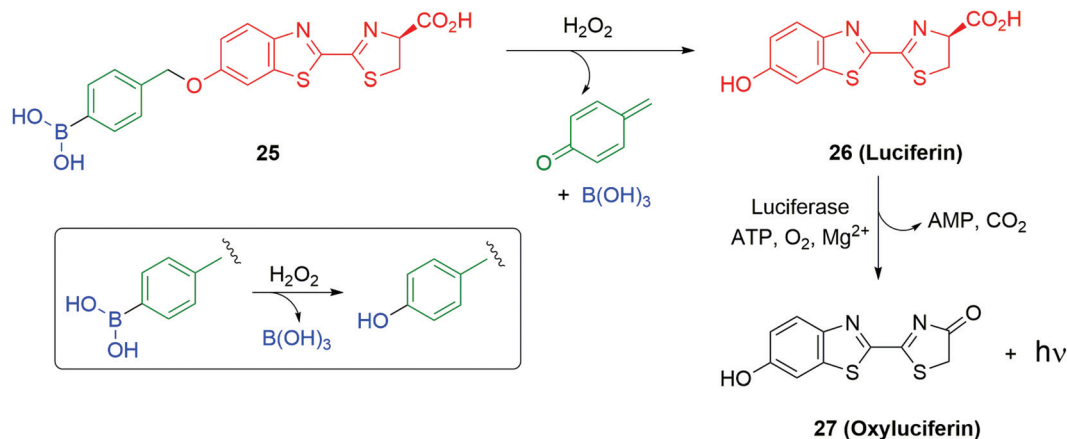
Use of a trigger group based on oxidation of a C–B bond has been reported by Chang and co-workers (Scheme 6).<sup>80</sup> Specifically, the use of hydrogen peroxide to mediate the oxidation is of medicinal significance as elevated levels in a cell are often correlated to significant disease states such as cancer and neurodegenerative diseases. Earlier work from this group has established the selectivity of this type of trigger for hydrogen peroxide over other reactive oxygen species.<sup>81</sup> Chang reported a SIE system 25 that is capable of releasing firefly luciferin with a view to quantifying the level of hydrogen peroxide in a cell. Thus, exposure of boronic acid 25 to intracellular H<sub>2</sub>O<sub>2</sub> releases 26 (firefly luciferin) that, in turn, upon exposure to luciferase, gives oxyluciferin 27 and chemiluminescence (612 nm).

Further studies on such SIE systems, by Cohen and co-workers,<sup>82</sup> has mapped out several useful design features (Fig. 3). In a comparative experiment, measuring rates of release of the phenol methyl salicylate ( $pK_a$  9.8), from three precursors 28–30, the carbonate 29 showed a slightly higher rate of release when compared to the phenol 28 but was subject to some background hydrolysis. Removing the self-immolative linker to give 30 revealed a significantly slower rate of formation; this latter issue highlights the general point that a self-immolative linker offers a consistent substructure within the molecule, with predictable kinetics and attenuated influence from changes in the reporter group structure, even when it is not an enzyme catalysed reaction that is under consideration. Amine-based reporter groups were unsuccessful *e.g.*, 31a unless part of a carbamate (32); a thiophenol (31b) also proved ineffective. At the reaction pH of 7.5, the amine-based reporter

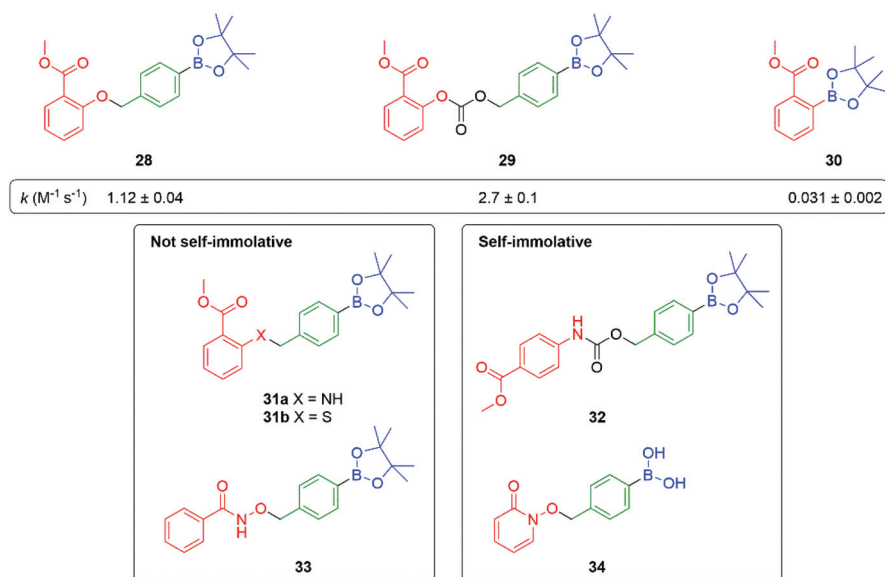


Fig. 2 Protected 4-aminobenzylalcohol linker that facilitates phenol release at neutral pH (for  $pK_a \leq 11.5$ ).<sup>49</sup>





**Scheme 6** Oxidatively driven SIE for release of luciferin: quantification of intracellular  $\text{H}_2\text{O}_2$ .<sup>80</sup>



**Fig. 3** Effectiveness of C–B bond oxidation to trigger release of various reporter groups.<sup>82</sup>

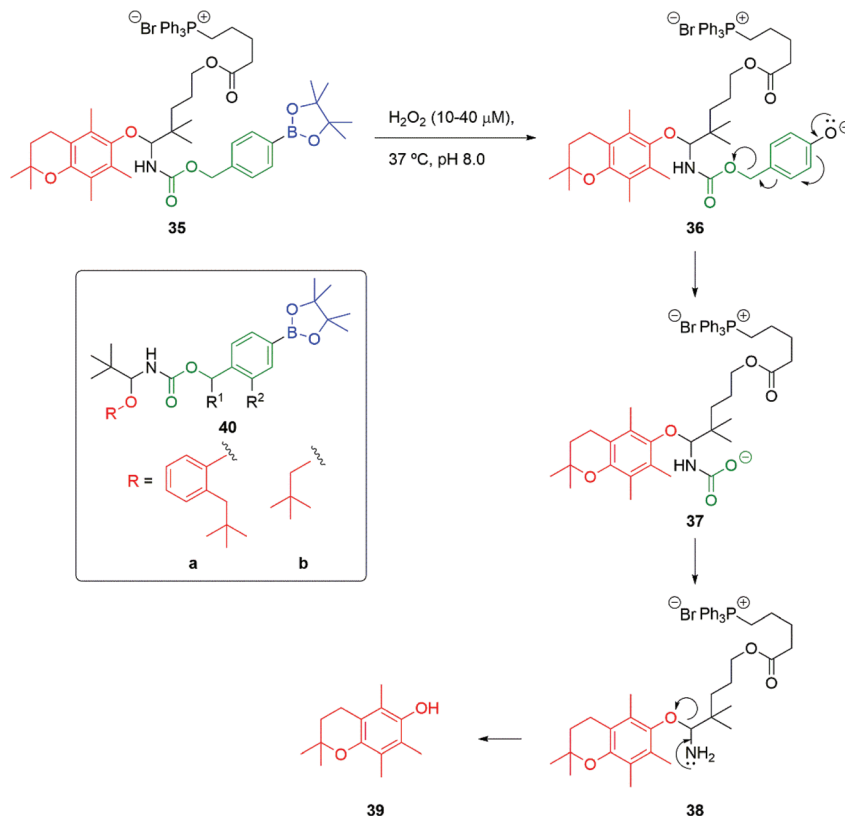
groups would be protonated to a very small extent, but this provided insufficient drive to eliminate, presenting an interesting contrast to *N*-alkylation (see Schemes 9, 33 and Fig. 12). Interestingly, **33**, containing a hydroxamic acid reporter group, also failed to self-immolate, perhaps reflecting the acidity of the NH group. The related compound **34** fragmented readily. Boronic acids were generally cleaved more rapidly than their corresponding esters, as well as improving aqueous solubility.

An alternative approach to the release of alcohols that addresses the difficulty of self-immolative release of alkyl alcohols has been advanced by Mosey and Floreancig (Scheme 7).<sup>83</sup> Building on the body of work reported by Chang and co-workers,<sup>80</sup> using a C–B bond oxidation of *e.g.*, **35** to **36** triggered by exposure to hydrogen peroxide, a key  $\alpha$ -alkoxy carbamate **37** is released. Of significance is the observation that self-immolation of the linker is slow compared to decarboxyl-

ation to give **38** and subsequent breakdown of the resultant tetrahedral intermediate, leading to **39**. When **40a** and **40b** ( $\text{R}^1 = \text{R}^2 = \text{H}$ ) are treated with hydrogen peroxide, the corresponding phenol and neopentyl alcohol were released at comparable rates, despite their difference in nucleofugacity. Interestingly, the authors also note the rate enhancement of linker fragmentation that attends the presence of a OMe at  $\text{R}^2$  in **40** or a methyl group at  $\text{R}^1$ , (*cf.* Scheme 4 and Fig. 2).

Overall, compound **35** is an interesting example of the general method; it is designed to deliver an antioxidant reporter group **39** to mitochondria, directed by the triphenylphosphonium group, as initially described by Murphy and co-workers.<sup>84,85</sup> It could be considered that the *O,N*-acetal functional group forms a second part of the linker moiety, as well as affording an attachment point for the directing group. In the latter sense, Santi has applied this type of *O,N*-acetal in the





**Scheme 7** Hydrogen peroxide induced self-immolative release of alcohols under *pseudo* biological conditions.<sup>83</sup>

delivery of SN-38.<sup>86</sup> Kolakowski and Jeffrey have shown this type of linker to be effective in drug delivery from antibody–drug conjugates.<sup>87</sup> A related approach was exploited independently by Wang and Xian for the delivery of persulfides (*vide infra*).<sup>88,89</sup> In later work, Floreancig and Deiters utilised hydrogen peroxide to trigger disassembly of *O,O*-acetals.<sup>90</sup>

In contemporaneous studies, Phillips and co-workers demonstrated release of two alcohols from symmetric or asymmetric acetals of the type present in **41**, at pH 7 under the influence of hydrogen peroxide (Scheme 8).<sup>52</sup> The amino benzaldehyde acts simultaneously as a reporter group (by colour, see Scheme 77 for the likely origin of the yellow colour) and a second linker group to the alcohol reporters. The observation of the secondary products **42** and **43** formed during fragmentation of **41** relates to the original suggestion by Katzenellbogen<sup>11</sup> that the fate of the linker could be influenced by nucleophiles in the system, other than water. Presumably, these arise *via* the *para*-quinone methide **44**; however, as these are also coloured, fortuitously they do not influence that part of the read-out.

The modular approach to synthesis of the detection system allows ready construction of detectors that respond to a range of environmental triggers; for example, UV radiation (**45a**), fluoride (**45b**), Pd(0) (**45c**), PGA (**45d**) and  $\beta$ -glucuronidase (**45e**) (see exemplars in Fig. 4).<sup>52</sup>



**Scheme 8** Hydrogen peroxide responsive detector that releases alcohols from an acetal under *pseudo* biological conditions.<sup>52</sup>

In addition to amine reporter groups being released as carbamates, ammonium ions have also been used to significant advantage. For example, Peng and co-workers have applied this approach to the delivery of nitrogen mustard anticancer agents *e.g.* mustine **46** (Scheme 9).<sup>91–93</sup> Utilising the nitrogen's



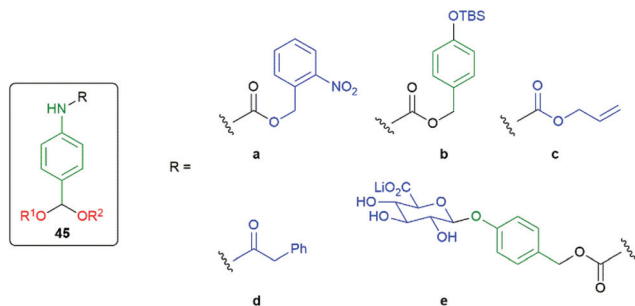
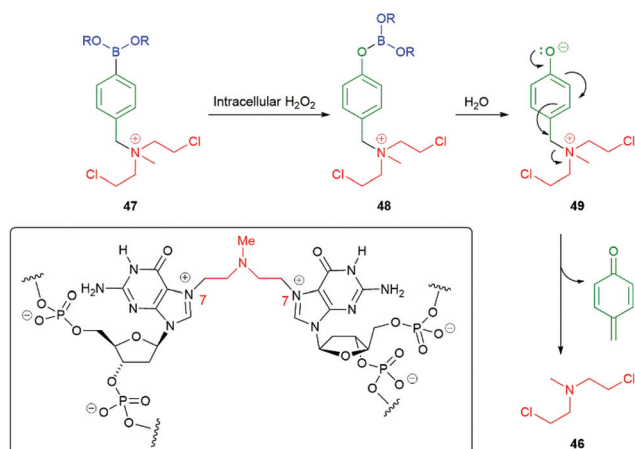


Fig. 4 Detectors that respond to a range of environmental triggers.<sup>52</sup>

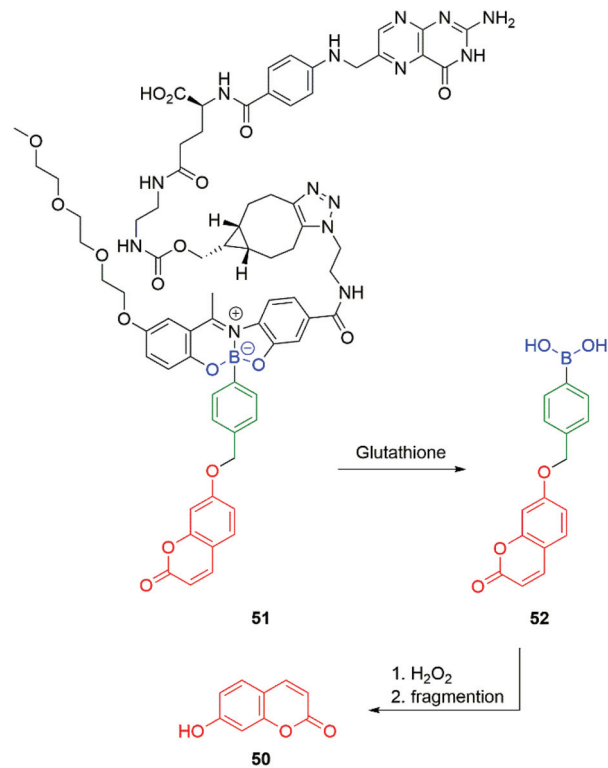


Scheme 9 Hydrogen peroxide induced self-immolative release of a nitrogen mustard.<sup>91–93</sup>

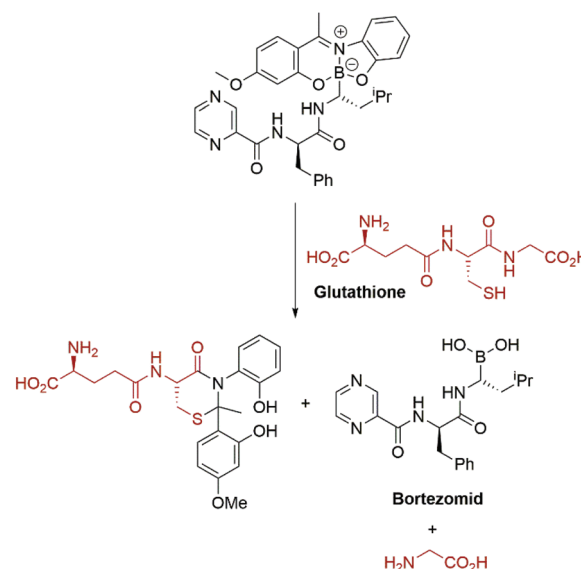
lone pair in bonding to the linker within **47** simultaneously forms a leaving group and prevents its use in neighbouring group participation, a key step that precedes DNA strand cross-linking, such as that to guanine *N*-7 illustrated in the boxed structure in Scheme 9. As noted above, intracellular hydrogen peroxide, frequently present in elevated levels in cancer cells, oxidises C–B bonds delivering borate esters such as **48** and thence *via* hydrolysis to phenols/phenolates **49** that self-immolate to release **46**. A related use of ammonium ion reporter groups has been discussed by Taran and Le Gall, *vide infra*.<sup>9</sup> In addition, Staben *et al.* have described the use of ammonium ions as leaving groups in self-immolative drug delivery systems based upon *para*-aminobenzyl alcohol and cyclization-based linkers.<sup>94</sup>

Gois and co-workers have adapted the C–B bond oxidation method to the targeted delivery of the fluorescent imaging agent 7-hydroxycoumarin **50** to folate-positive cancer cells (MDA-MB-231). Thus, **51** in the presence of glutathione releases **52** which will undergo oxidation and self-immolative cleavage to afford **50** (Scheme 10).<sup>95</sup>

Again, the modular approach for assembling the molecules greatly facilitates development of a glutathione triggered release of the cytotoxic drug Bortezomid.<sup>95</sup> A model study identified the cleavage products (Scheme 11) and led to a proposal for the mechanism of release of the boronic acid.



Scheme 10 Glutathione/hydrogen peroxide induced self-immolative release of a fluorescent coumarin.<sup>95</sup>



Scheme 11 Glutathione mediated release of Bortezomid.<sup>95</sup>

Fréchet *et al.* have prepared a modified version of the bio-compatible polymer dextran that is sensitive to the presence of H<sub>2</sub>O<sub>2</sub> (Scheme 12).<sup>96</sup> This new polymer, named OxiDEX, was found to be soluble in organic solvents, facilitating formation of microparticles (100–200 nm) capable of carrying a payload. OxiDEX was demonstrated to encapsulate ovalbumin to a





**Scheme 12** The modified dextran carrier polymer that was sensitive to  $\text{H}_2\text{O}_2$  as reported by Fréchet *et al.*<sup>96</sup>

protein loading of  $1.6 \pm 0.1$  wt%. In the presence of  $\text{H}_2\text{O}_2$ , the particles were shown to degrade with a half-life of  $36 \pm 1$  minutes. The OxIDEX particles were found to provide effective antigen presentation.

The value of C–B bond oxidation in affecting/investigating function within a cell was further exemplified by Pluth and co-workers by the development of a range of SIEs (**53**) capable of controlled release of COS and thence, by action of carbonic anhydrase, to accelerated release of  $\text{H}_2\text{S}$  (some non-enzymatic background release).<sup>97–99</sup> The discovery of  $\text{H}_2\text{S}$  as a gasotransmitter implicated in human health and disease has heightened interest in such molecules and **54** was shown to afford protection against oxidative stress in HeLa cells: its mode of action, *via* **55**, is illustrated below (Scheme 13). Release was preferentially triggered by  $\text{H}_2\text{O}_2$  but  $\text{O}_2^-$  and  $\text{ONOO}^-$  were also found to be competent oxidants; this being

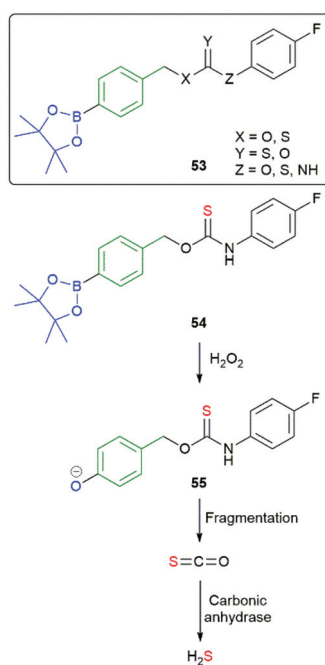
less discriminating than in its preferred oxidant than the systems reported by Chang and co-workers.<sup>81</sup> An alternative approach to the delivery of sulfur species has been developed by Toscano *et al.* *via* a cyclisation linker strategy (see section 2.2).<sup>100</sup>

Significant efforts have been expended to develop a range of self-immolative molecules, based upon 1,6-elimination, that deliver COS/ $\text{H}_2\text{S}$  but are triggered by a range of methods.

As a variation on **54**, Chakrapani and co-workers prepared a range of compounds exemplified by **56** (Fig. 5). The key feature of these compounds being the sulfur atom through which the linker is attached to the leaving group.<sup>101</sup> The significantly lower C–S as compared to C–O bond energy being considered advantageous during fragmentation. Similar compounds have also been reported by Pluth and their degradation pathways were subject to detailed theoretical analysis.<sup>99</sup> Despite the change of linking atom in **56**, it fragments efficiently to deliver, initially, COS and thence  $\text{H}_2\text{S}$ . The co-released aniline is the methyl ester of the non-steroidal anti-inflammatory drug mesalamine, used in the treatment of colitis. Together, the concept was to co-release a drug (mesalamine) and the cell-protective agent  $\text{H}_2\text{S}$ . The correlation of the  $\text{pK}_a\text{H}^+$  of the various amines/anilines employed in the study to the rate of release of  $\text{H}_2\text{S}$  (*via* COS) was also considered.

An alternate system, triggered by visible light, was also reported by the Chakrapani group.<sup>102</sup> Thus, **57** was prepared that featured a BODIPY-based photolabile trigger group (Fig. 5); this group being modified by ‘click’ methodology to append an oligo-ethylene glycol unit so as to improve aqueous solubility. Irradiation of **57** for 2 minutes at 470 nm afforded cleavage of the trigger group, within HeLa cells. Successful cleavage was established by observation of fluorescence at 540 nm. Additionally, compound **57** was found to be non-toxic. Klán and co-workers have reported use of BODIPY-based prodrug systems, but without use of a self-immolative linker.<sup>103</sup> Chakrapani and co-workers have also developed hydrogen peroxide triggered nitric oxide donors; whereas, Yuan *et al.* have reported a hydrogen peroxide triggered  $\text{H}_2\text{O}_2$  sensor with NO detection capability.<sup>104,105</sup>

Developing the 1,6-elimination system in **56** and **57**, Chakrapani and co-workers have exploited enzymatic trigger-



**Scheme 13** Reactive oxygen species triggered release of COS and thence gasotransmitter  $\text{H}_2\text{S}$ .<sup>97–99</sup>





Fig. 5 COS/H<sub>2</sub>S donor compounds **56** and **57**, triggered by H<sub>2</sub>O<sub>2</sub> and visible light, respectively.<sup>101,102</sup>

ing of COS/H<sub>2</sub>S release by protecting the phenolic OH as a POM (PivaloylOxyMethyl) group to afford compounds **58** (Fig. 6).<sup>106</sup> For the examples when X = O, rapid cleavage of the pivalate ester occurred upon exposure to an esterase followed immediately by sequential 1,6-elimination and formation of COS with the rate largely invariant with nature of R. Broadly the same mechanistic observations were made for examples when X = NH; however, some evidence for formation of a short-lived intermediate **58a** was presented. Additionally, for the X = NH compounds, the rate of release of COS/H<sub>2</sub>S was variable with the nature of R; for example, a benzyl group was found to generate the gasotransmitters more slowly than a *para*-methoxyphenyl group.

In a related study, Pluth and co-workers noted the advantage of intracellular cleavage in concentrating the release of H<sub>2</sub>S where required to solicit its action.<sup>107</sup> The relatively slow non-catalysed rate of hydrolysis associated with the sterically demanding pivalate ester in **59** was noted, a particular concern for a phenolic ester (Fig. 6). By contrast, rapid hydrolysis was demonstrated in the presence of porcine liver esterase. The generation of H<sub>2</sub>S in this manner does not directly consume intracellular nucleophiles, such as glutathione; however, the potential of consuming them by reaction with the *para*-quinone methide by-product was noted (much as suggested in the original paper by Katzenellenbogen). Compound **59** was noted to be cytotoxic and the cause was attributed to inhibition of mitochondrial respiration.

The abundant intracellular nucleophile cysteine has been utilised by Pluth in a two-step triggering of release of COS/H<sub>2</sub>S from **60** (Scheme 14).<sup>108</sup> Following an initial conjugate addition of thiolate to the acrylate moiety in **60** to afford **61**, cyclisation to  $\epsilon$ -lactam **62** releases the linker/reporter unit **63** that undergoes rapid 1,6-elimination to release COS. The two-step activation does make **60** vulnerable to trapping of the

acrylate moiety by alternative nucleophiles, such as glutathione or *N*-acetyl cysteine, that can only function in the first step. Competitive hydrolysis by porcine liver esterase was also noted, though the rate of release of COS/H<sub>2</sub>S was slower than that with cysteine.

Recognizing that self-immolation by 1,6-elimination can be initiated by an aniline as well as a phenoxide, reductively triggered self-immolative systems have been reported by Pluth, and by Singh and Chakrapani (Fig. 7).<sup>97,109</sup> Compound **64** was designed as an analytical tool for H<sub>2</sub>S and takes advantage of the well-known reduction of azides by two equivalents of H<sub>2</sub>S to afford the corresponding amine. The subsequent 1,6-elimination and release of COS, following hydrolysis by carbonic anhydrase, replaces one half of the consumed H<sub>2</sub>S analyte. The highly fluorescent methylrhodol ( $\lambda_{em}$  480–650 nm) is simultaneously released allowing quantification. A self-immolative polymer, triggered by azide reduction, for amplified release of COS, has recently been reported by Matson and co-workers (see section 4).<sup>110</sup> An additional method for release of COS, based upon a *trans*-cyclooctene trigger/linker system is discussed later on in this section.<sup>111</sup>

Rather than first releasing COS, Singh and Chakrapani utilised reduction of the nitro groups in molecules such as **65** to release H<sub>2</sub>S directly, following 1,6-elimination of the so-formed aniline/hydroxylamine (Fig. 7). *E. coli* nitroreductase (NTR) would be expected to reduce to the nitro group to the corresponding hydroxylamine **65a** or amine **65b** (see also Scheme 4). Exposure of **65** to NTR was shown to liberate H<sub>2</sub>S, as was its intracellular release in a variety of bacteria. As NTR is found in bacteria but not mammalian cells, **65** can be seen as a species selective H<sub>2</sub>S donor.

By adapting the enzymatically triggered species **58** and **59** to sulfonate **66** and analogues, Chakrapani was able to prepare cell-permeable, self-immolative molecules for controlled deliv-



Fig. 6 The esterase triggered COS/H<sub>2</sub>S donors **58** and **59** reported by the Chakrapani and Pluth groups, respectively.<sup>106,107</sup>





**Scheme 14** Pluth's cysteine-mediated two-step triggering of COS release from acrylate **60**.<sup>108</sup>



**Fig. 7** Reductively triggered COS/H<sub>2</sub>S donors **64** and **65**.<sup>97,109</sup>



**Scheme 15** The esterase triggered SO<sub>2</sub> donor **66** reported by Chakrapani and co-workers.<sup>112</sup>

ery of SO<sub>2</sub>; a cellular signalling compound (Scheme 15).<sup>112</sup> The cyclopropyl ester was selected according to its typically slower background rate of hydrolysis than simple aliphatic esters. The bond dissociation energy of the C–S bond was assessed to be comparable to a C–O bond; thus, fragmentation during 1,6-elimination and  $\alpha$ -elimination of SO<sub>2</sub> was anticipated to be facile. Forming the sulfonate ester with, *inter alia*, a 7-hydroxycoumarin (umbelliferone) facilitated fluorescence monitoring of fragmentation (phenyl sulfonate esters were also effective SO<sub>2</sub> donors). As an alternative to aromatic sulfonates, some alkyl sulfonate esters were examined and found to be relatively poor SO<sub>2</sub> donors, reflecting their inferior leaving group ability. As expected, the more reactive benzyl and allyl sulfonate esters were subject to significant background hydrolysis at pH 7.4, though no generation of SO<sub>2</sub> was observed from the resultant sulfonate. Exposure of **66** to an esterase led to consumption

with a half-life of 5 minutes. Umbelliferone was formed at a comparable rate and co-formation of SO<sub>2</sub> was established by its reaction with a coumarin-hemicyanine dye.

Interest in this area has also embraced hydropersulfides, such as cysteine and glutathione hydropersulfide, as ubiquitous in mammalian cells with protein-based cysteine hydropersulfides also being significant. Together, such hydropersulfides are considered mediators of biological function. The development of small molecules capable of effecting delivery of hydropersulfides, as reagents for the formation of their biologically significant counterparts, has become a matter of interest and self-immolative linkers have played a role in their design. In particular, the instability of persulfides, especially when an unprotected SH is present, suggests that selective release of such species from a protected form is important. For example, in the style of Mosey and Floreancig's hemiaminal-



based linker **35** (Scheme 7), a persulfide donor **68** that liberates an unstable disulfaneylmethanol **69**, upon cleavage with an esterase, was developed by Wang (Scheme 16a).<sup>88</sup> Once formed, **69** spontaneously undergoes a 1,2-elimination to release a single hydropersulfide species **70** allowing a detailed study of its biological effects. Reaction of **70** with thiols also generates the gasotransmitter H<sub>2</sub>S. Variation of the structure of R<sup>1</sup> allows control of the rate of release; whereas, changes to R can tune its aqueous solubility, e.g. **68a** (R<sup>1</sup> = Et) was found to exhibit protective effects in a murine model of heart myocardial infarction-reperfusion-injury studies. Xian has described a range of self-immolative persulfide donors of which **71** serves as an example, these are triggerable by fluoride/acid, Scheme (15a).<sup>89</sup> Of further interest is the conversion of **71** into the potentially esterase sensitive compound **72**. Additionally, related H<sub>2</sub>S and HSNO donors were reported. Overall, these silyl-triggered SIEs appear very flexible synthetically.

Two related reports have appeared, by Chakrapani and Matson, that target elevated levels of hydrogen peroxide in cells undergoing oxidative stress (*vide supra*) by oxidative cleavage of the C–B bond in **73** and **74** (Scheme 16b and c).<sup>101,113</sup> These reagents utilise 1,4- and 1,6-elimination to liberate **70b** and **75** from **76** and **77**, respectively. In each case, these compounds were shown to offer protection to cells undergoing oxidative stress. Chakrapani and co-workers noted that the cinnamaldehyde by-product **78** is a Generally Regarded As Safe (GRAS) compound, though it does offer some potential for re-

trapping **70b**. In each case, the oxidation with hydrogen peroxide was found to be chemoselective for the boronate ester over the persulfide moiety. These and other studies on reactive sulfur species has been expertly reviewed by Bora *et al.* in 2018.<sup>114</sup>

Using new versions of Schaap's dioxetane,<sup>115–117</sup> such as **79**, with improved chemiluminescence properties, Shabat and co-workers have developed a range of self-immolative detectors e.g. for galactosidase **80** and glutathione **81a** (Fig. 8).<sup>118</sup> A particular advantage of these new dioxetanes is that they maintain high light emission efficiency in aqueous solutions, greatly assisting their application in biological systems. The fragmentation of dioxetane **79** affords a deprotonated, excited state benzoate, as the final emissive species. Attachment of an acrylate/acrylonitrile moiety *ortho* to the phenolic OH was key to the improved emissive properties. The *ortho*-chloro substituent lowers the pK<sub>a</sub> of the phenol, increasing the percentage that is deprotonated at a given pH, a prerequisite for chemiexcitation and chemiluminescence.<sup>119</sup> Compound **79** exhibits  $\phi_{\text{CL}}$  13.8% ( $\lambda_{\text{max}} = 525 \text{ nm}$ ); in the absence of the acrylonitrile moiety, the chemiluminescent quantum yield falls to  $\phi_{\text{CL}}$  0.003% ( $\lambda_{\text{max}} = 470 \text{ nm}$ ).<sup>32</sup> A detailed summary of the chemistry underpinning these dioxetanes has been reported by Gnaïm *et al.*<sup>28</sup> Additionally, Shabat and co-workers were able to demonstrate further enhancements to light emission by formation of an inclusion complex between a range of dioxetane probes, e.g. **80** and trimethyl  $\beta$ -cyclodextrin; further, some of these were



**Scheme 16** (a) Esterase or fluoride/acid mediated release of a hydropersulfide from **68** or **71** via a 1,2-elimination; (b) hydrogen peroxide triggered release of hydropersulfide from **73** by 1,4-elimination; (c) hydrogen peroxide triggered release of hydropersulfide from **74** by 1,6-elimination.<sup>88,107,113</sup>



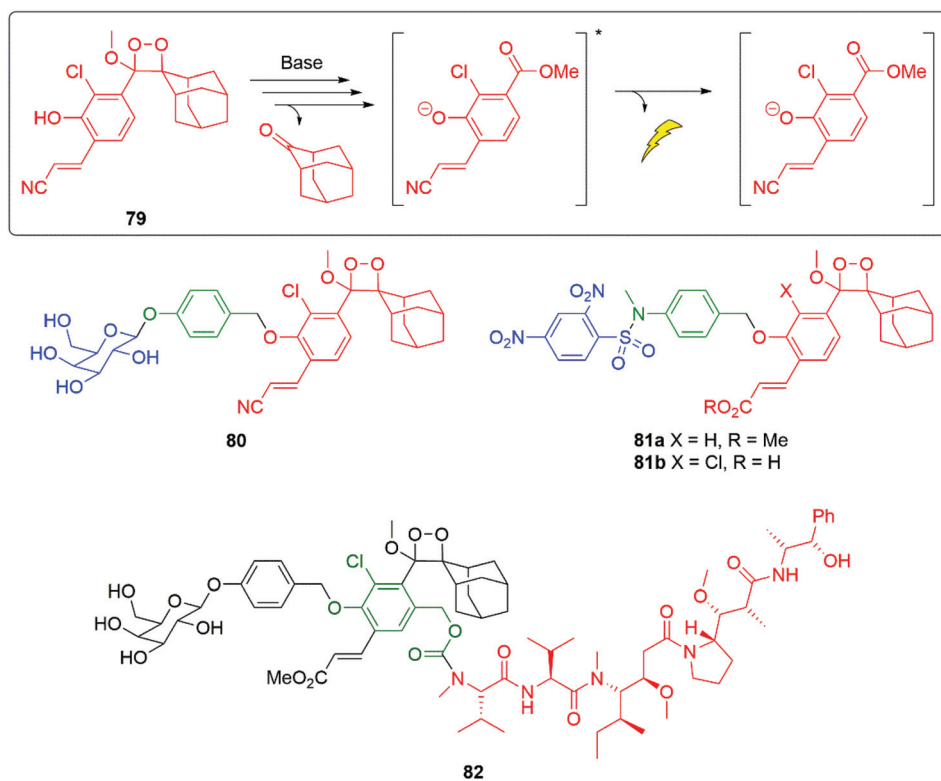


Fig. 8 Modified Schaap's dioxetanes for improved chemiluminescence.<sup>118</sup>

shown to be effective for *in vivo* imaging.<sup>120</sup> Utilising the H<sub>2</sub>S released by biodegradation of  $\beta$ -lactam antibiotics, following ring opening by a  $\beta$ -lactamase, Spitz and Shabat have developed several H<sub>2</sub>S sensitive probes *e.g.* **81b** that allow screening for antibiotic resistance.<sup>121</sup> Wu and Zheng have used a similar trigger to that in **81a-b** to release camptothecin (see section 3.1).<sup>122</sup>

Developing self-immolative entity **80** into **82**, to make the aromatic ring of the chemiluminescent moiety a second linker unit, allows the luminescent reporting to be accompanied by delivery of the chemotherapeutic agent monomethyl auristatin E (Fig. 8).<sup>123</sup> Of significance is that such reporting was established to work *in vivo* in mice bearing CT26-LacZ tumours.

Developing the applications of these new 1,2-dioxetanes has facilitated ultrasensitive self-immolative sensors for the key food pathogens *Salmonella* and *Listeria monocytogenes*. The limit of detection of these sensors outperforms common fluo-

rescent probes. The sensors **83** and **84** function by targeting, respectively, a *Salmonella* esterase and a phosphatidylinositol-specific phospholipase C that is species specific (Fig. 9).<sup>124</sup>

Building on earlier work by Renard and Romieu,<sup>125,126</sup> connecting the chemiluminescent probe through a self-immolative aniline linker, giving probes of type **85** (see Fig. 10), allows a range of peptide triggers to be attached that can target specific proteases. For example, Brik and Shabat reported that attaching the C-terminal sequence of ubiquitin protein (Ub (1-75)) to the aniline nitrogen through a glycine residue (**85a**) allows an assay for deubiquitinase activity to be developed.<sup>127</sup> Since deubiquitinating enzymes are involved in various human diseases, monitoring of their activity is valuable. Probe **85a** was found to be effective at detecting activity from three different deubiquitinases by cleavage of the scissile bond: UCH-L3, UCH-L1 and USP-2, with the first two giving the stronger response. Kitamura, Shabat and Vendrell have shown

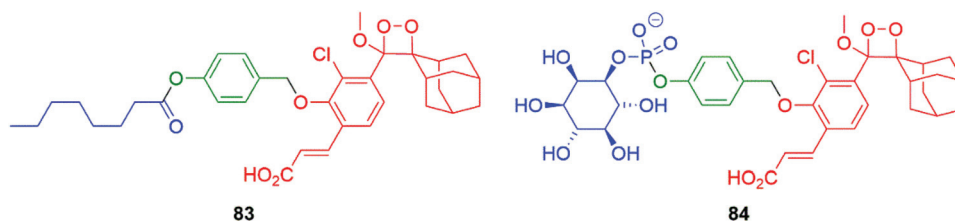


Fig. 9 Selective chemiluminescent sensors **83** and **84** for rapid detection of *Salmonella* and *Listeria monocytogenes*.<sup>124</sup>





**Fig. 10** Chemiluminescent probes **85a–d** that target of protease activity in four different contexts.<sup>127–130</sup>

that appending peptide **85b** was found to selectively target granzyme B, a key enzyme in the functioning of natural killer cells; these cells can kill certain types of cancer cells. This probe has allowed imaging of granzyme B activity in mouse models.<sup>128</sup> Attaching the peptide sequence in **85c** allows targeting of prostate specific antigen proteolytic activity; this has been applied to the forensic detection of human semen on fabrics.<sup>129</sup> Bogoy *et al.* have studied the imaging of the clinically very important disease tuberculosis; this has been by addressed with the peptidic sequence in **85d**. This sequence targets the Hip1 protease in *Mycobacterium tuberculosis*, allowing imaging of such cells either in culture or in human sputum samples.<sup>130</sup>

Using solid-phase methods, a general approach to the synthesis of these self-immolative, chemiluminescent probes that are triggered by proteases, has been described by Ponomariov *et al.*<sup>131</sup>

As an alternative to targeting proteases, conjugation of the nitrogen of the aniline linker to a substrate for the copper dependent enzyme tyrosinase allows selective oxidation from sensor **86** to *ortho*-quinone **87** (Scheme 17).<sup>132</sup> When **87** forms in the presence of thiols, for example, glutathione then cleavage occurs to **88** and sets in train disassembly of the linker and ultimately chemiluminescence from an excited state of **89**. The electrophilicity of *ortho*-quinones toward thiols is known and has been examined in a biological context by Fellmann, Doudna and Francis.<sup>133</sup> Such conjugate addition is expected to form a catechol, allowing the trigger to cleave. The presence of the 2-dimethylaminoethyl unit facilitates cell permeability. The typically high levels of tyrosinase expressed in melanoma cells makes this probe of significance in cancer imaging.

Similar metabolic activity of tyrosinase has been shown as effective at triggering self-immolation by Ma and Zhang, in turn acting as sensors for that enzyme.<sup>134,135</sup>

Further studies by Shabat and co-workers have seen deployment of chemiluminescent 1,2-dioxetanes in a polymeric framework (see section 4.1).<sup>43</sup>

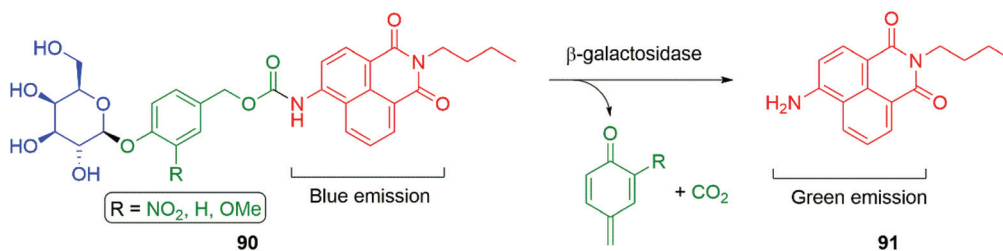
Hou *et al.* have developed a ratiometric self-immolative probe **90** for  $\beta$ -galactosidase that changes from blue (475 nm) to green (545 nm) fluorescence upon triggering to release the 4-amino-1,8-naphthalimide fluorophore **91** (Scheme 18).<sup>136</sup> They report an interesting observation with respect to the substituent R on the linker, finding that the rate limiting step for the probe was enzymatic hydrolysis and thus the primary contribution of the substituent was to affect the Michaelis-Menten constant ( $K_m$ ) of the substrate for the  $\beta$ -galactosidase, the nitro substituted compound having the lowest value.

Probing redox biology is important in understanding cellular function. Yang has introduced an innovative method for sensing hydrogen peroxide based upon sequential Payne and then Dakin reactions; hydrogen peroxide is converted into a reagent suitable for rapid Dakin oxidative conversion of an aromatic aldehyde into a phenol (Scheme 19).<sup>137</sup> When applied to pro-fluorescent agents **92** or **93**, the presence of hydrogen peroxide triggers 1,6-elimination and release of their strongly fluorescent reporter groups at a rapid rate. It was found that  $\text{Cl}_3\text{CCN}$ , **92** and **93** were non-toxic to RAW264.7 macrophages and were successful in imaging hydrogen peroxide activity in RAW264.7 cells. Shabat and Yang successfully extended this methodology to chemiluminescence by preparing probe **94** and demonstrating its effectiveness in imaging live cells and real-time monitoring of rat brain.<sup>138</sup>





**Scheme 17** Satchi-Fainaro, Shabat and Sessler's sensor **86** for a chemiluminescent response to the simultaneous presence of tyrosinase and thiols.<sup>132</sup>



**Scheme 18** The  $\beta$ -galactosidase probes **90** developed by Hou and co-workers.<sup>136</sup>

By varying the trigger group and a subtle modification to the linker, Shabat and Yang have extended this work to the sensing and real-time imaging of HOCl in mice (Scheme 19).<sup>139</sup> Thus, in **95** a phenoxy trigger group has been attached to the linker; the two *ortho*-chloro substituents on the trigger ( $pK_a$  6.8) ensured that at physiological pH greater than half of the phenol will be ionised, enhancing the nucleophilicity of the aromatic ring. It would also resist chlorination of this ring by HOCl. When exposed to HOCl, oxidative cleavage occurred with loss of quinone **96** and release of the linker reporter unit **97**; this will fragment by 1,6-elimination leading, after fragmentation of **98**, to chemiluminescence. The addition of a chloro substituent to the linker resisted further chlorination and lowered the  $pK_a$  of the phenol.

Antibiotic resistance is one of the major challenges in medicine and medicinal chemistry. The role of  $\beta$ -lactamases is central to that challenge and probes that can offer an easily applied diagnostic tool to a given sample, for their presence, is of considerable importance. Spitz and Shabat have

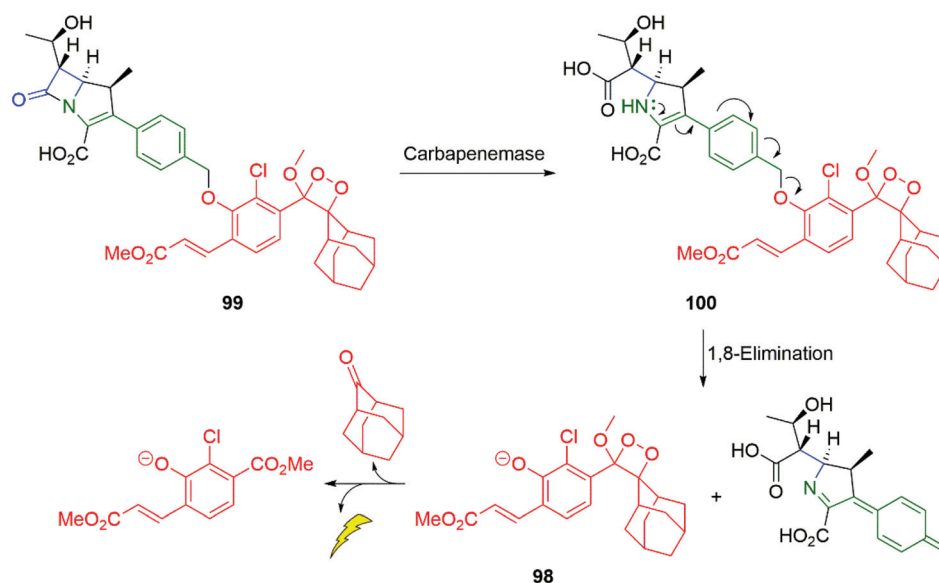
reported such a probe **99** for carbapenemase activity (Scheme 20).<sup>140</sup> In the presence of a carbapenemase *e.g.* SPM-1 (a metallo- $\beta$ -lactamase), the  $\beta$ -lactam ring of **99** undergoes hydrolysis to give **100**, setting up an enamine-driven 1,8-elimination to give the chemiluminescent dioxetane **98** discussed above.

Formaldehyde is an important one carbon source for biological systems, frequently stored as part of a folate molecule. The low concentrations and transient nature of formaldehyde in biological systems has resulted in an interest in developing probes for its detection. Building on Chang's extensive studies on the self-immolative aza-Cope rearrangement strategy to trigger a fluorescent response to the presence of formaldehyde, chemiluminescent probe **101** was developed by Chang and Shabat (Scheme 21).<sup>141–144</sup> Upon exposure to formaldehyde, the primary amine of the Chang trigger condenses with it to give the corresponding imine **102** that undergoes an aza-Cope rearrangement to afford **103**. Hydrolysis of **103** delivers ketone **104** that undergoes  $\beta$ -elimination to release the dioxetane **98**





**Scheme 19** Yang and Shabat's sensors for oxidative activity the cell triggered by  $H_2O_2$  or  $HOCl$ .<sup>137–139</sup>



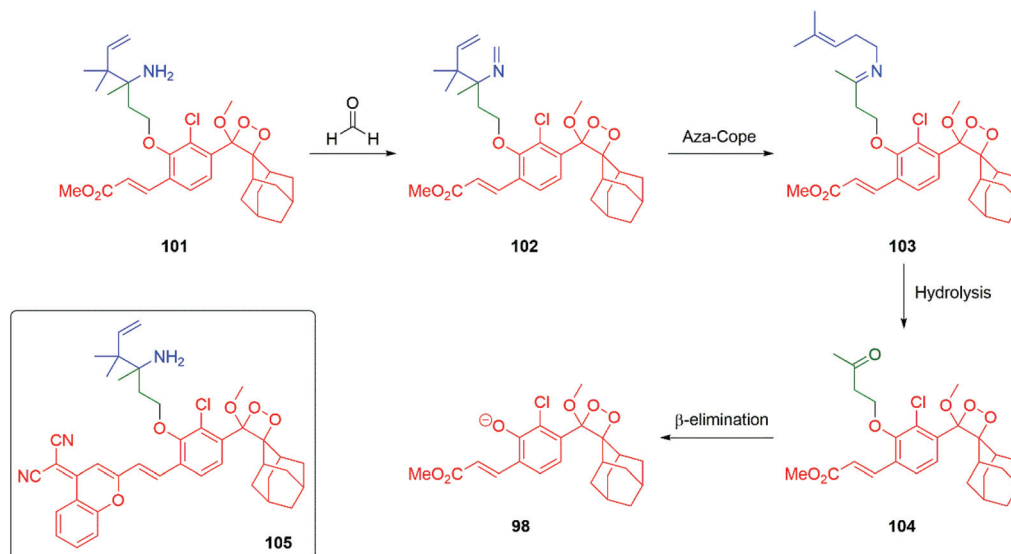
**Scheme 20** Spitz and Shabat's probe **99** for carbapenemase activity.<sup>140</sup>

that undergoes decomposition with release of a photon at 540 nm. To improve imaging *in vivo* imaging probe **105** was developed that emits radiation at 700 nm.

By contrast, Ma has demonstrated that imine formation by oxidation of an amine, followed by hydrolysis and  $\beta$ -elimination of acrolein, to release a self-immolative phenol, can serve as a selective sensor for monoamine oxidase A (MAO-A) over MAO-B.<sup>145</sup>

The Staudinger reduction of  $\alpha$ -azido-ether groups to generate unstable *N,O*-acetal moieties that collapse with the release of a reporter group have been important, *inter alia*, in nucleic acid detection studies and have been reviewed by Winssinger, Seitz and Kool.<sup>146–148</sup> The utility of the *N,O*-acetal functional group in SIEs has been illustrated in Scheme 7. The development of templated Staudinger azide reduction into a SIE technology for release of functional molecules has been

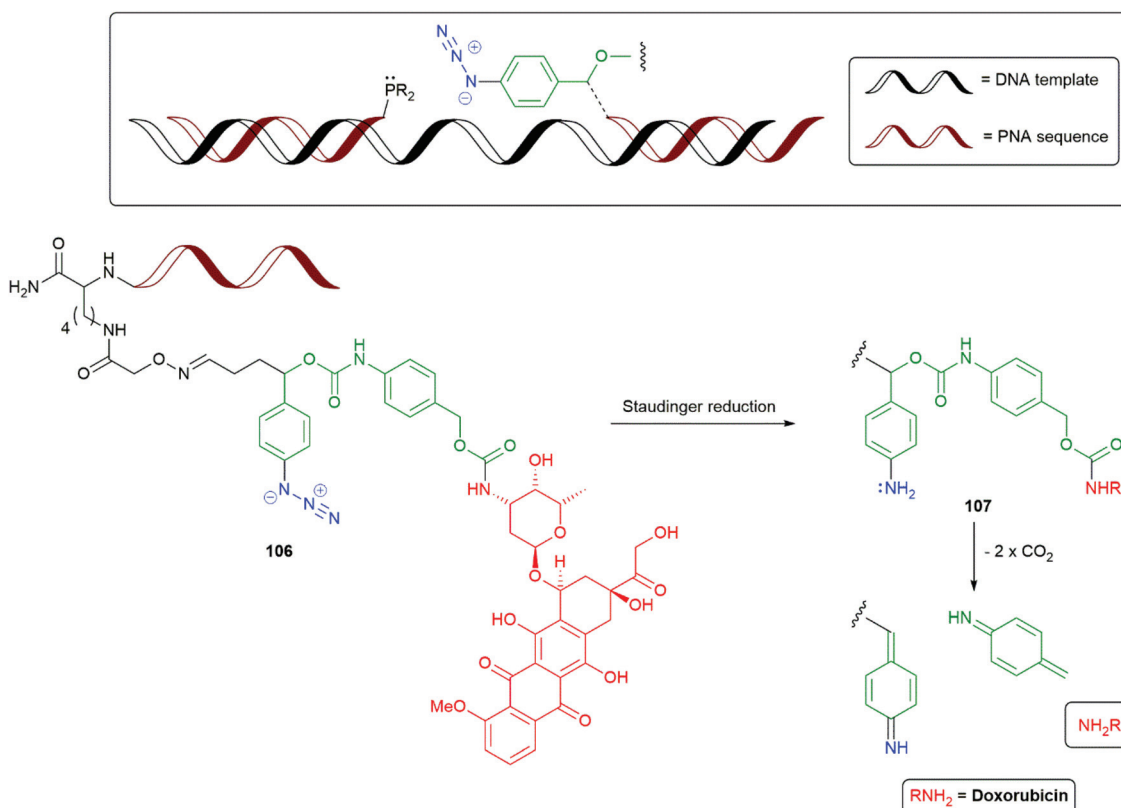




**Scheme 21** Chang and Shabat's aza-Cope driven probe **101** for folate-derived formaldehyde.<sup>144</sup>

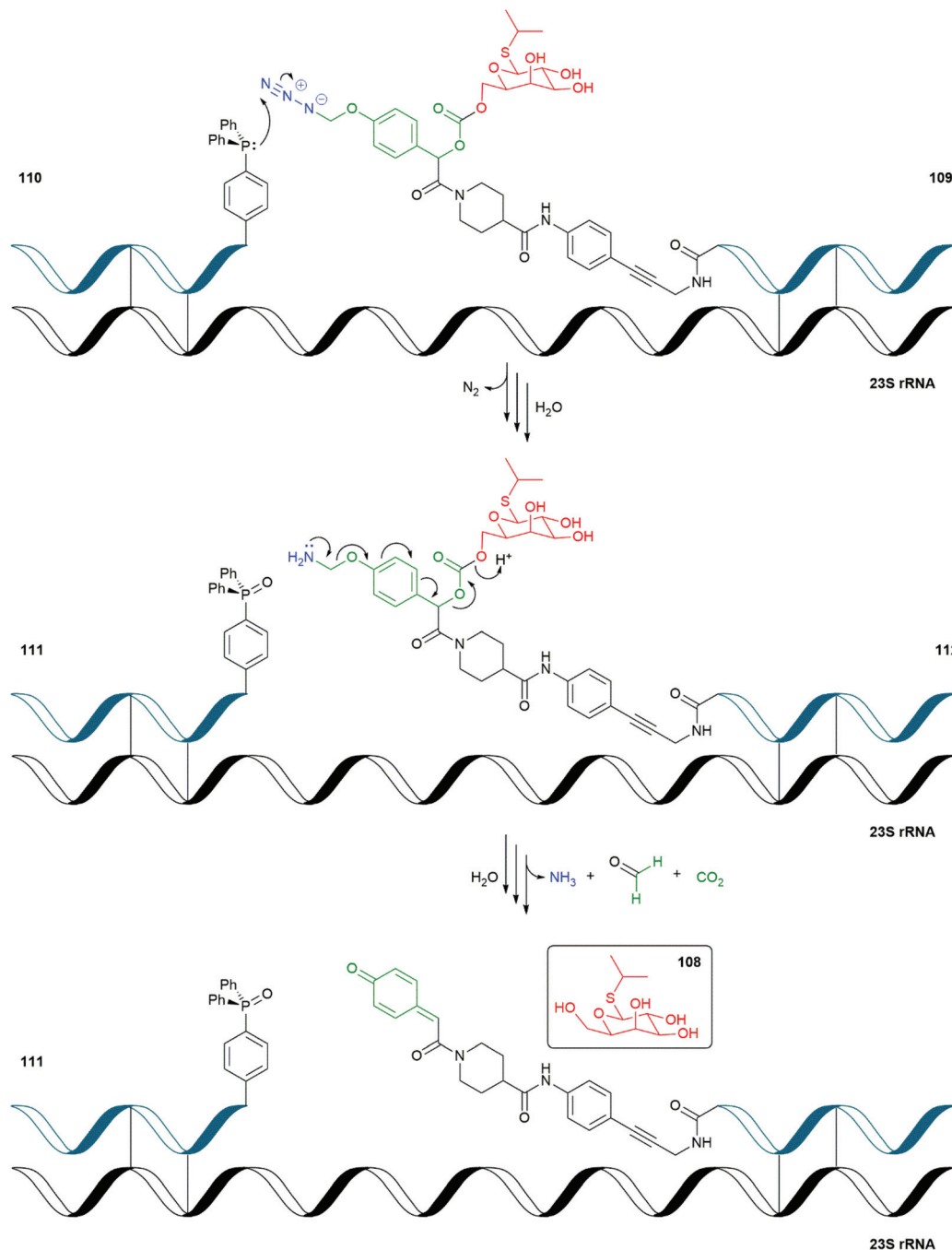
reported independently in 2013 by Sadhu and Winssinger (Scheme 22), and by Ito and Abe (Scheme 23).<sup>149,150</sup> In particular, the bioorthogonality of the azide group was seen as important in allowing the method's implementation within cells. Winssinger employed a strategy of synthesising a peptide

nucleic acid then condensing it with the SIE to afford oxime **106** (Scheme 22). Subsequent reduction of the azide in **106** generates the corresponding aniline **107**, that then permits degradation to liberate doxorubicin as the reporter group. The alternative reporter groups rhodamine methylurea and estra-



**Scheme 22** The templated Staudinger azide reduction triggered SIE **106** reported by Winssinger and co-workers.<sup>149</sup>





**Scheme 23** The RNA templated self-immolative system **109** reported by Ito and Abe.<sup>150</sup>

diol were also examined. Model azide reductions indicated Staudinger reduction and fragmentation of the first linker stage to be very fast; whereas, the second linker self-immolated at a rate related to the  $pK_a$  of the reporter group, with some attenuation for the carboxyl linker.<sup>151</sup> However, even the slowest system examined, doxorubicin, was found to have a  $t_{1/2}$  of 21 minutes. Further studies by Winssinger have utilised templated azide photoreduction, mediated by a Ru(II) complex, in live cells.<sup>152</sup> The method was found to give very high turnover in the reduction and high sensitivity in nucleic acid sensing.

Ito and Abe have described an RNA-templated SIE decomposition that releases isopropyl- $\beta$ -D-thiogalactoside (IPTG) **108** within an *E. coli* cell (Scheme 23).<sup>150</sup> IPTG, when present in a bacterial cell, induces expression of plasmid-based genes that are under the control of the *lac* operator by binding to the *lac* repressor. In their study, Ito and Abe have used the Staudinger reduction of azide triggered *para*-hydroxymandelic acid-based SIE **109** by RNA bound triphenylphosphine **110** affording, after hydrolysis, the corresponding phosphine oxide **111** and linker system **112**. Upon loss of for-



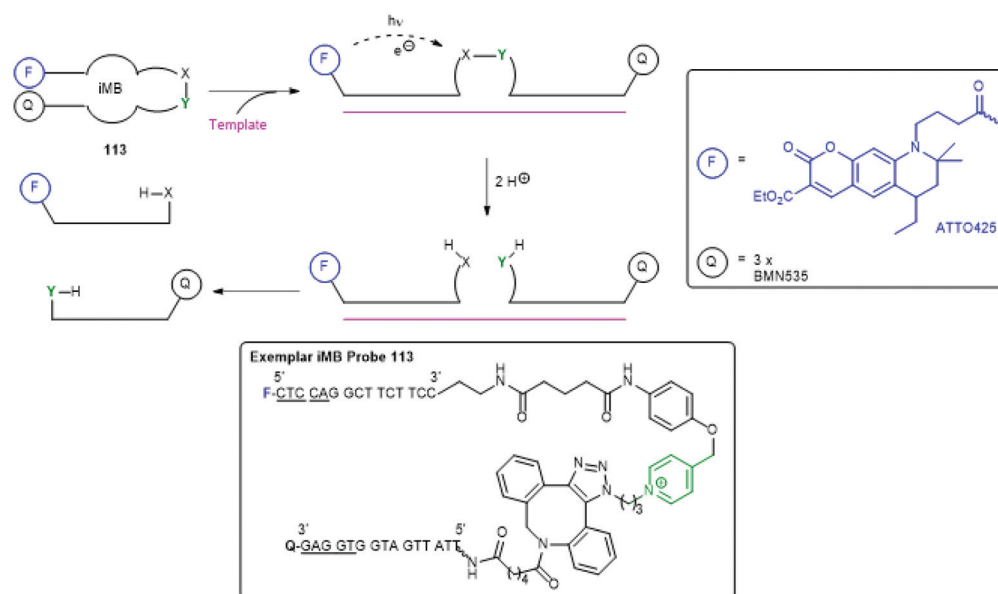
maldehyde imine and 1,6-elimination of the mandelate unit, decarboxylation releases IPTG **108**. Additional DNA-templated FRET systems were also reported.

Recently Seitz and co-workers have presented an interesting, templated SIE method (an immolative Molecular Beacon iMB) that allows amplification of a fluorescence signal, facilitating detection of RNA/DNA target sequences at pM levels (Scheme 24).<sup>153</sup> It involves a novel and unusual situation in which the trigger and reporter group are the same, activation of which photosensitises cleavage of a remote linker. Thus, an immolative molecular beacon **113** was prepared that uses a pentamer stem (underlined nucleotides) to give a hairpin structure that brings the fluorescent reporter group (ATTO425) into proximity with a quencher group (three copies of BMN535). Upon exposure to the target RNA/DNA template, the hairpin opens allowing fluorescence upon exposure to 455 nm light. Simultaneously, this photosensitises cleavage of the

*N*-alkylpicolinium-phenol ether linker, mediated by ascorbic acid. Each fragment of the cleaved probe has a lower binding energy for the template than the probe itself, allowing dissociation, continued fluorescence and reuse of the template.

The mechanism illustrated in Scheme 25 has been proposed<sup>153</sup> to account for reductive cleavage of the *N*-alkylpicolinium-phenol ether (NAP) linker.

Building upon earlier work on light activation of **114**, Schmidt, Jullien and co-workers studied light activation ( $365 \pm 25$  nm) of SIEs of type **115** to underpin a detailed assessment of the kinetics of disassembly of representative self-immolative systems, such as **116**, and the relationship their of structure to the observed rates (Fig. 11).<sup>151,154</sup> The results emphasise the speed and utility of photochemical triggering, a technique that has found a number of applications in the field, *e.g.* Schemes 47 and 57. The data reported are of general importance; for example, the relative rates of decarboxylation of carbamates



Scheme 24 The immolative molecular beacon (iMB) **113** reported by Seitz and co-workers.<sup>153</sup>



Scheme 25 The proposed mechanism for cleavage of the NAP-phenyl ether linker **113**.<sup>153</sup>



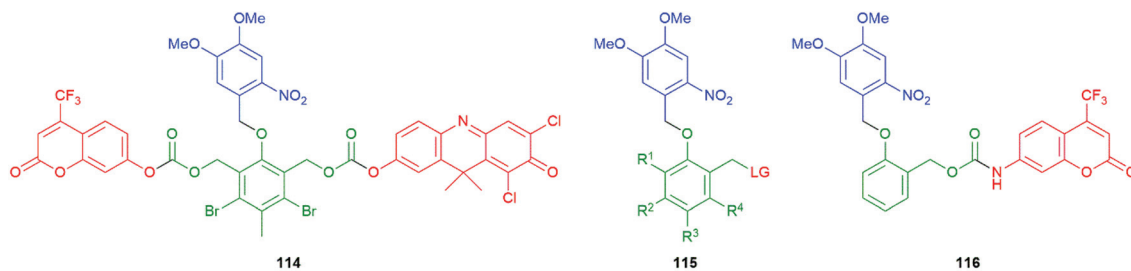
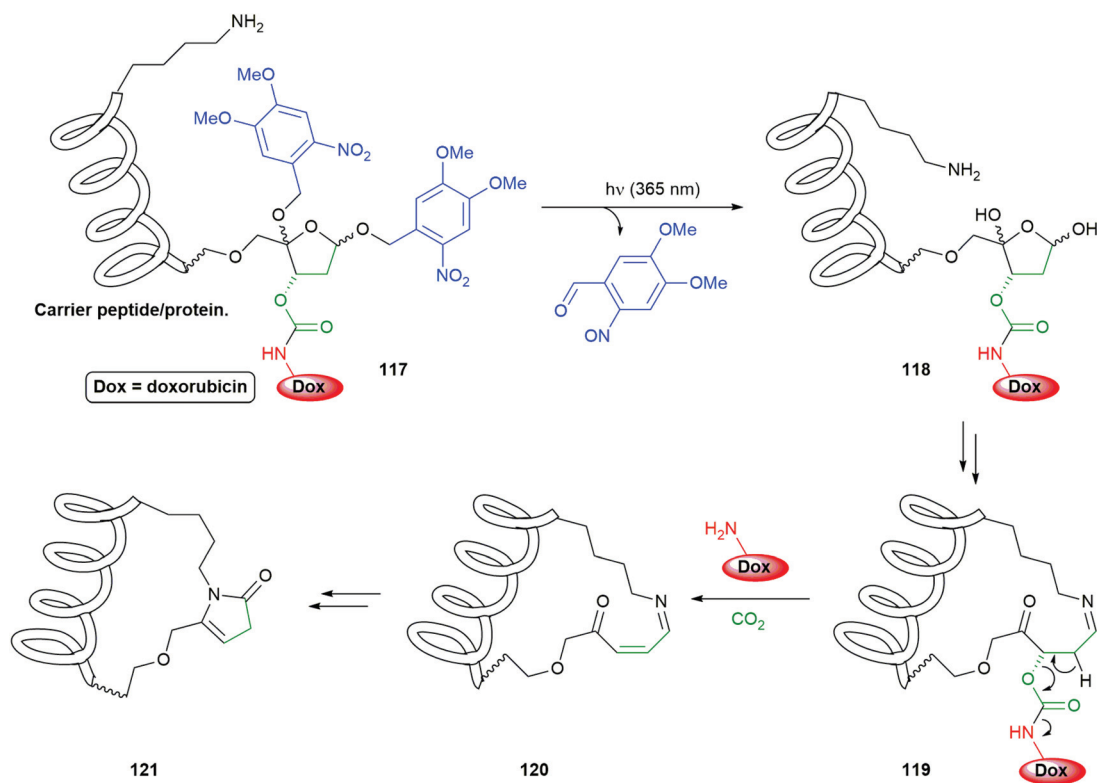


Fig. 11 The photoactivatable self-immolative systems **114**–**116** subject to kinetic studies by Schmidt, Jullien and co-workers.<sup>151,154</sup>

and carbonates, two commonly employed parts of SIE design, are determined. Also, quantitative data on the effect of electron withdrawing and electron donating groups on the linker add further useful design information. The authors have drawn attention to the idea of a self-immolative linker as a 'molecular clock' and report further quantitative information on the importance of pH on their disassembly. The significance of such considerations is given useful focus in the recent results reported<sup>155</sup> by Bradley and co-workers that show reaction-condition-dependent stability of a self-immolative (SI) linker. This phenol-based linker–reporter system proved isolable under some conditions yet disassembled expeditiously under others (see Schemes 35 and 36). A broader consideration of the kinetic aspects of SIE disassembly, across many systems, was covered in their recent review.<sup>21</sup>

An interesting application of photo-triggered self-immolative linkers has been reported by Zhou (Scheme 26).<sup>156</sup> The system **117** conjugates a new self-immolative linker/reporter group to a carrier peptide or protein; this peptide/protein has an appropriately placed primary amine *e.g.* a lysine residue, the  $\epsilon$ -amino group of which then becomes critical to fragmenting the system once photo-decaging has taken place. The method is based upon earlier work on the fragmentation of DNA by primary amines at C4'-oxidized abasic sites (referred to as C4APs) and has focused upon the biocompatibility of both the initial system and the breakdown products, with the added advantage that the carrier could assist with important functions such as cell penetration. Thus, irradiation of **117** at 365 nm led to quantitative cleavage of its two *ortho*-nitrobenzyl trigger groups to afford **118**. Equilibria with ring-opened forms



Scheme 26 Zhou's PC4AP (photocaged C4'-oxidized Abasic site) self-immolative linker attached to a carrier peptide to form a delivery system for doxorubicin.<sup>156</sup>



of **118** facilitates formation of imine **119** using the intramolecular  $\epsilon$ -amino group of a lysine side-chain. Elimination of the carbamate, possibly *via* the enamine form of **119**, releases the doxorubicin reporter group. Cyclisation of **120** with step-wise addition and re-elimination of water gives **121** as the final product. Release of doxorubicin was found to reach 85% within 1 h, following irradiation for 5 min at 365 nm, when H3-V35C was used as the carrier peptide. The conjugate was also shown to be transported into the cytoplasm of HeLa cells and release its doxorubicin upon irradiation, only then did the drug move to the nucleus. The new linker was also shown to be compatible with antibody directed methods.

Though an amine-containing reporter group (doxorubicin) is illustrated in Scheme 26, alcohol bearing reporter groups are also usable.

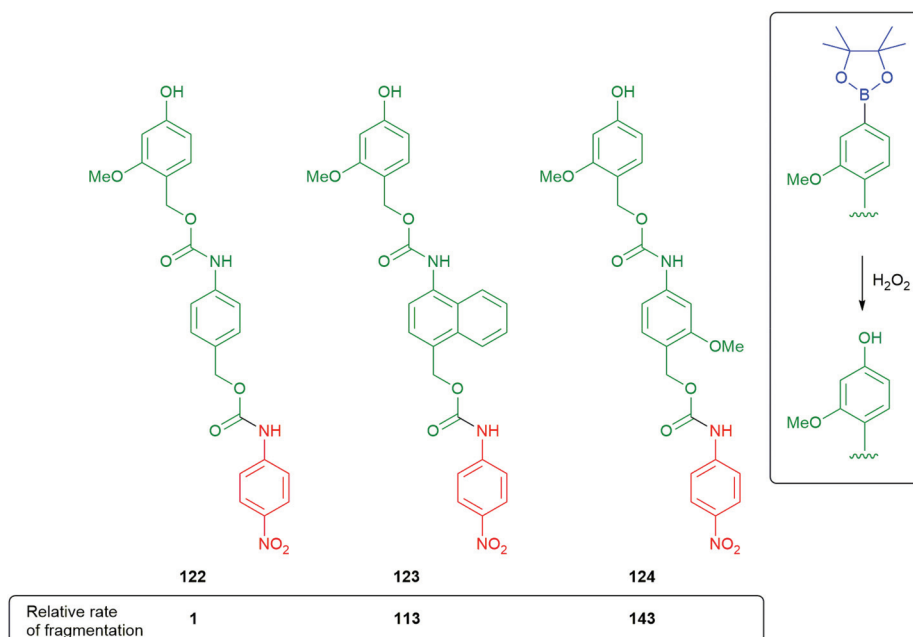
The design of linkers with varying rates of release has been important to the advancements in the field. In respect of linkers based upon an aromatic core, in addition to the use of judiciously placed donor substituents on the ring, employing an aromatic ring of lower resonance energy can also be useful; for instance, Shabat's pyridine linker<sup>66</sup> (*vide supra*) and the use of polycyclic aromatics. Indeed, Gillies has utilised the facile thermal reversibility of a furan Diels–Alder reaction, coupled with furan's electron rich 2 and 5 positions, to facilitate fragmentation of a self-immolative polyglyoxylate polymer, see section 4.4. Some measure of relative aromaticity can be garnered, *inter alia*, from aromaticity indices; for example, those proposed by Hess and Schaad which relate a number of heterocycles to benzene as 100%. Thus, pyridine (82%), pyrrole (37%), furan (12%) can be seen as having lower aromaticity.<sup>157</sup>

Phillips has shown that naphthyl linkers can be effective, if designed to give 1,6-elimination.<sup>158</sup> As part of this study, the

contributions of resonance energy of a particular aromatic were considered and evaluated against a benzene ring as standard (Scheme 27). The results were applied to the fragmentation rates of oligo-linkers **122–124**, formed after triggering of the corresponding boronate esters. The naphthyl linker disassembled a little slower than a methoxy bearing benzene ring; however, it still represents a valuable, alternative approach to varying fragmentation rates. Solvent polarity effects were also considered with more polar solvent mixtures encouraging faster fragmentation rates. The naphthyl and methoxybenzene linkers **123** and **124** were able to function effectively in a significantly less polar medium than **122**.

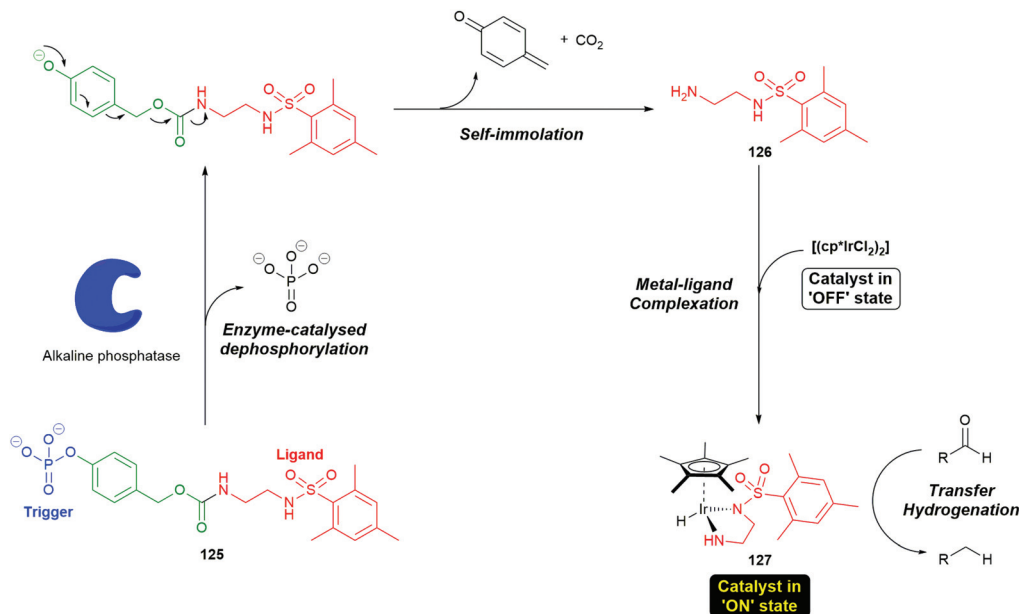
Self-immolative systems that operate, post-triggering, *via* an electronic cascade have been utilised in innovative synthetic processes. For example, Goggins *et al.* have described the use of a self-immolative electronic cascade process to permit signal transduction and amplification *via* an enzymatically-triggered ligand release and accelerated catalysis process.<sup>159</sup> The pro-ligand enzyme substrate **125** was designed to selectively self-immolate in the presence of an alkaline phosphatase enzyme to release a ligand **126** that can bind to a metal pre-catalyst  $[(cp^*IrCl_2)_2]$  to afford **127**, thus accelerating the rate of a transfer hydrogenation reaction (Scheme 28). Using SI proligands to facilitate a change in the properties of metals may prove quite generally significant (*vide infra*).

Using an esterase driven cleavage of a SIE, Gale and co-workers have described a very interesting means by which the magnetic properties of a complex can be profoundly changed, from antiferromagnetic to paramagnetic (Scheme 29).<sup>160</sup> A proligand was designed into the  $Fe^{3+}$   $\mu$ -oxo-bridged dimer complex **128** that, upon exposure to a porcine liver esterase, triggered cleavage of the pivalate ester to afford **129**; concomi-



Scheme 27 Comparative rates of fragmentation of modified, aromatic self-immolative linkers **122–124**.<sup>158</sup>





**Scheme 28** The self-immolative electronic cascade process to permit signal transduction and amplification via an enzymatically triggered ligand release from the polyligand system **125** and accelerated catalysis process.<sup>159</sup>



**Scheme 29** Gale's porcine liver esterase sensitive SIE that drives conversion of an antiferromagnetic complex **128** into a paramagnetic complex **131**.<sup>160</sup>

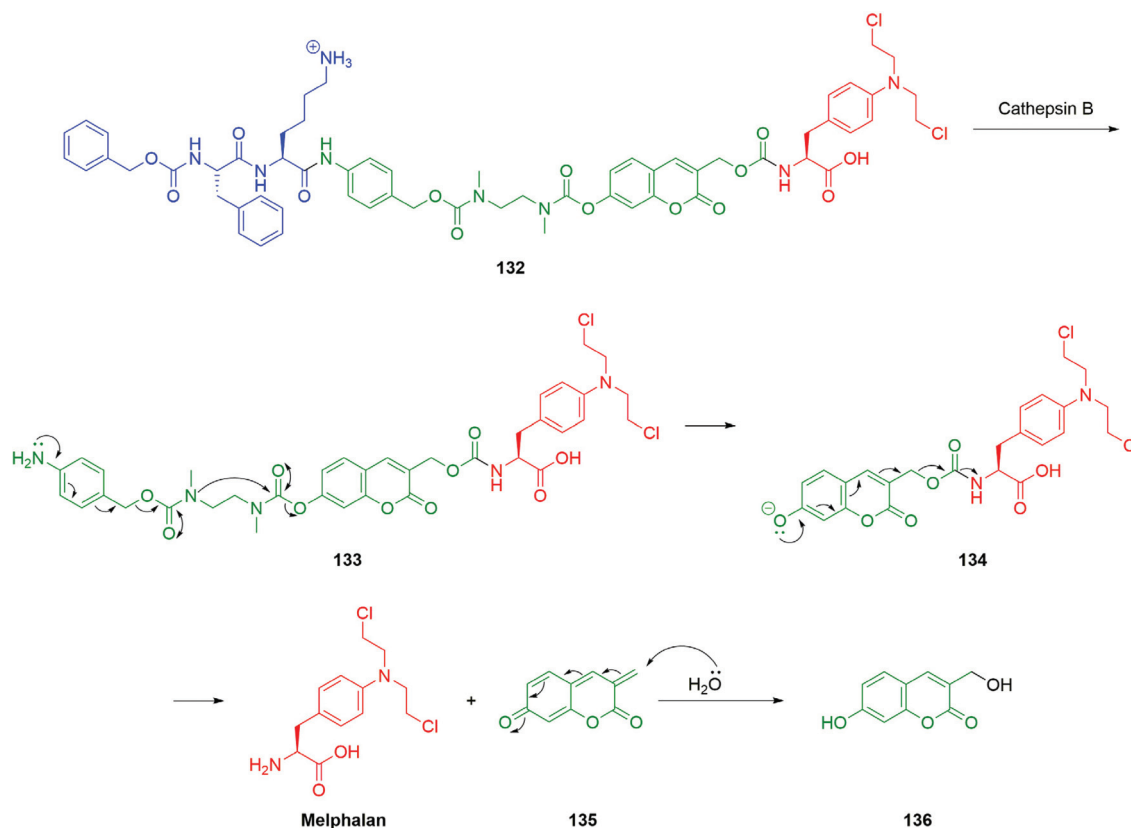


tant 1,6-elimination gave **130**. The facility with which elimination of the phenol occurs probably reflects the predominantly aqueous solution in which the reaction takes place, as noted by Phillips (*vide supra*).<sup>49</sup> By bonding of the newly generated phenolic ligand in **130** it spontaneously splits into two equivalents of a monomeric, distorted octahedral, high-spin  $\text{Fe}^{3+}$  complex **131** that displays paramagnetic properties. This change in magnetic properties can support, *inter alia*, magnetic resonance imaging experiments.

An alternative approach to the targeted delivery of nitrogen mustards to that described by Peng and co-workers (Scheme 9) has been reported by Shabat *et al.* An elegant prodrug system based on a 7-hydroxycoumarin fluorophore-linker was developed which allowed for an efficient 1,8-elimination cascade (Scheme 30).<sup>161</sup> The success of a 1,8-elimination across a coumarin mirrors that across cinnamyl alcohol systems but contrasts with that attempted across a naphthalene ring system.<sup>162,163</sup> The prodrug **132** was comprised of a dipeptide, Z-Phe-Lys, the 4-aminobenzyl alcohol linker, an ethylenediamine-derived cyclisation spacer, coumarin-based fluorophore-linker and the anticancer agent, melphalan. Exposure of the prodrug **132** to cathepsin B, an enzyme found in elevated levels in cancer cells and tumour endothelial cells, resulted in cleavage of the trigger group to reveal the aniline moiety **133** capable of 1,6-elimination to yield a secondary amine that in

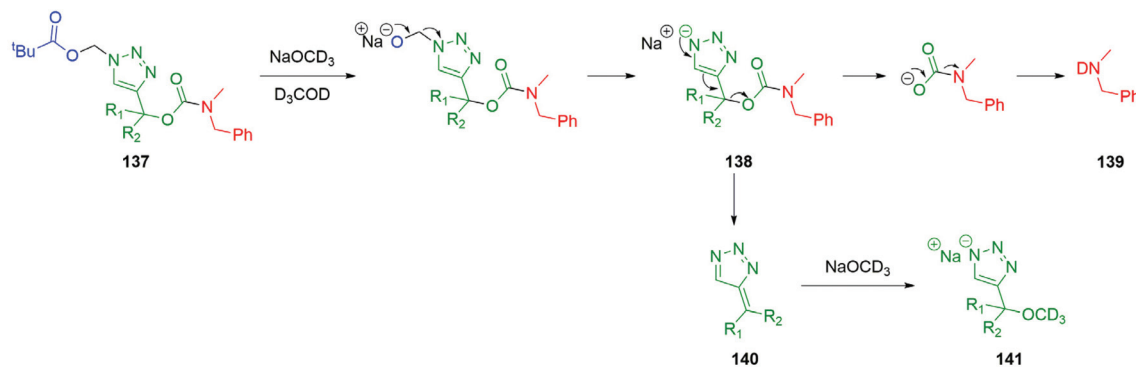
turn cyclises to afford a urea and the free ionised hydroxycoumarin species **134**. The phenolate species **134** fragmented *via* a 1,8-elimination process, resulting in the release of melphalan and the coumarin-quinone-methide **135**, which is then subject to hydration in the aqueous medium to afford the highly fluorescent coumarin derivative **136**. This design facilitates monitoring of fragmentation by fluorescence.

Inspired by the work of Bertrand and Gesson on acid sensitive triazolymethylcarbamate linkers,<sup>164</sup> Blencowe *et al.*<sup>165</sup> demonstrated the base sensitivity of triazolymethylcarbamate self-immolative systems **137**, capable of a 1,4-elimination cascade with a pivaloyloxymethyl (POM) trigger (Scheme 31). It was highlighted that the rate of self-immolative elimination was tuneable by the degree and nature of substitution at the triazole  $\alpha$ -methine position ( $\text{R}_1$  and  $\text{R}_2$ ), with the fastest rate of self-immolation when  $\text{R}_1$  and  $\text{R}_2$  were *gem*-dimethyl groups. Self-immolation was triggered in a mixture of  $\text{NaOCD}_3$  and  $\text{MeOD}_3$  with formaldehyde generated as a by-product, affording the triazole anion **138**. Under these experimental conditions, the triazole anion **138** initiates a 1,4-elimination to allow for release of the carbamic anion which subsequently underwent a decarboxylation event resulting in the formation of the deuterated benzylamine **139**. The so-formed triazafulvene **140** was trapped by excess base to afford **141**. Acid



**Scheme 30** Melphalan release upon exposure of prodrug **132** to cathepsin B featuring 7-hydroxycoumarin fluorophore-linker as reported by Shabat and co-workers.<sup>161</sup>





**Scheme 31** Base mediated disassembly of self-immolative triazole **137** via 1,4-elimination reported by Blencowe *et al.*<sup>165</sup>

mediated degradation of polymer bonded triazoles have also been described.<sup>166</sup>

Roberts and Stevens further developed the 1,2,3-triazolyl-based self-immolative scaffold to afford a dynamic, pH sensitive switch that allows controlled delivery of the reporter group. A double linker system was prepared that combined the triazole moiety with a 1,2-diamine cyclisation stage to facilitate the use of carbamate trigger moieties.<sup>48</sup> Removal of the trigger from **142** with a Pd(0) catalyst and morpholine as stoichiometric nucleophile yielded the free amine **143**. Cyclization to a urea, with concomitant elimination of formaldehyde, gave triazolide anion **144**. The triazolide anion then underwent a pH dependent 1,4-elimination; under basic conditions, release the

reporter moiety together with carbon dioxide and triazafulvene **140** occurred. In turn, **140** undergoes a Michael addition with the excess morpholine to give **145** (Scheme 32). Alternatively, upon the addition of acid, the triazolide anion protonates, thus pausing the self-immolation. Treatment with base was observed to restart the paused 1,4-elimination. The 1,4-elimination was found to be faster in the presence of D<sub>2</sub>O, in accord with other fragmentations discussed above.

Subsequently, the authors have applied this methodology to 'click' their self-immolative unit to a polymer with pendant alkyne groups in order to develop a material with tuneable properties.<sup>167</sup> Further work, with Gillies, has seen the method used to effect post-polymerisation modification of self-immolative



**Scheme 32** Dynamic pH responsive self-immolative triazole **142** with an ethylenediamine linker permitting the use of carbamate trigger groups as described by Roberts and Stevens.<sup>48</sup>



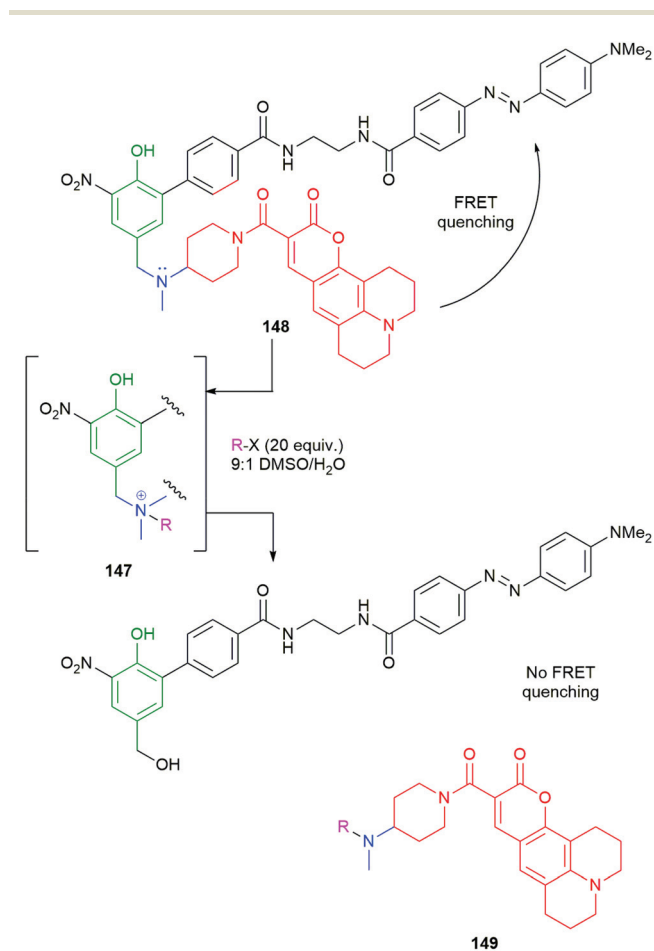
lative polymers (SIPs), allowing depolymerisation<sup>168</sup> under selective conditions *e.g.* Pd(0) catalysts or UV light (365 nm) *e.g.* **146**, for related SIPs, see section 4.4.

The effectiveness of ammonium ions as leaving groups in self-immolative processes has been exemplified in drug deliv-

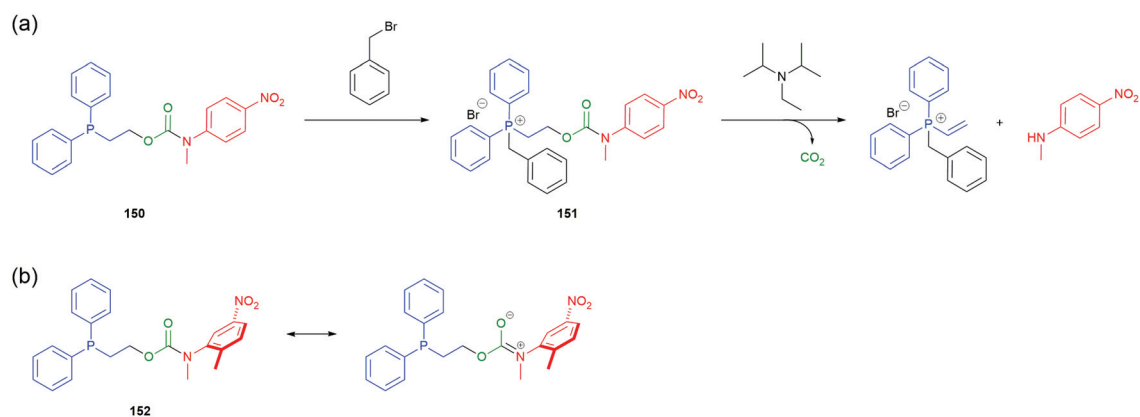
ery by Peng, using hydrogen peroxide triggering (Scheme 9).<sup>91–93</sup> Pillow *et al.* have used both glutathione and enzymatic triggering to release drugs, in ammonium ion form, from antibody–drug conjugates.<sup>94</sup> By contrast, Taran and Le Gall have used the generation of an ammonium ion (**147**) by alkylation of **148** as a means of triggering its self-immolative fragmentation (Scheme 33).<sup>9</sup> By this means, the FRET quenching apparent in **148** is removed in **149**, allowing quantitative detection of a variety of alkylating agents by fluorescence upon excitation of coumarin **149** at 365 nm. This method is particularly interesting as one of the early examples of an electrophilically triggered SIE and, as with Seitz's iMB, has the rare property that the reporter group and trigger are in the same moiety. The self-immolative linker features an *ortho*-nitrophenol, to enhance the acidity of the phenolic OH; an alternative role for the nitro group, in enzyme catalysed reactions, was discussed by Hou and co-workers (Scheme 18).<sup>136</sup>

The utility of the related iminium ions, as leaving groups in SIEs, has also been used in an elegant DNA ‘walking’ mechanism of a 2,6-disubstituted phenol system by Fakhiri and Rokita (see section 3).<sup>53</sup>

Acton *et al.* reported a self-immolative system triggered by non-acidic electrophilic species such as methyl, allyl and benzylic halides.<sup>8</sup> Inspired by work from Kunz<sup>169</sup> and Verducci,<sup>170</sup> 2-(diphenylphosphino)ethyl group (DPPE) was conjugated with *N*-methyl-4-nitroaniline *via* a carbamate to afford **150** (Scheme 34). Subjecting phosphine **150** to a Type II S<sub>N</sub>2 alkylation resulted in formation of the corresponding phosphonium salt **151**, thus increasing the acidity of the  $\alpha$ -methylene protons and activating the trigger towards base mediated elimination. Addition of *N,N*-diisopropylethylamine (DIPEA) to a solution of **151** in acetonitrile led to 1,2-elimination, releasing the nitroaniline reporter moiety, confirmed visually by the distinct yellow colour of the solution (Scheme 34). A one-pot procedure proved equally effective. Recent optimisation studies by Gavriel *et al.*, to probe both electronic and steric effects of the reporter unit, identified the self-immolative system **152** as the best balance of stability and reactivity.<sup>171</sup>



**Scheme 33** Taran and LeGall's FRET-based detection system **148** for electrophilic alkylating agents.<sup>9</sup>



**Scheme 34** (a) Self-immolative system **150** for disclosure of electrophilic alkylating agents, as described by Acton *et al.*,<sup>8</sup> (b) optimisation of **150** to afford compound **152**.<sup>171</sup>



Bradley and co-workers have recently adapted a self-immolative electronic cascade process, that affords a quinone methide intermediate, to give an elegant protecting group strategy and demonstrated its application to solid-phase peptide synthesis.<sup>155</sup> In this approach, the side chain amine of a lysine residue is protected in the form of a modified benzylic carbamate that uses a 4-demethoxyveratryl alcohol unit that bears a *para*-vinyl ether (referred to as the vinyl ether benzyloxycarbonyl (VeZ) protecting group), for example **153** (Scheme 35). The vinyl unit of the VeZ protecting group allows a thermally induced triggering event that is orthogonal to the standard range of protecting groups used in peptide synthesis. Thus, treatment of **153** with tetrazine **154**, induces a tandem inverse electron-demand Diels–Alder reaction, retro-Diels–Alder affording, after tautomerism, **155**. An eliminative rearomatization released the linker–reporter unit **156**; indeed, this elimination could be regarded as an additional linker unit (*vide infra*).<sup>172,173</sup> The stability of **156** proved condition dependent, with isolation being possible.

Consistent with Phillips' observations on the fragmentation of phenolic systems (Fig. 2),<sup>49</sup> plus those of Roberts and Stevens<sup>48</sup> on the fragmentation of triazole carbamate systems (Scheme 32), an increase in the percentage of water in the solvent assisted the rate 1,6-elimination of **156**. Thus, the reaction conditions of 50% water/DMF mixture (buffered to pH 5 using sodium citrate), in conjunction with exposure to microwave radiation, allowed for an accelerated Diels–Alder reaction and a facile self-immolative deprotection step: these con-

ditions could be employed when generating peptides on solid-supports (Scheme 36). Fmoc-Lys(VeZ)-OH was applied to the synthesis of two cyclic peptides, melanotan II (MTII) and a constrained BAD BH3 peptide analogue – both of which are examples of side-chain to side-chain lactam-bridge peptides. Additionally, the approach has proved effective at drug release from prodrug systems.<sup>174</sup>

The use of thermal triggering of SIE systems, using Diels–Alder reactions, has also proved advantageous in SIE polymer systems (see section 4.4).<sup>175</sup>

The method has proved effective at release of doxorubicin (for its structure see Schemes 22 and 39) from an amphiphilic methyl methacrylate/PEG copolymer **157** in HEK273 T and PC3 cells (Scheme 37).<sup>176</sup> In view of the vinyl ether unit, the polymer was best prepared by RAFT. When in water, the copolymer formed nanoparticles of 35 nm diameter with PEG at the surface and four doxorubicin moieties in the hydrophobic core.

This work was developed from reports of effective bioconjugation and protein activation of tetrazines with *trans*-cyclooctene derivatives.<sup>177–179</sup> Robillard developed this facile ligation method into an interesting self-immolative method termed 'click to release' (Scheme 38).<sup>180</sup> Of particular interest is the innovative way that the triggering event simultaneously completes construction of a self-immolative unit. The nature of the R group on the tetrazines, *e.g.* **158–159** being found to exert a significant effect of its rate of reaction, alkyl substituents enhancing reactivity over their aromatic counterparts. Thus,

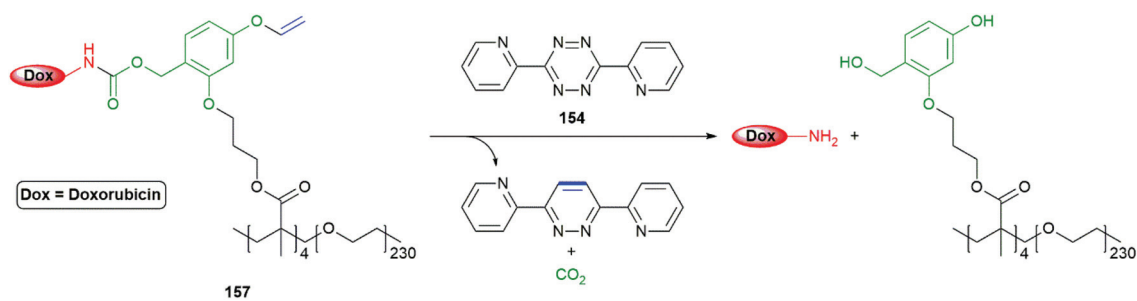


**Scheme 35** The thermally induced cleavage of the trigger moiety of the vinyl ether benzyloxycarbonyl (VeZ) protecting group on **153** with tetrazine **154** reported by Bradley and co-workers.<sup>155</sup>





**Scheme 36** Fragmentation of the conjugate base of SIE linker **156** and a target peptide melanotan II.<sup>155</sup>



**Scheme 37** VeZ protecting group methodology adapted to controlled release of doxorubicin from an amphiphilic copolymer, initiated by biocompatible tetrazine **157**.<sup>176</sup>



**Scheme 38** 'Click to release' reaction of tetrazines with *trans*-cyclooctenes **160** and **165**.<sup>180</sup>



*trans*-cyclooctene **160** (X = O) undergoes the previously discussed tandem inverse electron-demand Diels–Alder reaction, retro-Diels–Alder, under physiologically compatible conditions, affording **161**. Dihydropyridazine **161** undergoes tautomerism to give **162**, completing the self-immolative unit. Once formed, **162** undergoes 1,4-elimination to release the reporter group (a detailed analysis of this process was reported), CO<sub>2</sub> and **163** that, in turn, isomerises to aromatic pyridazine **164**. The significance of water in the reaction medium was again noted.

For the case when X = S, Pluth has cleverly adapted the approach to delivery of COS, mediated by tetrazine **159**, and thence by catalysis with carbonic anhydrase to gasotransmitter H<sub>2</sub>S.<sup>111</sup>

The use of the *trans*-cyclooctene-based methodology has also been adapted to the release of oxygen-connected reporter groups by inserting an aniline-based linker and exemplified by preparation of the Triclosan donor **165** by Bernardes (Scheme 38).<sup>181</sup> Release of this antibacterial agent was demonstrated within live *E-Coli* cells by reaction with tetrazine **166**: restoration of triclosan's activity was observed.

Further, Robillard has substituted the benzylamine reporter group in **160** for doxorubicin in **167** and demonstrated its release in A431 cell culture upon treatment with **158**, as well as noting the method's potential for use in antibody drug conjugates (Scheme 39).<sup>180</sup> The delivery of doxorubicin by this approach has been further extended by Mejia Oneto *et al.* to target soft tissue sarcoma by using an injectable polymeric reagent **168**; specifically, an alginate hydrogel modified with tetrazines (Scheme 39).<sup>182</sup>

Further impressive advances in the application of *trans*-cyclooctene, tetrazine methodology in the anticancer area have

been published.<sup>183,184</sup> Very recently, Fan and Chen have reported a novel approach to on-demand pyroptosis *via* tetrazine mediated activation of a cytosine base editor, blocked by a *trans*-cyclooctene.<sup>185</sup>

An interesting variation on the method is the use of a 1,3-dipolar cycloaddition of an aromatic azide *e.g.* hydrogelator **169** to a *trans*-cyclooctene **170** to give an unstable adduct **171** that fragments to diazonium species **172** with concomitant ring contraction to deliver, after hydrolysis, an aniline **173** (Scheme 40). This aniline undergoes 1,6-elimination to yield dipeptide **174**; in so doing, a gel–sol transition takes place raising the potential of such systems to be employed in *inter alia* a drug delivery role *e.g.* for doxorubicin.<sup>186</sup> This reaction has also proved successful in prodrug systems *e.g.* for doxorubicin and profluorescence compounds.<sup>187,188</sup> Such a change of physical properties of a gelator has also been used as part of a dendritic chain reaction (see section 3.3).

Reduction of azides to initiate 1,6-elimination and targeted release of reporters by cyclisation–elimination, triggered by saccharide azides, has also been achieved by Staudinger reduction.<sup>189,190</sup>

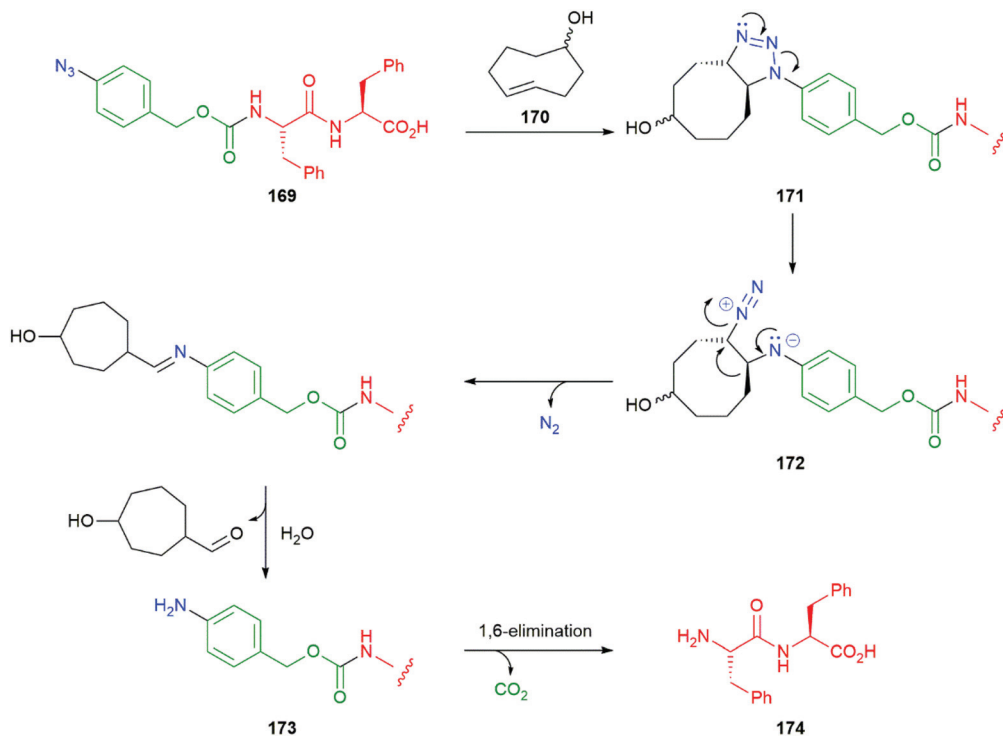
Alternative reactive alkenes have also been used in ‘click to release’ reactions of tetrazenes; for example, Franzini has demonstrated the effectiveness of 7-oxa/azabenzonbornadienes *e.g.* **175** (Scheme 41).<sup>191,192</sup>

Developing work by Imming *et al.* and Leeper *et al.*, Franzini has also reported a distinctive method for dual reporter group release from a combination of tetrazines and isonitriles and found this to work *in vivo*, using zebra fish embryos (Scheme 41).<sup>193–196</sup> The capacity for dual release offers an interesting alternative to the use of dendrons and can be used,



Scheme 39 'Click to release' of doxorubicin system **167**, modified with *trans*-cyclooctene, by tetrazines **158** or **168**.<sup>180,182</sup>





**Scheme 40** 1,3-Dipolar cycloaddition of **169** to a *trans*-cyclooctene **170** triggers a gel-sol transition.<sup>186</sup>



**Scheme 41** Franzini's isonitrile and norbornadiene triggered release systems from and with tetrazines.<sup>191–194</sup>

for example, to deliver two different, synergistic drugs, in therapeutic applications or to release two distinct fluorescent molecules (see pro-fluorescent **176** and **177**). Thus, treatment

of tetrazines **178** with isonitriles **179** results in a tandem cheletropic reaction, retro-[4 $\pi$  + 2 $\pi$ ] cycloaddition to afford pyrazole **180**. Hydrolysis of **180** liberates aldehyde **181** that undergoes



$\beta$ -elimination to deliver one reporter group; whereas, **182** undergoes 1,4-elimination to give the second reporter group.

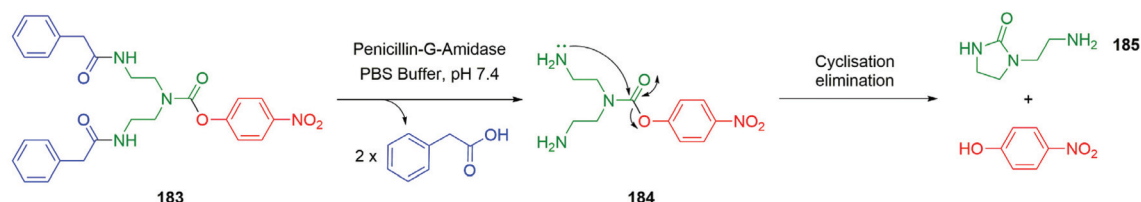
Related results have been reported for release of sulfonamide groups by Houk and Liang using cycloaddition of sydnoimines onto the strained alkyne, dibenzoazacyclooctyne. An orthogonality of delivery was noted between this system and the benzonorbornadiene-terazine system of type **175**, mentioned above.<sup>197</sup>

## 2.2 Self-immolation via cyclization elimination

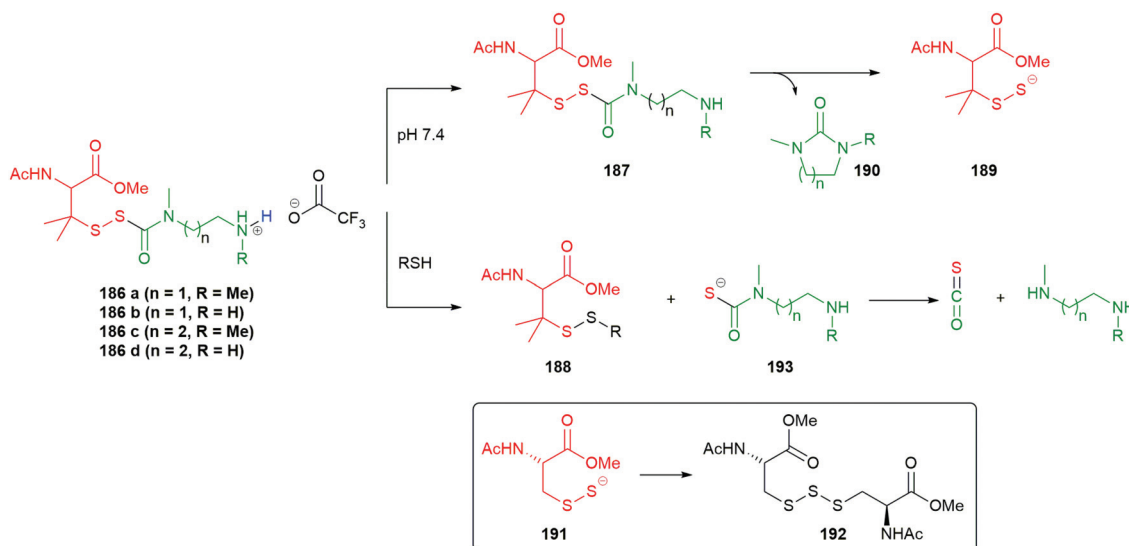
Self-immolative linkers that utilize cyclization for disassembly *via* activation of a latent nucleophile (*e.g.* amine,<sup>198</sup> phenol,<sup>199</sup> and thiol groups<sup>200,201</sup>) followed by an intramolecular *exo-trig* type cyclization mechanism are driven by (i) an increase in entropy coupled with (ii) the irreversible formation of thermodynamically stable products (*e.g.* CO<sub>2</sub>). For example, this degradation pathway was demonstrated by Amir and Shabat with the release of *para*-nitrophenol from a first-generation diethylene tri-amine-based dendron **183** (Scheme 42) using ethylenediamine as the linker.<sup>202</sup> The amide linkage is stable under physiological conditions; however, the selection of the amide side chain of penicillin G affords an elegant solution for mild cleavage of an otherwise stable functional group. Thus, cleavage of the two trigger groups by the enzyme penicillin-G-

amidase affords the nucleophilic amine species **184** that participates in a favourable 5-*exo-trig*-cyclisation to liberate *para*-nitrophenol (the reporter unit in this model study) with concomitant formation of imidazolidinone **185**. The cyclisation-elimination approach to self-immolative linkers, either alone or in tandem with other linker types, has been applied in a number of ways in recent years and below we illustrate some of these.

The biological significance of controlled release of COS/H<sub>2</sub>S and persulfides has been discussed above (Schemes 13, 14, 16, 38 and Fig. 5–7). Additionally, Toscano notes the recent discovery of the use of tRNA bound Cys-SSH in protein synthesis.<sup>100</sup> Toscano and co-workers have thus prepared a range of self-immolative molecules of which compounds **186a–d** were found to be effective for persulfide or COS/H<sub>2</sub>S delivery (Scheme 43). They are triggered by deprotonation of its terminal nitrogen, at physiological pH, to give free amines **187** or by nucleophilic attack by thiols to give persulfides **188** and thence COS/H<sub>2</sub>S. The predictable cyclisation rate (pH dependent) of the linker affords a suitable release profile for hydropersulfide **189**, with ureas **190** as by-product. The rate of release of the persulfide **189** is slowed at lower pH, or with the absence of a terminal methyl group (**186b** and **186d**) or a longer linker (**186c–d**). The steric bulk presented by the *gem*-



Scheme 42 Penicillin-G-Amidase triggered self-immolative system **183** featuring a cyclisation linker as described by Shabat and co-workers.<sup>202</sup>



Scheme 43 The pH/thiol triggered SIEs **186** for release of a hydropersulfide **189** or COS/H<sub>2</sub>S reported by Toscano and co-workers.<sup>100</sup>

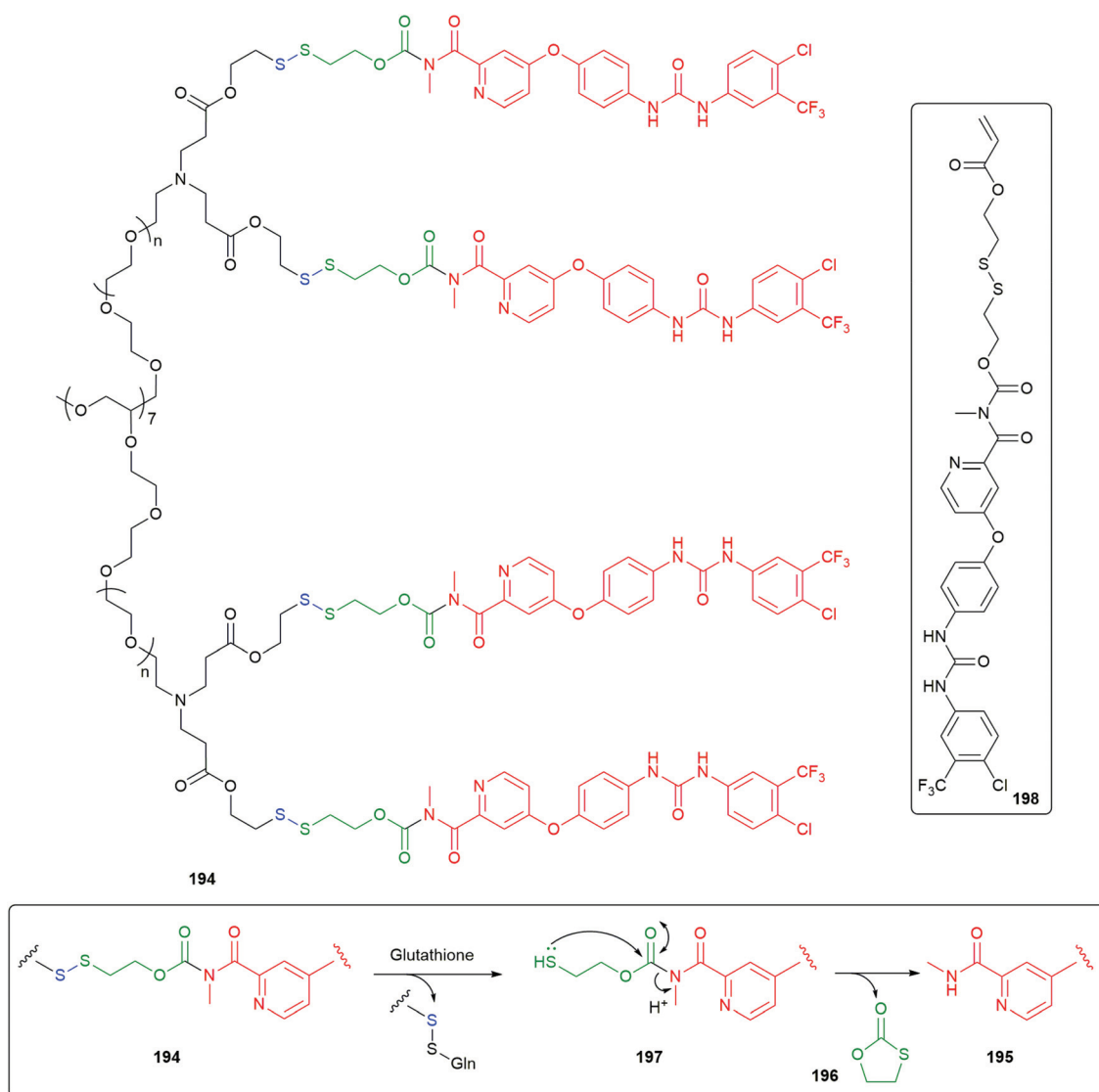


dimethyl group in the *N*-acetyl penicillamine unit of **186** is significant. The analogue of **186** derived from *N*-acetylcysteine methyl ester releases hydropersulfide anion **191** that reattacks the S-S bond of the starting material to deliver trisulfide **192** as a significant by-product. In the presence of thiols, in competition with cyclisation to cyclic ureas **190**, attack on the persulfides **186** occurs to give **188** and **193**, and thence release of COS, with subsequent hydrolysis, catalysed by carbonic anhydrase, to deliver H<sub>2</sub>S (see also Scheme 13). Though a minimal pathway with **186a**, slower cyclising compounds *e.g.* **186c–d** led to this becoming a major pathway. Thus, linker design is crucial to achieving a desired mode of action. In addition, **188** also reacts with *N*-acetylcysteine to afford polysulfides. Artaud and Galardon have also described a pH sensitive persulfide donor molecule based on penicillamine.<sup>203</sup>

The cleavage of disulfide bonds in **194** by cellular thiols has been described by Feng and co-workers as means of controlled release of sorafenib **195** *via* a cyclisation–elimination event to

yield 1,3-oxathiolan-2-one **196** as the by-product *via* the thiol intermediate **197** (Scheme 44).<sup>204</sup> The drug release system **194** was prepared from multi-armed PEG-NH<sub>2</sub> adding to acrylate **198** to deliver an amphiphilic polymer that exhibited good aqueous solubility and self-assembled into micellar-like nanoparticles (hydrodynamic diameter *ca.* 150 nm). Sorafenib could be released *in vitro* by treatment with dithiothreitol. Dose dependent cytotoxicity was observed toward HeLa and HepG2 cells, with evidence for improved intracellular localization; in addition, *in vivo* activity was reported. A similar cyclisation–elimination, but onto a carbonate group, was reported by Low for the delivery of camptothecin.<sup>205</sup>

As part of their studies on traceless linkers to quaternary ammonium ions, Pillow *et al.* have used a glutathione sensitive persulfide trigger to initiate a tandem cyclisation–elimination, 1,6-elimination sequence to release tubulysin from tripartite antibody–linker–drug conjugate **199** *in vitro* (Fig. 12).<sup>94</sup>



**Scheme 44** The PEG-based SIE **194** for intracellular delivery of sorafenib as described by Feng and co-workers.<sup>204</sup>





Fig. 12 Pillow's glutathione triggered antibody-double linker-drug conjugate **199**.<sup>94</sup>

Perez has developed a SIE that combines targeting of doxorubicin delivery with a folate unit and a cyclisation-elimination linker that was triggered by intracellular cleavage of a persulfide bond to release the drug.<sup>206</sup>

The ethylenediamine-carbamate module has been shown to be highly versatile, and has been used in combination with self-immolative triggers that are activated upon the application of different stimuli (*e.g.* enzymatic action,<sup>64,201,207</sup> irradiation with UV,<sup>208</sup> or near-infrared light<sup>209</sup>). However, as noted by Dal Corso, Gennari and co-workers, the cyclisation can prove to be rate-limiting and ultimately affect prodrugs' therapeutic efficacy.<sup>210</sup> In 2020, Dal Corso and Gennari proposed a suitable modification of the ethylenediamine-carbamate resulting in a proline-derived self-immolative linker with an enhanced rate of cyclisation whilst retaining the desirable features of the ethylenediamine linker (Scheme 45).<sup>210</sup> The reactivity of the proline-derived linker in **200** was compared directly to the ethylenediamine linker in **201** in their trifluoroacetic acid (TFA)-salt pro-drug forms. The half-life for cyclisation of **201** was 10.6 hours; whereas, **200** was found to release the reporter moiety with a half-life of only 1.6 hours. In this system, the cyclic amine attacks the carbamate connected to the exocyclic amine thus forming a bicyclic urea.

Subsequently, this was extended to a trifunctional linker system **202** which functions by non-sequential, dual activation wherein the presence of a protease enzyme, though sufficient to remove the dipeptide trigger, with concomitant 1,6-elimination to give **203**, is insufficient to give rapid cyclisation to release the camptothecin reporter group (Scheme 46).<sup>39</sup> This is thought to arise because of extensive protonation of the proline-derived amine, preventing its nucleophilic cyclisation

onto the carbamate in **203**. By contrast, the combined presence of both a protease and a phosphatase converts **202** into **204** which undergoes rapid cyclisation-elimination forming bicyclic urea **205** and releasing the reporter group. This nuanced approach allows for the general idea of selecting for environments in which two analytes must be present *e.g.* a cell type that contains two enzymes; this should allow for more selective targeting of a reporter group.

In a related study, the rates of cyclisation of variously substituted 4-aminobutyric acids were examined by Gillies as potential self-immolative linkers.<sup>211</sup>

Schermann has developed a number of drug delivery systems, based around a cyanine caging group, of which the antibody-cyanine-drug conjugate **206** serves as an example (Scheme 47). These are triggered by irradiation with near-IR light (780 nm), affording good tissue penetration of the light and lower risk of tissue damage than UV radiation.<sup>212–216</sup> Formation of singlet oxygen allows cleavage of the indicated double bonds *via* the corresponding dioxetanes **207**. Once cleaved to compounds **208** and **209**, the enamine moiety becomes susceptible to hydrolysis releasing self-immolative linker-reporter unit **210** that undergoes cyclisation-elimination to afford cyclic urea **211** and release of the duocarmycin reporter group. It should be noted that these systems also allow for fluorescence monitoring of the systems distribution *in vivo*.

The *E/Z*-isomerism of *ortho*-hydroxycinnamates of type **212** leads to spontaneous cyclisation from **213** to coumarin **214** with release of the reporter group (Scheme 48). Such self-immolation may be regarded as an example of a reagentless form of activation in that no formal trigger group is present



Scheme 45 The proline-derived self-immolative linker in **200** as described by Dal Corso and Gennari *et al.*<sup>210</sup>





Scheme 46 Dal Corso and Gennari's dual triggered SIE for camptothecin delivery **202**.<sup>39</sup>



Scheme 47 Schnermann's near-IR triggered drug delivery system **206** for duocarmycin.<sup>213</sup>



Scheme 48 Drug delivery platforms **215** and **216** based around photoisomerism of cinnamate linkers.<sup>217,218</sup>



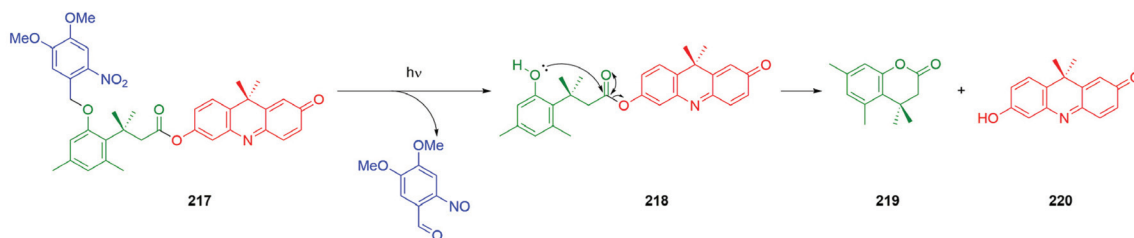
and the only 'reagent' is a UV or near IR two-photon excitation. However, this approach does allow for double targeting, as exemplified by Wang and Zhang's theranostic pro-prodrug **215** where reduction of the aromatic nitro group by nitroreductase directs release toward cells over expressing this enzyme *e.g.* hypoxic solid tumours, after which external irradiation (365 nm) effects *E/Z* isomerism and release of the gemcitabine reporter group.<sup>217</sup> Concomitant with this is formation of a strongly fluorescent coumarin reporter from the self-immolative linker. A related double activation strategy has also been exemplified by Zeng and Wu (see Scheme 52).

Sasmal *et al.* have recently reported drug delivery platform **216** based upon a key cinnamate photoactivation.<sup>218</sup> In the same way as Mosey and Floreancig (Scheme 7), Sasmal *et al.* have employed Murphy's triphenylphosphonium directing group to target the mitochondria of the relevant cell type, and the success of this approach was evident in the fluorescence microscopy studies following treatment of HeLa cells with **216** (92% of cellular uptake into the mitochondria within 2 h). Use of one (365 nm) or two-photon irradiation (700 nm)<sup>219</sup> of **216** proved successful in releasing the doxorubicin reporter group.

An alternative platform for effective intramolecular cyclisation systems have been realised by the trimethyl-lock linkers,

these take advantage of a Thorpe–Ingold effect in tandem with repulsion from an adjacent aromatic methyl group: recently, these have been thoroughly reviewed by Klahn.<sup>220–223</sup> Jullien and Schmidt have reported valuable kinetic data of their rates of cyclisation, utilising a photoactivatable self-immolative system **217** that, upon trigger activation, results in a 6-*exo-trig*-cyclisation (**218**), favoured by steric hindrance, resulting in lactonization of the linker to give **219** in *ca.* 3 minutes liberating the fluorescent reporter **220** (Scheme 49).<sup>199</sup> This sterically induced effect occurs on account of the unfavourable interactions between the methyl residue at the *meta*-position on the phenolic core and *geminal* methyl groups at the benzylic position of the alkyl chain. Further data is reported on a phenol-carbamate cyclisation linker. They note the general point that cyclisation-based linkers tend to self-immolate less rapidly than elimination-based linkers.

Wang and co-workers have used the trimethyl-lock linker as an esterase-triggered source of the gasotransmitter H<sub>2</sub>S (Scheme 50).<sup>224</sup> Treatment of **221a–b** with porcine liver esterase gives rapid cleavage of the trigger group. The resultant phenol **222** undergoes facile cyclisation, possibly following protonation to the thioacid, to give  $\delta$ -lactone **219** and the reporter group, H<sub>2</sub>S. By variation of the ester group, the rate of



**Scheme 49** Near-UV triggered self-immolative system **217** capable of undergoing a trimethyl-lock accelerated cyclisation event resulting in the release of a fluorescent reporter moiety as described by Jullien, Schmidt and co-workers.<sup>199</sup>



**Scheme 50** The esterase/alkaline phosphatase triggered trimethyl-lock linker for controlled release of H<sub>2</sub>S and H<sub>2</sub>S<sub>2</sub> reported by Wang, Zheng and co-workers.<sup>224,225</sup>





**Scheme 51** Cheng's DT-diaphorase triggered SIE **225** for release of *N*-azidoacetylmannosamine.<sup>226</sup>

hydrolysis could be tuned (**221a**  $t_{1/2}$   $13.0 \pm 2.4$ ; **221b**  $t_{1/2}$   $28.7 \pm 1.5$ ). Additionally, the absence of the aromatic methyl groups could significantly slow the rate of the cyclisation reaction. Together these allow variation in the rate of delivery of the  $H_2S$  gasotransmitter. Zheng and Wang have also modified this approach to deliver hydrogen persulfide using **223a–b** (Scheme 50).<sup>225</sup> By altering the trigger group to a phosphate in **224**, triggering can occur using alkaline phosphatase.

By coupling the ability of some 1,4-benzoquinones to function as substrates for DT-diaphorase, being reduced to the corresponding hydroquinone, a combined trigger–linker of the trimethyl-lock type has been used by Cheng as part of a delivery system **225** for *N*-azidoacetylmannosamine (Scheme 51).<sup>226</sup> The trigger–linker and reporter group are connected by a second, *N,N'*-dimethylethylene diamine, linker; this linker was established to give negligible non-specific hydrolysis. Thus, following reduction of **225** by DT-diaphorase, **226** undergoes cyclisation to eliminate  $\delta$ -lactone **227**. The *N,N'*-dimethylethylene diamine linker in **228** then cyclises to urea **190** to deliver *N*-azidoacetylmannosamine **229**; the latter is known to be incorporated into cell surface saccharides, offering a partner for subsequent 'click' chemistry modifications. The overexpression of DT-diaphorase in multiple cancer cell lines makes this of particular interest in the study of cancer biology; for example, **225** was shown to deliver **229** in Bxps-3 cells (pancreatic cancer cells).

In 2015, Zeng and Wu used the combined trigger–linker of the trimethyl-lock type with an aniline-based 1,6-elimination linker to give a camptothecin delivery system **230** (Fig. 13).<sup>227</sup> In this system, an additional feature is the ability to self-indicate fragmentation by the loss of fluorescence quenching (photo-induced electron transfer – PeT – from the camptothecin to the quinone). Simultaneously, this also functions as diagnostic for DT-diaphorase activity, with the fluorescence intensity being



**Fig. 13** Zeng and Wu's theranostic SIE **230** for camptothecin delivery.<sup>227</sup>

shown to reflect the levels of the enzyme. This strategy has been adapted to a dendritic platform (see section 3).<sup>228</sup>

In 2018, Wu and Zeng developed a selective methotrexate delivery system **231**, in a liposome carrier; as it requires two triggering stimuli, it may be designated as a pro-prodrug (Scheme 52).<sup>229</sup> First, reduction/cyclisation of the DT-diaphorase sensitive 1,4-benzoquinone trigger/linker in **231** leads to selective cleavage in cells overexpressing that enzyme. Concomitant with this, activation of fluorescence (475 nm) of the coumarin moiety in **232** occurs, facilitating assessment of the enzyme's levels. Subsequent irradiation by one-photon (visible – 400–450 nm) or two-photon (near infrared) light cleaves the coumarin to release the dihydrofolate reductase inhibitor, methotrexate. Critically, in the absence of DT-Diaphorase, cleavage of the coumarin under irradiation at 400–450 nm is blocked. Such double triggering offers the potential of detection and selective cytotoxicity toward cancerous cells overexpressing DT-diaphorase *e.g.* HeLa and A549.





**Scheme 52** Wu and 's pro-prodrug system **231** for selective targeting of cancer cells.<sup>229</sup>

A practically interesting *in vivo* imaging application of the 1,4-benzoquinone trigger/linker has been reported by a collaboration between Kwak, Sessler, Shabat and Kim, utilising an optimised chemiluminescent reporter group described by Sigman and Shabat, comparison was made between the pro-chemiluminescence **233** and pro-fluorescence probes **234** shown in Fig. 14.<sup>230,231</sup> Amongst the advantages attributed to chemiluminescence is good penetration depths into tissue, higher signal-to-noise ratios than fluorescence and reduced interference from autofluorescence. Upon exposure to DT-diaphorase (NQO1), the chemiluminescent probe **233** was observed to rapidly begin emission of green light ( $\leq 90$  s, monitored at 515 nm), undergoing rapid reduction, cyclisation, 1,6-elimination and fragmentation of the dioxetane without an observed intermediate. *In vitro*, this probe was found to differentiate between A549 cells (elevated NQO1 levels) and H596/WI-38 cells (low NQO1 levels). The fluorescence-based probe **234**, developed by McCarley, was also effective;<sup>232,233</sup> however, chemiluminescence was found to deliver a higher signal-to-

noise ratio in reporting on NQO1 activity in A549 cells. *In vivo* imaging of NQO1 activity in A549-tumour-bearing mice, by chemiluminescence, was effective whilst no signal was seen with H596 derived xenografts.

Ji and Miller have developed a self-immolative system **235** for the selective transport of the antibiotic ciprofloxacin into bacterial cells, utilizing the microbial iron acquisition system (Fig. 15).<sup>234</sup> The targeting is achieved by a siderophore (desferrioxamine B) that is attached to a succinate trigger; in turn, this connects to a trimethyl-lock linker and, finally, the reporter group. As a cautionary note, whilst displaying antibiotic activity, it proved less active than ciprofloxacin alone, raising the probability that the enzymatic cleavage of the trigger was inefficient. Linkers were originally introduced to ease the problem of enzyme access to a scissile bond, but here a problem remains.

In an ingenious adaptation of the Julia olefination, Wang and Wang have reported an esterase sensitive prodrug **236** for delivery of the potential gasotransmitter SO<sub>2</sub> (Scheme 53).<sup>235</sup> A

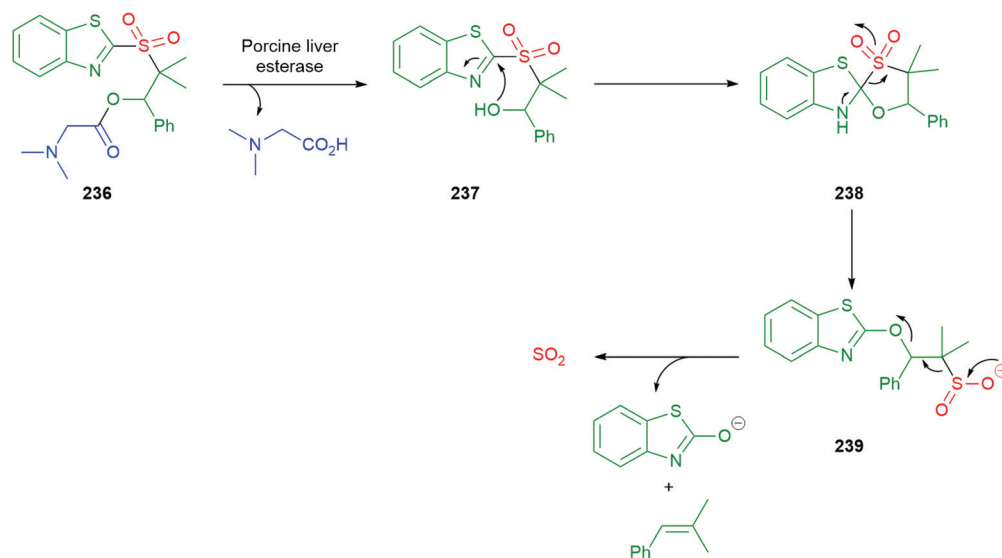


**Fig. 14** Chemiluminescence **233** and fluorescence-based **234** trimethyl-lock linker probes for *in vitro* and *in vivo* imaging of NQO1 activity.<sup>230–233</sup>





Fig. 15 The siderophore directed SIE **235** for delivery of ciprofloxacin reported by Ji and Miller.<sup>234</sup>



Scheme 53 Wang and Wang's esterase triggered  $\text{SO}_2$  release SIE **236** based on a modified Julia reaction.<sup>235</sup>

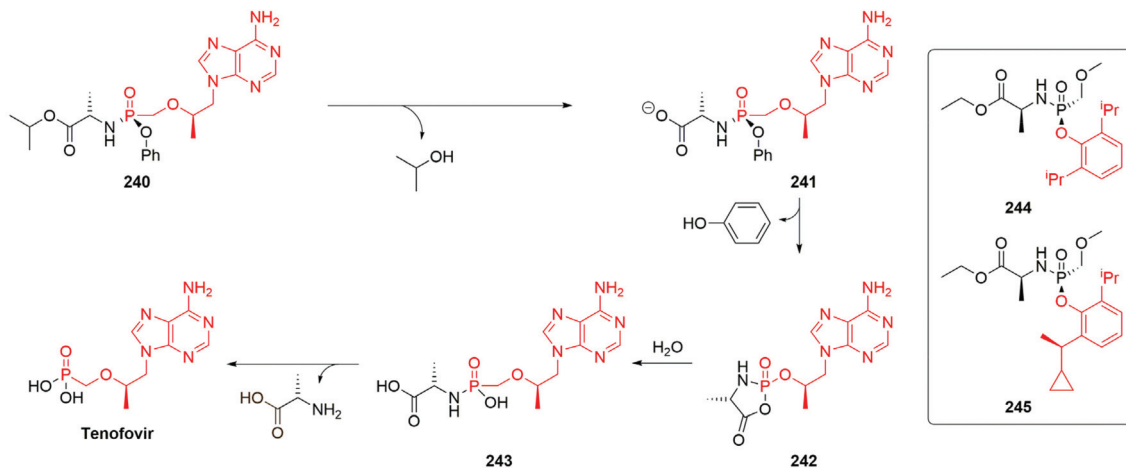
range of molecules related to **236** were prepared, with the glycinate ester shown below facilitating rapid hydrolysis and enhanced aqueous solubility. The substituents on the linker facilitates rearrangement *via* **237** and **238** to give **239**, the *gem*-dimethyl precludes  $\beta$ -elimination of the ester prior to hydrolysis, then, critically, stabilises the antiperiplanar transition state for fragmentation of **239** to release  $\text{SO}_2$ . Compound **236** was shown to release  $\text{SO}_2$  in HeLa cells.

Linkers featuring a phosphate/phosphonate unit have proved to be of significant value, in both the cyclisation–elimination mode and from *para*-aminobenzylalcohol<sup>236</sup> linkers where they may readily replace the role played by carbonates or carbamates in connecting to the reporter group (see Scheme 50 for use as a trigger group). These groups have found an early implementation in prodrugs; for example, they have been employed in the form of ester hydrolysis triggered phosphoramidates for the delivery of tenofovir<sup>237</sup> and Propofol,<sup>238</sup> building upon earlier technology reported by McGuigan *et al.* (Scheme 54).<sup>239–243</sup> Thus, following administration of Tenofovir alafenamide **240**, hydrolysis to carboxylate

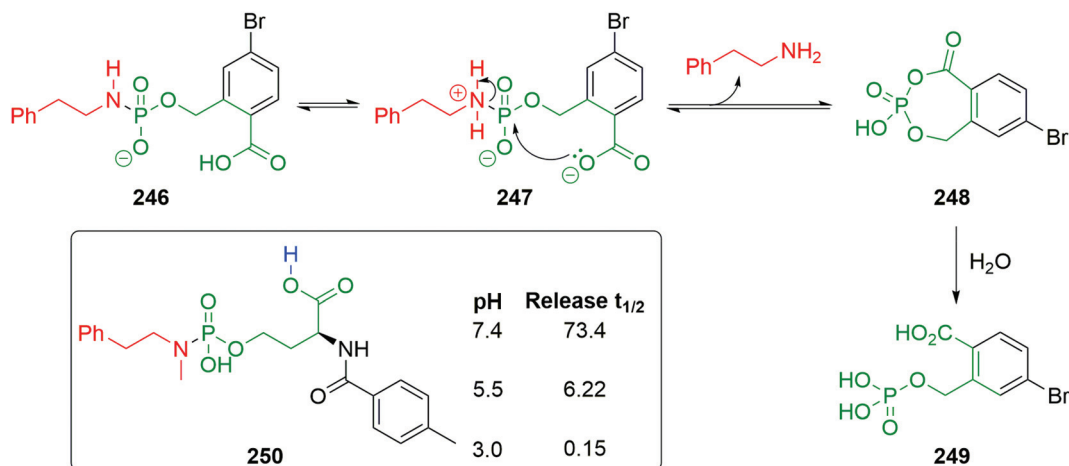
**241** is thought to occur and that spontaneously cyclises to **242**; in turn, this hydrolyses twice to give first **243** then release of the drug Tenofovir (NB the usual colour scheme has been abandoned as trigger, linker and reporter groups overlap). This approach was adapted by Wei *et al.* to give prodrugs **244** and **245** for the phenolic reporter groups Propofol and HSK3486, respectively: compounds with a variety of uses including starting and maintaining anaesthesia. This approach offers a general platform for the delivery of phenolic drugs.

Berkman and co-workers have reported a number of pH triggered phosphoramidate-based systems for the delivery of amines, with general acid catalysis of cleavage of the P–N bond being noted (Scheme 55). The  $\text{pK}_a$  of the amine reporter group was found to be important in determining the rate of hydrolysis.<sup>244</sup>  $^1\text{H}$  and  $^{31}\text{P}$  NMR studies on **246** revealed cleavage of **247** proceeding *via* a two-step mechanism, passing through an acylphosphate intermediate **248** to give **249**.<sup>245</sup> Further work on a series of compounds related to **250** confirmed the importance of the nature of the amine reporter group and established the significance of the carboxylic acid (or other acid





Scheme 54 The release of Tenofovir from prodrug Tenofovir alafenamide **240**.<sup>237,238</sup>



Scheme 55 The pH triggered phosphoramidate-based systems for the delivery of amines reported by Berkman and co-workers.<sup>244–246</sup>

group), its  $pK_a$  and its position relative to the phosphoramidate in labializing the P–N bond.<sup>246</sup> In studies on the rate of hydrolysis of **250**, it was shown to vary significantly over the pH range 3–7.4.<sup>246</sup>

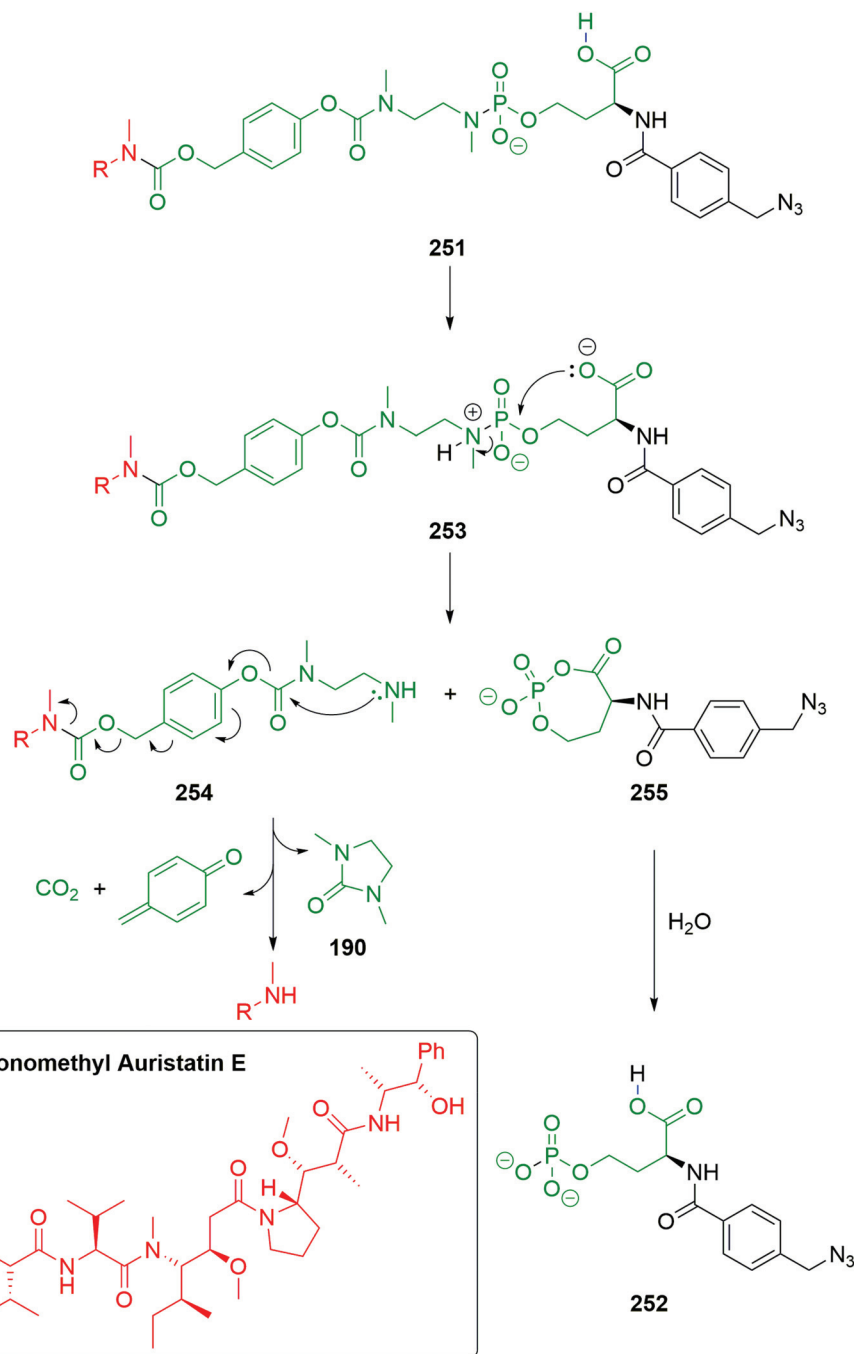
Building upon this work, a SIE **251** for the delivery of the antimetabolic agent monomethyl auristatin E has been reported (Scheme 56).<sup>247</sup> Inclusion of an  $N,N'$ -ethylenediamine cyclisation linker, coupled with a 1,6-elimination linker in **251** achieved consistent rates of hydrolysis, regardless of varying steric hindrance of the reporter group, the proposed mechanism of fragmentation of **251** to yield the antimetabolic agent and the phosphate **252** via intermediates **253–255** is illustrated in Scheme 56. The presence of an azide in **251** makes it adaptable to a number of purposes through ‘click’ chemistry *e.g.* the potential for incorporation into an antibody–drug conjugate. This methodology has also been applied to controlled release of *t*-Dopa.<sup>248</sup>

Recently, Baszczyński and Procházková have described a set of UV light triggered, phosphate-based self-immolative entities that facilitate the release of two reporter groups, exploiting

that particular advantage of using a phosphate over, say, a carbamate (Scheme 57).<sup>249</sup> The release of more than one reporter group has mainly been achieved by the use of dendritic and polymeric systems (*vide infra*) though, for example, Phillips has described an acetal-based system for achieving this (Scheme 9, and Fig. 4). The rate of release from **256** proved tunable by a combination the Thorpe–Ingold effect on the cyclisation step and variation of the  $pK_a$  of the reporter group. The first reporter to be released occurs *via* an SI mechanism (**257** to **258a–b**, then hydrolysis to **259a–b**); whereas, the second release to **260** occurs by direct hydrolysis. Phenols were found to be good leaving groups; whereas, alkanols were retained on the phosphate. A particularly rapid release of phenols was observed when a *gem*-dimethyl group was present on the linker (**256**,  $R^1 = R^2 = \text{Me}$ ).

Recently, Rotger has introduced a new linker based upon a squaramide group **261** (Scheme 58).<sup>250</sup> When the linker nitrogen proximal to the squaramide is *N*-methylated, the preferred *E,Z*-conformation **261** (boxed structure) favours cyclisation





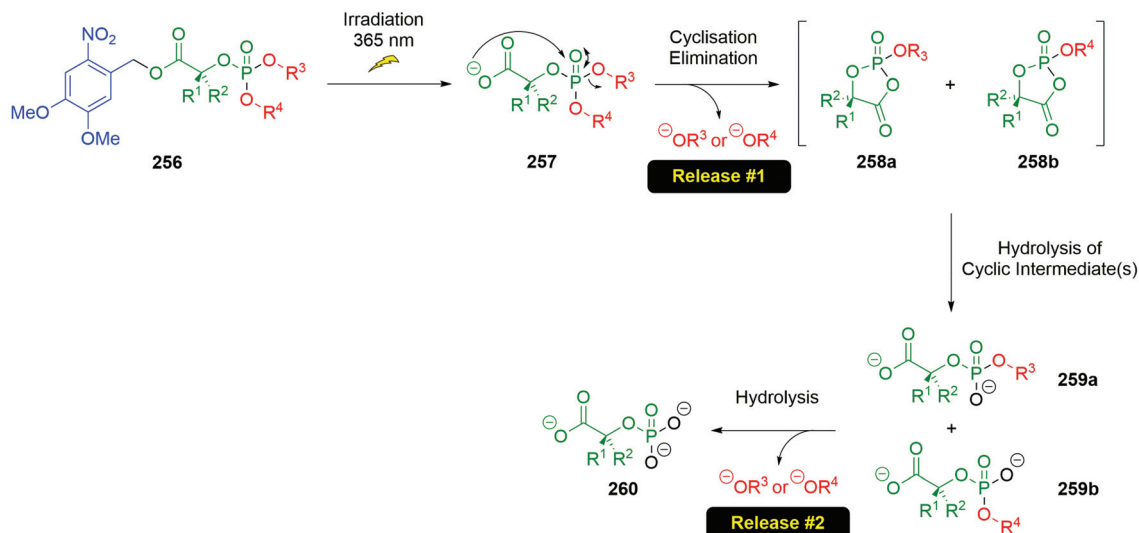
Scheme 56 The pH triggered release of monomethyl auristatin E from the SIE 251.<sup>247</sup>

through an apparent *7-endo-trig* mode. The combination of stability of linker under physiological conditions, with a good rate of cyclisation–elimination for aniline-based reporter groups (alkylamines are significantly slower) makes this a valuable addition to the chemist’s arsenal. Use of the linker was exemplified with delivery system 262 which undergoes reduction of the nitro group with nitroreductase in the presence of NADH, followed by 1,6-elimination of 263 to give 264. Cyclisation of 264 occurs smoothly to release the aniline-based nitrogen mustard 265 and bicyclic squaramide 266.

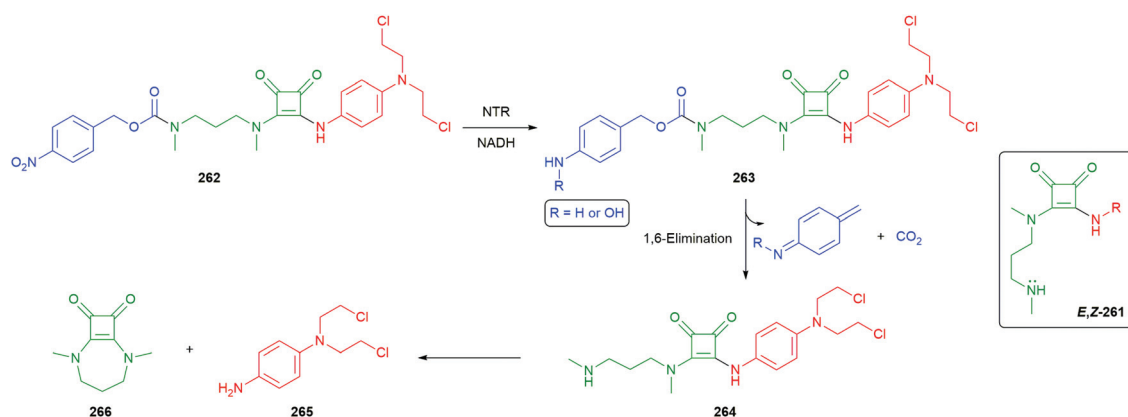
### 3 Amplification of self-immolative systems through dendron-based and related approaches

It was quickly understood that release of reporter groups could be amplified following a single triggering event by either linking self-immolative units together in the appropriate manner (to yield self-immolative polymers, see section 4 below) or alternatively utilising multiple electronic cascade





Scheme 57 Baszczyński and Procházková's phosphate-based self-immolative entity **256** for release of two reporter groups.<sup>249</sup>



Scheme 58 Rotger's novel squaramide self-immolative linker, illustrated with delivery of a nitrogen mustard **265** following triggering by nitroreductase (NTR).<sup>250</sup>

processes through branching units (*i.e.* self-immolative dendritic systems). To this end, self-immolative dendritic systems are a unique class of molecules defined by the release of multiple reporter groups *via* a series of electronic elimination processes arising from a *single* activation event.<sup>23,208,251,252</sup> Suitable structural modification of linear self-immolative aromatic linker units to permit degradation *via* additional pathways enables the creation of branched self-immolative linker systems and ultimately amplified release of multiple reporter groups following the triggering event.

In the past decade, the synthetic focus towards self-immolative systems capable of amplified release of reporter units has shifted from the construction of dendritic compounds of high generation number; their syntheses are frequently far too complex and practically challenging, not to mention extremely costly in terms of labour, in relation to the advantage of amplification offered. More pragmatic studies on self-immolative systems offering amplified release have thus focused primarily

on the use of first generation dendrons to demonstrate amplification for new trigger or linker groups or indeed application of these systems under realistic environmental conditions.

### 3.1 Phenol-based AB<sub>2</sub>, AB<sub>3</sub> and AB<sub>6</sub> based linkers

Shabat and co-workers described an example of a phenol-based AB<sub>2</sub> linker system to control the disassembly rate of self-immolative dendrons.<sup>208</sup> Dendrons **267** and **268** contained the methyl and ethylcarboxy-ester substituent on a core benzene building-block (Scheme 59). Upon a single trigger event *via* photo-irradiation of the *ortho*-nitrophenyl residue to promote 1,6- and 1,4-elimination, the dendrons release *para*-nitroaniline from **269/270** *via* diamine cyclisation and fragmentation from the cresol derivative **271**. The dendron **268** featuring the electron-withdrawing substituent exhibited a higher disassembly rate when compared to dendron **267** that possessed a *para*-methyl substituent. It was proposed that control of the rate of self-immolative dendrimer disassembly would be applicable in





**Scheme 59** Chemical structure and disassembly of second-generation 2,4-bis(hydroxymethyl)phenol AB<sub>2</sub> linker-based self-immolative dendrons.<sup>208</sup>

the field of diagnostic or therapeutic applications when a specific release of reporter rate is needed.

Shabat and co-workers subsequently developed a divergent strategy wherein a phenol-based self-immolative dendritic pro-drug system,<sup>198,253</sup> featuring a 2,4,6-tris(hydroxymethyl)phenol branching unit, allowed preparation of a number of derivatives. This approach facilitated the stepwise coupling of doxorubicin (DPX) directly *via* its primary amine, whereas etoposide (ETP) and camptothecin (CPT) were coupled through the *N,N'*-dimethylethylenediamine self-immolative cyclisation linker (as exemplified in Scheme 43, **186a**). Self-immolative elimination was carried out under physiological conditions in the presence of catalytic antibody 38C2 enzymes<sup>198</sup> and facilitated the disassembly *via* retro-aldol, retro-Michael cleavage of the trigger group and release of three different drugs (*i.e.* from a single molecular scaffold) through a combination of 1,6- and two 1,4-elimination processes after only a single trigger event. It was, however, observed for self-immolative higher generation dendrons based on AB<sub>2</sub> repeat units that the aqueous solubility was compromised in the light of their hydrophobic character, which in turn led to aggregation in this protic medium.<sup>254,255</sup> An alternative approach was thus developed to overcome this solubility issue whereby the multiplicity of a low generation self-immolative dendron was increased to permit high substrate loading and also improve the aqueous solubility.<sup>256</sup> The self-immolative dendron **272** featured 2,4,6-triformylphenol as the branch point, phenylacetamide as the trigger and six tryptophan reporter groups (Scheme 60). The self-immolative dendron was then incubated in phosphate buffer of saline (PBS, pH 7.4) both in the presence and absence of penicillin G amidase (PGA). PGA cleaved the phenylacetamide from dendron **272** and the resulting phenoxide **273** disassembled to release a total of six equivalents of tryptophan

and the hexahydroxyphenol **274**. The release of tryptophan was completed within 48 hours in the presence of PGA; whereas, release was not observed in the absence of the enzyme.

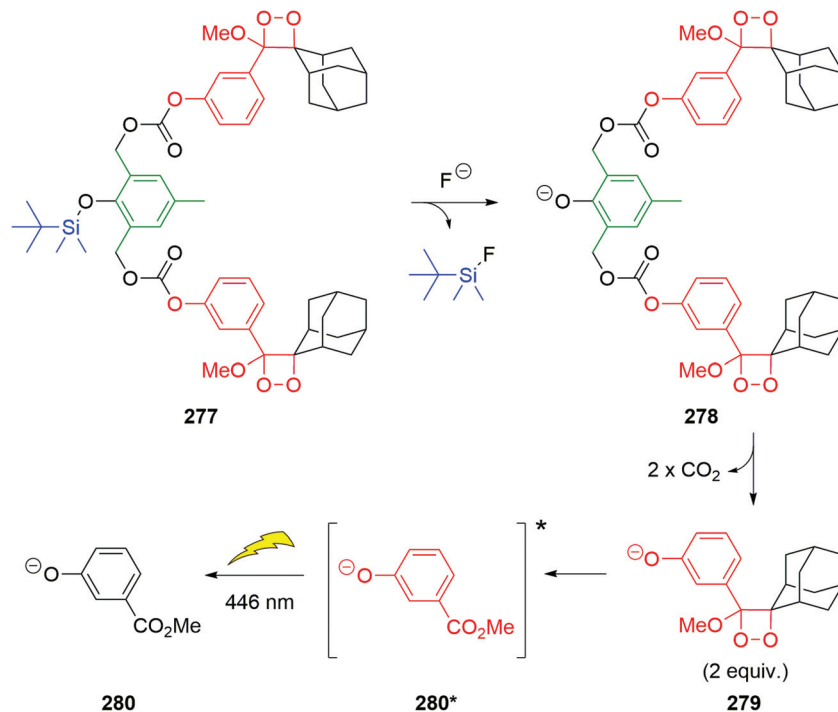
Shabat and co-workers have also utilised a first generation dendritic system where the trigger unit was a phenyl boronic ester (susceptible to the presence of hydrogen peroxide, *vide supra*) to develop FRET sensors (see **275** and **276** in Fig. 16).<sup>257</sup> These dendrons feature fluorophores (a fluorescein system and CY5, respectively) whose visible emission was suppressed by the close proximity of the quencher compounds coupled onto the branched unit. The turn-on FRET sensors shown in Fig. 16 operate by exposure to hydrogen peroxide (in buffered PBS plus DMSO as a co-solvent) to facilitate release of the fluorophores and quencher compounds into solution *via* two 1,4-elimination processes thus permitting observation of the fluorescence.

Akkaya has demonstrated the applicability of an AB<sub>2</sub> dendron **277** to the detection of fluoride, utilising Schaap's 1,2-dioxetane-based chemiluminescent reporter group (Scheme 61).<sup>258</sup> Related reporter groups have also made a significant impact in a number of areas; in particular, the compounds developed by Shabat (see Fig. 8).<sup>118</sup> Treatment of dendron **277** with a source of fluoride ions chemoselectively cleaves the Si–O bond of the trigger group and releases phenoxide **278** that subsequently undergoes successive 1,4-elimination reactions to liberate two equivalents of chemiluminescent reporter group **279** for each ion sensed. The reporter group fragments to **280\***, relaxation of which to its ground state occurs with emission in the blue region of the spectrum. The sensor proved effective both in solution and when impregnated into a polymer support (PMMA).<sup>258</sup>

Use of two-photon excitation, with near infrared (NIR) light, to trigger a self-immolative delivery system allows good spatial and temporal control of the process and is effective in biologi-







**Scheme 61** Chemiluminescent sensor for the detection of fluoride using an AB<sub>2</sub> linker-based self-immolative dendron **277**.<sup>258</sup>

cal systems. An action cross-section of 1 GM (Goeppert–Mayer) units at 740 nm has been reported for a 4-bromo-7-hydroxycoumarin chromophore. As an alternative to redesigning the trigger chromophore, to increase the action cross-section and hence its efficiency at triggering an SIE, Almutairi and co-workers have prepared a second-generation (G2) dendritic system **281** that should release four L-glutamic acid units per two-photon excitation (see Fig. 17).<sup>209</sup> In practice, some background hydrolysis and side reactions from the irradiation of **281** were observed, but the amount of L-glutamic acid released

from the dendron, after 30 minutes exposure to NIR light, was 2.8-fold higher than that from the coumarin conjugate of L-glutamic acid **282**. Thus, this work demonstrates the important lesson that while dendrons are effective in this role, it is important to consider potential side reactions.

Hennig has described a range of efficiently quenched, NIR fluorescent, activatable (PGA) probes based on the compounds **283** and **284** but varying the fluorescent species, here illustrated with a fluorescein reporter group that forms a non-fluorescent H-dimer in the dendron (Fig. 18).<sup>259</sup> The particular

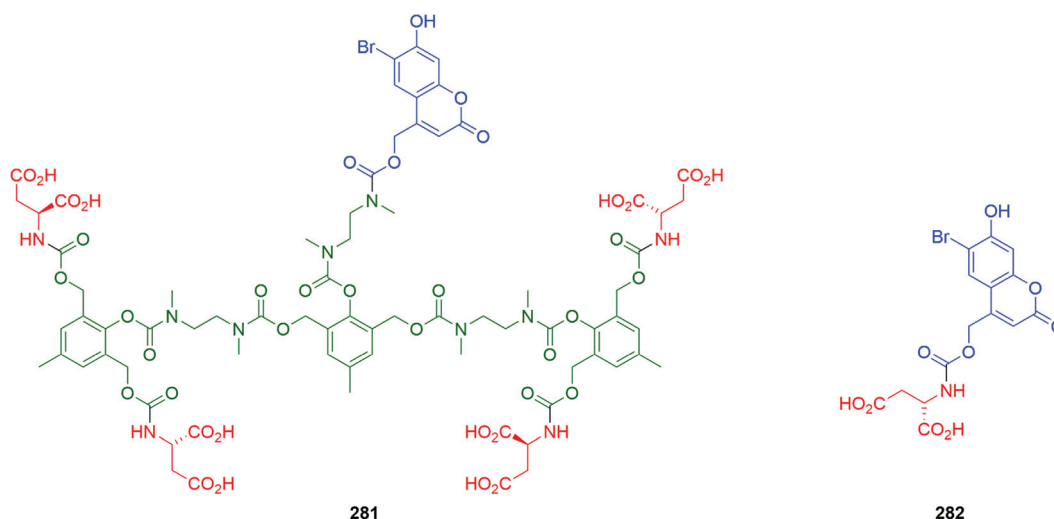


**Fig. 17** Almutairi's two-photon, NIR triggered G2 dendron **281** for the release of L-glutamic acid.<sup>209</sup>





Fig. 18 Self-immolative probes 283 and 284 used to detect PGA *via* a NIR fluorescence response.<sup>259</sup>

advantage of such systems being that once the dye and quencher interaction is optimised, to give the maximum change from the quenched to free state, the trigger component can be varied with little effect on those optical properties. Investigation of the optical properties of these compounds led to a detailed understanding of their behaviour. Interestingly, whether a 2,6 or 2,4-substitution pattern was used in the dendron portion of the molecule had little effect on the relative quantum yields.

Gillies and co-workers have developed a route to photo-triggered self-immolative hydrogels<sup>260</sup> using a combination of cycli-

sation linkers and electronic cascade processes. The bis-alkyne dendron 285 shown in Scheme 62 was crosslinked with the four-armed PEG featuring azide end groups *via* the well-established copper-catalysed 'click' cycloaddition to yield a network hydrogel. The dendron component of this network featured an *ortho*-nitrobenzyl unit end group that could be photochemically triggered to permit liberation of the secondary amine and induce self-immolation *via* an initial cyclization event followed by electronic cascade (1,4-elimination) to degrade the links of the network, thus disrupting the physical form of the hydrogel as established by studying the compressive moduli.



Scheme 62 The light-triggered self-immolative hydrogel reported by Gillies and co-workers.<sup>260</sup>



An excellent example of how self-immolative electronic cascade processes can be utilised in biotechnology has been reported<sup>53</sup> by Fakhari and Rokita in the development of dynamic DNA crosslinking agents to modify biochemical transportation and ultimately disrupt DNA repair as part of a strategy for cancer chemotherapy. A silyl ether protected phenol **286** featuring a DNA intercalator (acridine) unit and two benzyl acetates was synthesised – triggering with a fluoride ion source activated the system to the corresponding phenolate which then could degrade *via* 1,4-elimination to afford a quinone methide intermediate (Scheme 63). This intermediate was able to reversibly couple to DNA *via* the nucleophilic nitrogen atoms of adenine or guanine in turn leading to formation of another quinone methide that can then bind to the nitrogen base of an adjacent nucleotide to form a crosslink (either intra or interchain crosslinking is viable). This crosslinking process was shown to be reversible and thus the quinone methide unit can migrate along the DNA duplex in a bipedal fashion.

Zhang and co-workers have cleverly deployed an AB<sub>3</sub> dendron, conjugated to a range of DNA strands by azide ‘click’ chemistry, to create amphiphiles.<sup>261</sup> These amphiphiles assemble into micellar nanostructures in water, whose structure can be varied, that undergo ready endocytosis (within 6 hours). Subsequent UV irradiation (365 nm) triggers release of three equivalents of camptothecin (CPT). The conjugated system affords much lower cell toxicity than the camptothecin itself. For example, a DNA 20-mer **287** was conjugated to an AB<sub>3</sub> dendron **288** to afford the amphiphile **289** (Scheme 64).

In 2017, Zeng and Wu described<sup>122</sup> a glutathione (GSH)-triggered and self-immolative ABB' dendritic platform **290** comprising the reporter groups, the anticancer drug camptothecin (CPT) and a two-photon NIR fluorophore (dicyanomethylene-4H-pyran, DCM) for the *in situ* tracking of drug release and anti-tumour therapy (Scheme 65). GSH is an endogenous tripeptide that is present in cells at the millimolar concentration level and it serves as the major antioxidant in many biological systems. The dendritic drug release system

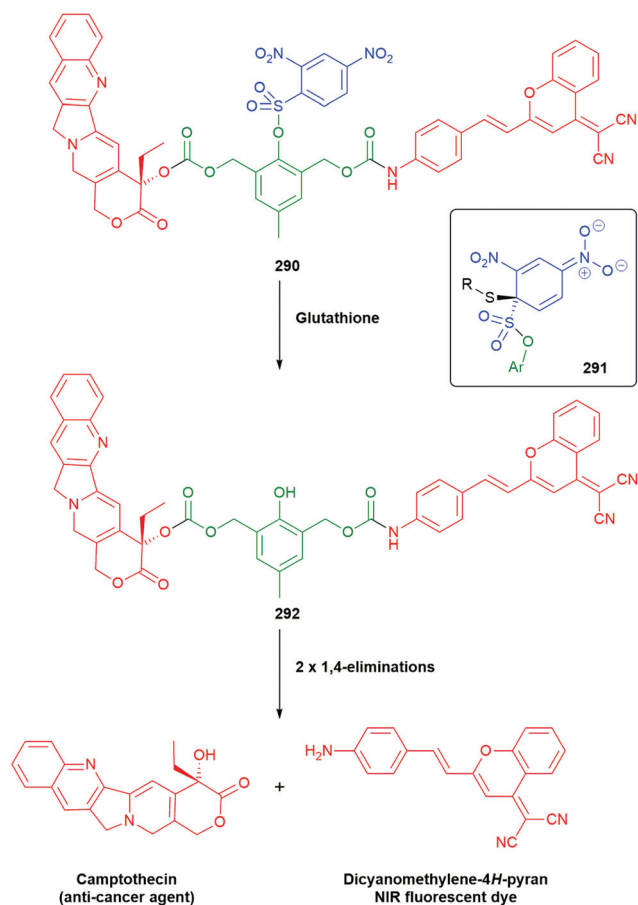


**Scheme 63** The self-immolative DNA crosslinking system **286** capable of migrating in a bipedal fashion along DNA sequences reported by Fakhari and Rokita.<sup>53</sup>





Scheme 64 A camptothecin bearing AB<sub>3</sub> dendron **288** equipped with a UV trigger, conjugated to a strand of DNA **287** to yield amphiphile **289**.<sup>261</sup>



Scheme 65 The self-immolative theranostic dendritic drug delivery system **290** reported by Zeng and Wu.<sup>122</sup>

featured 2,4-dinitrobenzenesulfonyl (DNS) as the thiol-responsive trigger group that was cleaved by the action of GSH, presumably *via* Meisenheimer complex **291**, to liberate the corresponding phenol **292** that in turn facilitated self-immolation *via* a combination of 1,4-elimination processes to deliver CPT and DCM within cellular environments. This prodrug was shown to be effective both *in vitro* and *in vivo* and was able to achieve sustained release of CPT to afford efficient inhibition of tumour growth.

In the same manner that the elevated levels of glutathione in some cancer cells was targeted by ABB' dendron **290** (Scheme 65), a number of malignant cancers *e.g.* non-small cell lung carcinoma, overexpress DT-diaphorase, sometimes by as much as 50-fold compared to normal cells also can be targeted. Developing their work on a drug delivery system that is both triggered by the enzyme DT-diaphorase and able to measure its level within the cell (Fig. 12), Zeng and Wu have prepared an AB<sub>2</sub> dendron **293** (Fig. 19).<sup>228</sup> Following reduction of the 1,4-benzoquinone to the corresponding hydroquinone, successive cyclisation of the trimethyl-lock and *N,N'*-ethylene-diamine linkers occurs, followed by 1,4-elimination of phenol moiety and decarboxylation to release the CPT reporter group. The fluorescence that arises from irradiation of camptothecin is quenched by the quinone in **293**. However, fragmentation of the dendron not only releases the topoisomerase I inhibitor, but restores camptothecin fluorescence ( $\lambda_{\text{max}}$  446 nm), self-indicating the fragmentation and quantifying DT-diaphorase activity. The release was shown to occur in A549 cells (a DT-Diaphorase overexpressing cell line) but not in L929 cells (a non-overexpressing cell line). Kim and Kim have used a related, theranostic dendron using biotin as a cancer targeting unit an SN-38 as the therapeutic agent.<sup>262</sup> *In vitro* and *in vivo* studies showed inhibition of tumour growth.





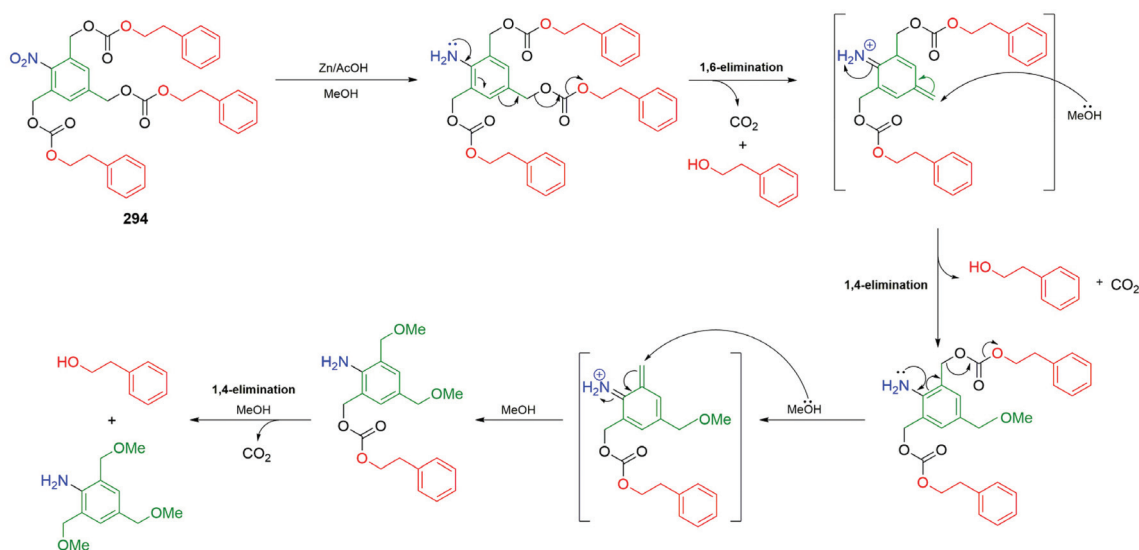
Fig. 19 The DT-Diaphorase triggered AB<sub>2</sub> dendron **293** for the amplified release of camptothecin reported by Zeng and Wu.<sup>228</sup>

### 3.2 Aniline-based AB<sub>2</sub> and AB<sub>3</sub> linkers

First and second-generation aniline-based self-immolative dendrons were first introduced in 2003 by De Groot *et al.*<sup>251</sup> A self-immolative second generation dendron featuring three 2-(4-aminobenzylidene)propane-1,3-diol AB<sub>2</sub> type self-immolative linkers was able to degrade *via* two 1,8-elimination processes from a single trigger activation event to liberate four equivalents of paclitaxel (PTX). The self-immolative process for this second generation dendron was triggered by reduction of the nitro focal point under mild acidic conditions (zinc in the presence of acetic acid in MeOH). Subsequent investigations by De Groot *et al.* assessed the potential of self-immolative AB<sub>3</sub> linkers featuring the same trigger group chemistries with the release of 2-phenylethanol from a first-generation dendron **294** with a 2,4,6-tris(hydroxymethyl)aniline dendritic core unit

(Scheme 66).<sup>251</sup> In the light of the modest basicity of anilines ( $pK_aH^+$  of aniline *ca.* 5) generated post-reduction of the nitro trigger group, a significant percentage was present in the non-protonated form and can, therefore, trigger 1,6-elimination to lead to decarboxylation and liberation of the reporter molecule and aza-quinone methide. Quenching the aza-quinone methide with methanol reformed the electron-donating aniline, which then in turn permitted two sequential 1,4-eliminations to occur with concomitant decarboxylation to release two additional reporter molecules. Overall, a total of three equivalents of 2-phenylethanol were released from a single reduction activation event in the appropriate solvents.

In 2011, Papot and co-workers demonstrated<sup>263</sup> successfully the action of an ABB' dendritic prodrug system that featured two back-to-back self-immolative linkers (Fig. 20). The first being phenol-based and attached to the glucuronic trigger group; whereas, the second is an aniline-based branched amplifier unit carrying two distinct reporter groups. This first generation dendron (**295**) featured doxorubicin and the histone deacetylase inhibitor MS-275 as the reporter groups. The phenol-based linker carried an *ortho*-nitro substituent that will serve to decrease the  $pK_a$  of the phenol and, as discussed by Hou in the context of their galactosidase-based SIE, it may affect the Michaelis–Menten constant ( $K_m$ ) of the substrate for the enzyme (Scheme 18).<sup>136</sup> This linker provides a suitable distance between the enzyme substrate and the two bulky drugs to allow easy recognition of **295** by  $\beta$ -glucuronidase. Enzyme-catalyzed cleavage of **295** led to the generation of a phenoxide intermediate that then induced the release of an aniline *via* a 1,6-elimination process. Once activated, the aniline amplifier unit first liberated doxorubicin *via* a 1,4-elimination followed by spontaneous decarboxylation. Reaction with the water in the aqueous environment traps the resultant *ortho*-azaquinone methide to regenerate the electron-rich aniline thereby permit-



Scheme 66 Triple self-immolation elimination of 2-phenylethanol from first generation 2,4,6-tris(hydroxymethyl)aniline based AB<sub>3</sub> dendron **294**.<sup>251</sup>





Fig. 20 The anti-cancer self-immolative dendritic prodrug systems (295 and 296) developed by the Papot group.<sup>263,265</sup>

ting the subsequent release of MS-275 *via* a 1,6-elimination process. Normally, 1,6-eliminations are observed to be faster than their 1,4 counterparts; however, this appears to be significantly influenced by the nature of the leaving group. The authors also note that as azaquinone methides are potential alkylating species (see Scheme 62 for a related example), there is potential for these intermediates to also prove toxic to cancerous cells. The one issue with **295** was effective cell penetration. Additional work on amplification, with delivery of two doxorubicin reporter groups was reported in 2012.<sup>264</sup> To enhance the cell specificity and efficiency of the action of drugs in dendritic prodrug systems, Papot and co-workers have cleverly refined their prodrug design to produce **296** that features a folate moiety to target the folate receptors frequently overexpressed in cancerous cell lines and facilitate endocytosis of the prodrug (Fig. 20).<sup>265</sup> The structure of the phenoxy linker was modified at the benzylic position to allow the folate to be attached by 'click' chemistry. The lysosomal enzyme,  $\beta$ -galactosidase, triggered self-immolation to release two doxorubicin molecules in a highly targeted fashion. A similar, folate directed approach has been reported for delivery of monomethylauristatin E.<sup>266</sup> More recently, Papot has extended

these studies to give a  $\beta$ -glucuronidase-responsive drug delivery system that contains a maleimide unit that allows *in vivo* functionalisation of cysteine-34 of plasmatic albumin.<sup>267,268</sup> Such albumin conjugates prevent rapid clearance of the drug and concentrate that conjugate in tumour tissues where  $\beta$ -glucuronidase triggers release of the anticancer agent *e.g.* monomethyl auristatin E or doxorubicin; these drug delivery systems were shown to be effective against, *inter alia*, pancreatic tumors and murine LLC xenografts. The studies were extended to include trimeric versions of the system.<sup>269</sup>

In the same paper<sup>257</sup> in which FRET sensors were reported from first generation self-immolative dendrons bearing a phenyl boronic ester trigger group to permit a turn-on FRET response upon exposure to hydrogen peroxide following two 1,4-elimination processes, Shabat and co-workers also reported an analogous Homo-FRET sensor (see **297** in Fig. 21). Unlike the phenol-based FRET dendritic systems, activation of this aniline-based Homo-FRET probe was triggered by the action of the enzyme PGA on the phenylacetamide group to liberate the Cy5 fluorophores *via* both 1,4- and 1,6-elimination processes from the branching unit to achieve the desired fluorescence response.





Fig. 21 The aniline-based self-immolative Homo-FRET system **297** reported by Shabat and co-workers.<sup>257</sup>

### 3.3 Dendritic chain reactions (DCR) and amplification systems

Although self-immolative dendrons are elegant systems, there are structural and practical limitations (*i.e.* very labour-intensive syntheses) in terms of achieving significant amplification values for reporter release from dendritic architectures as high generation dendritic species are required. In 2009 Shabat and co-workers reported a solution for this limitation in the form of the dendritic chain reaction (DCR).<sup>270</sup> This approach takes inspiration from the polymerase chain reaction (PCR) and Mirkin's example of a PCR-like cascade.<sup>271,272</sup> Shabat's initial DCR system **298**, a first generation dendron which featured an arylboronic acid was triggered in response to  $\text{H}_2\text{O}_2$  to provide a phenolic species capable of a 1,6-elimination *via* a quinone

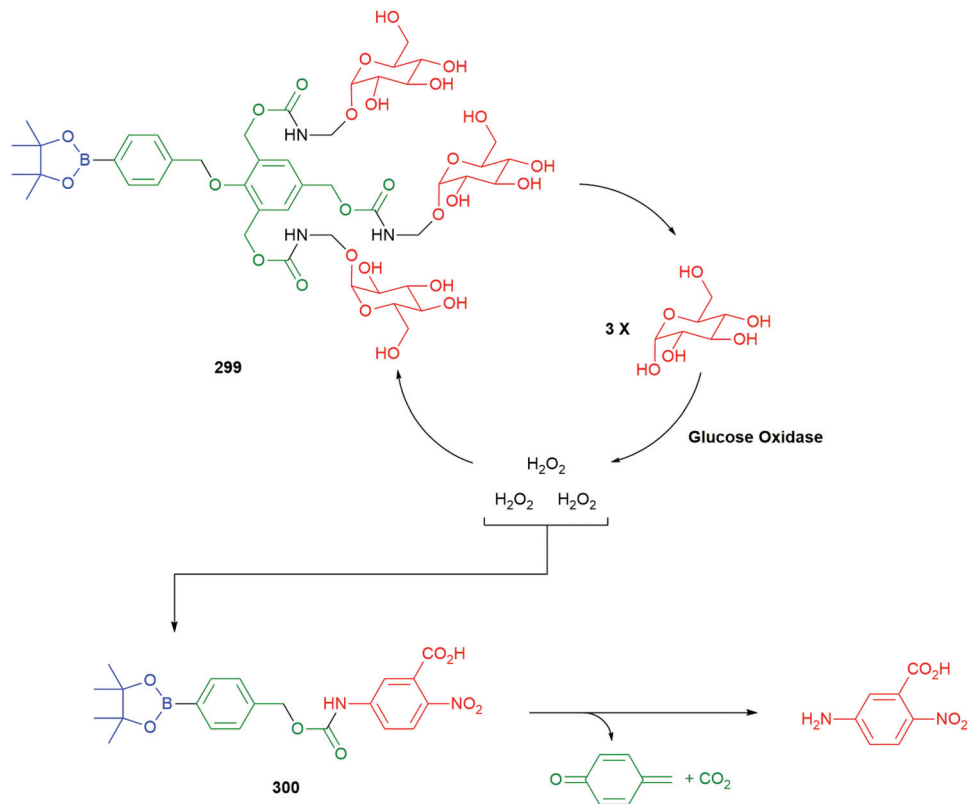
methide and decarboxylation reaction to release the core unit.<sup>227</sup> The core unit was able to undergo three further eliminations of the substituents in the *ortho*- and *para*-positions to release 4-nitroaniline (yellow) and the two choline molecules. The choline units were then oxidized by choline oxidase (COX) present in solution to produce four molecules of hydrogen peroxide, enabling amplification (Scheme 67).

Developing the concept of a hydrogen peroxide sensitive first-generation dendron **299** as amplifier, Shabat has reported an exponential signal amplification using a dendritic chain reaction. Thus, exposure of **299** to hydrogen peroxide releases three molecules of glucose that upon exposure to glucose oxidase generates three equivalents of hydrogen peroxide (Scheme 68).<sup>45</sup> This hydrogen peroxide generator is coupled with a second component **300**, sensitive to  $\text{H}_2\text{O}_2$ , that gives a



Scheme 67 Self-immolative dendritic chain reaction involving the dendron **298** triggered by the oxidation of a phenylboronic acid releasing 4-nitroaniline (coloured readout) and two choline molecules that undergo oxidation by COX generating  $\text{H}_2\text{O}_2$  for further trigger activation.<sup>270</sup>





**Scheme 68** Shabat's self-immolative dendritic chain reaction involving the AB<sub>3</sub> dendron **299**.<sup>45</sup>

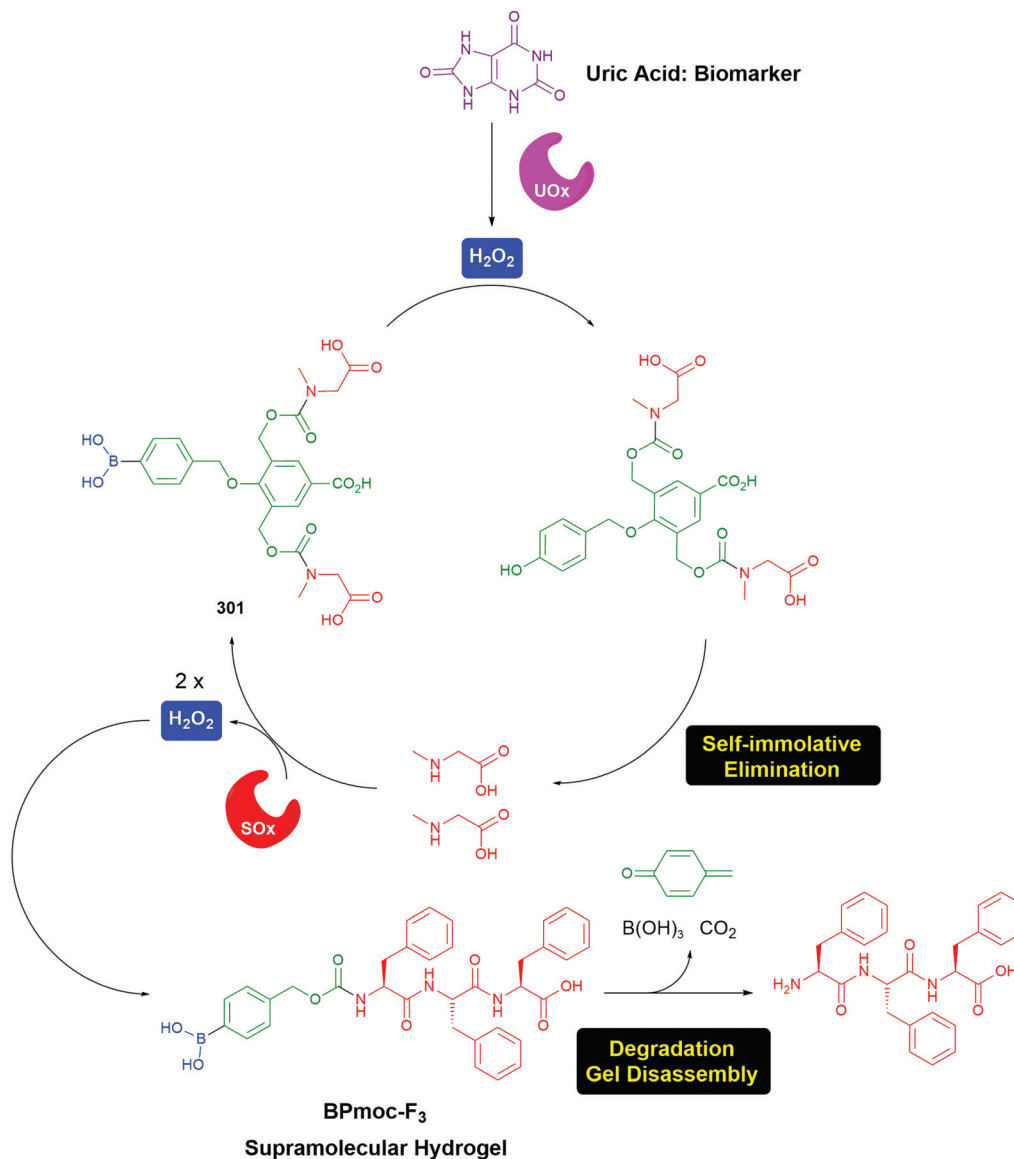
spectroscopically monitorable signal. During this work, the authors compared the effectiveness of the AB<sub>3</sub> dendron **299** with an AB<sub>2</sub> and two second-generation dendrons of AB<sub>4</sub> and AB<sub>6</sub> design, respectively. The higher order dendrons gave the fastest rate of disassembly but it was noted that they are subject to more background hydrolysis; overall, the AB<sub>3</sub> dendron **299** represents the best balance of stability and amplification.

In 2015, Hamachi and co-workers described the application of a dendritic chain reaction process within a multicomponent supramolecular hydrogel to permit detection of small-molecule biomarkers by a gel–sol transition, with the naked-eye.<sup>273</sup> The hydrogel was composed of a hydrogen peroxide-responsive supramolecular triphenylalanine-based hydrogel (Bpmoc-F<sub>3</sub>) plus an embedded dendritic self-immolative system and corresponding enzymes (sarcosine oxidase (SOx)/urate oxidase (UOx)) to afford a signal amplification system (see Scheme 69). Degradation of both the peptide Bpmoc-F<sub>3</sub> and self-immolative first generation dendritic system **301** was triggered by hydrogen peroxide, produced by reaction of the biomarker (uric acid) with UOx. In order to effect amplified degradation of the hydrogel network, the multi-component material was designed so that dendritic component would release two sarcosine units upon self-immolation; the sarcosine produced was then consumed by SOx present in the gel matrix, in turn liberating two equivalents of hydrogen peroxide to amplify degradation of Bpmoc-F<sub>3</sub> and **301**, producing the gel–sol transition.

Papot and Taran have used their β-glucuronidase sensitive trigger/linker combination to drive controlled release of a payload from a micelle effectively amplifying the analyte signal (Scheme 70).<sup>274</sup> An amphiphilic, micelle forming, compound **302** was synthesised around an iminosynone (coloured brown). The micelles formed from **302** (CMC = 50 μM, 10 ± 1 nm) were shown to carry payloads and to breakdown on exposure to a strained alkyne *e.g.* **303** to give **304** by a 'click' reaction with the iminosynone moiety, cleaving the hydrophilic from the hydrophobic segments. Breakdown of the micelle releases the payload. Use of a self-immolative molecule **305** with a hydrophilic tale slows transport of the strained alkyne into the micelle core; however, upon triggering with β-glucuronidase (a tumour associated enzyme), the released alkyne **303** rapidly penetrates to the hydrophobic core, reacting with concomitant release of the payload *e.g.* a fluorescent probe. This combination of reagents was found to be effective both in KB cells and subcutaneous KB mouth epidermal carcinoma xenografts in mice.

In 2012, Phillips described an autocatalytic signal amplification system that couples a molecule sensitive to a particular analyte (Pd(0)) that produces a chemical signal with another that serves to amplify that initial signal (Scheme 71).<sup>275</sup> Thus, **307** detects the analyte with decomposition initiated by a π-allylpalladium species, followed by rapid 1,6-elimination to release a molecule of piperidine. Once formed, the piperidine serves as a base to cleave the Fmoc group from amplifier **308**,





**Scheme 69** The enhanced degradation of a peptide hydrogel via a dendritic chain reaction from the first generation dendritic self-immolative system **301**.<sup>273</sup>

itself being regenerated in the process, and triggering formation of a second molecule of piperidine. The process then repeats with the total number of piperidine molecules being  $2^n$  ( $n$  = the number of cycles). As discussed previously, the methoxy group in **308** was found to confer an increase in rate of fragmentation (factor of 2.3) compared to its desmethoxy analogue. Additionally, a dendron-based amplification reagent **309** was also found to be successful in this process, but releases two additional molecules of the base for each complete cycle. Readout occurred spectroscopically, *via* dibenzofulvene ( $\lambda_{\max}$  = 305 nm), or *via* a pH indicator.

In a similar fashion to the palladium detection system outlined in Scheme 71, Phillips outlined<sup>275</sup> an amplification system for the detection of  $\beta$ -galactosidase as the analyte, with readout from the assay being colourimetric (2-hydroxy-1,4-

benzoquinone).<sup>276</sup> Exposure of **310** to  $\beta$ -galactosidase, followed by 1,6-elimination, releases hydroxyquinol **311** that is auto-oxidised in air to give coloured benzoquinone **312** and an equivalent of H<sub>2</sub>O<sub>2</sub> (Scheme 72). Compound **313** serves as a hydrogen peroxide sensitive amplifier.

Phillips and co-workers have described<sup>277</sup> a system for *in situ* signal amplification that is activated by the presence of the analyte (glucose) and minimises background reactions, an important issue for amplification processes. Thus, in the presence of the analyte (glucose), oxidation takes place by glucose oxidase delivering hydrogen peroxide with the expected lowering of pH. The hydrogen peroxide is used by amplification reagent **314** to mediate oxidation of the C–B bond with subsequent 1,4-elimination of glucose from the so-formed enol/enolate (Scheme 73). As the pH lowers from >6.2 to





**Scheme 70** Papot and Taran's self-immolative molecule **305** for biorthogonal 'click to release' degradation of a payload bearing micelle.<sup>274</sup>

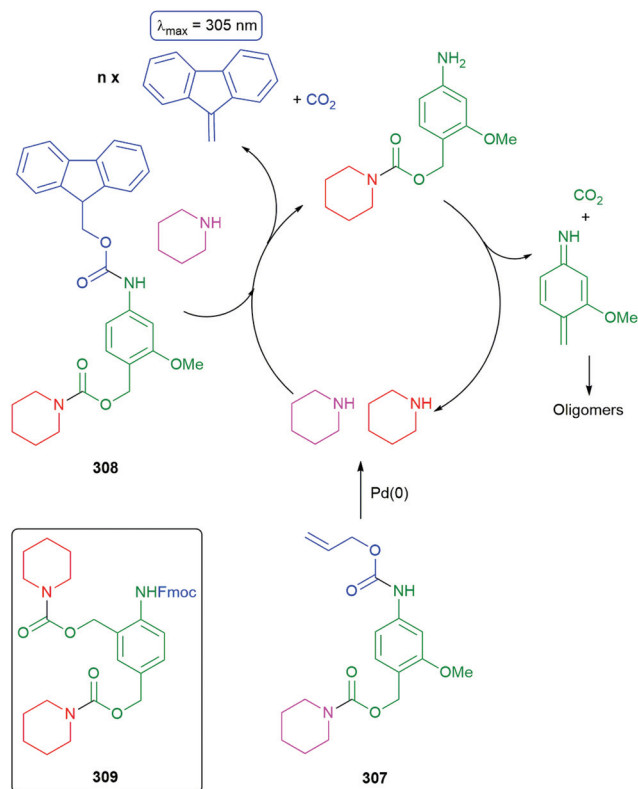
<4.2 methyl red **315** protonates to afford **316** with a concomitant colour change from yellow to pink, giving a colourimetric readout. In respect of background hydrolysis of the amplification reagent **314**, use of an ether bond to connect the linker to the reporter group affords a highly stable molecule that, when highly purified, gives a minimal background reading. A non-amplified assay for penicillin-G-amidase, based upon a self-immolative molecule that releases glucose has also been reported by Mohapatra and Phillips.<sup>278</sup>

Detection and amplification of the analyte fluoride has proved to be of significance in a number of roles *e.g.* the disclosure and quantification of G series nerve agents (*vide infra*). Shabat and co-workers have reported<sup>279</sup> a dendron-based

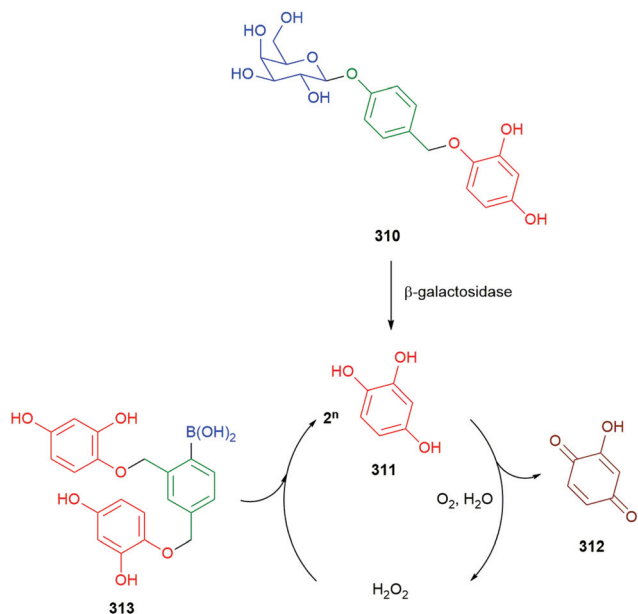
amplification system **317** that takes advantage of the high chemoselectivity of fluoride for silicon (Scheme 74). Treatment of **317** with as little as 0.004 equivalents fluoride leads to its complete disassembly with an exponential rate of progress. Each disassembly of **317** is accompanied by release of one equivalent of *para*-nitroaniline, facilitating spectroscopic readout.

Baker and Phillips have provided a further example of the flexibility of a two-component analytical system discussed in Schemes 71 and 72.<sup>280,281</sup> In the case below, the allylic carbamate in **318** again serves as the specifier for the Pd (0); whereas, **319** serves as the amplifier (Scheme 75). Following cleavage of the allylic carbamate, generation of two fluoride



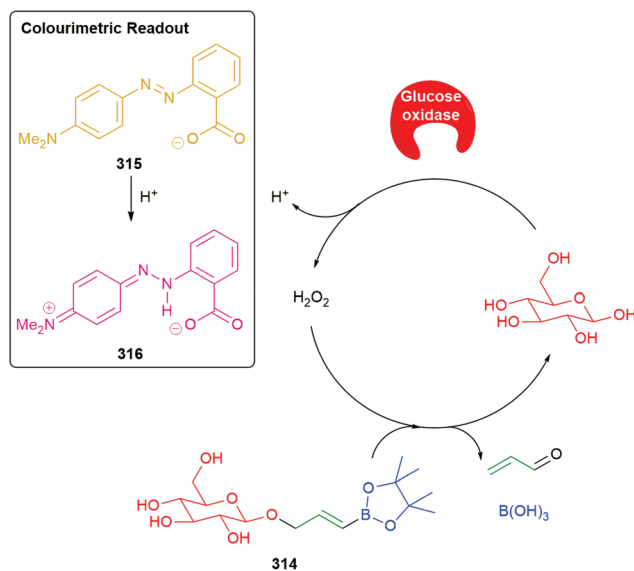


Scheme 71 Phillips's autocatalytic amplifier system for the detection of a palladium analyte.<sup>275</sup>



Scheme 72 Phillips dendron-based signal amplification system for colourimetric detection of  $\beta$ -galactosidase.<sup>276</sup>

ions by 1,6-elimination occurs with concomitant formation of *para*-aminobenzaldehyde, the latter allowing for colourimetric reporting. In respect of this reporting mechanism, see



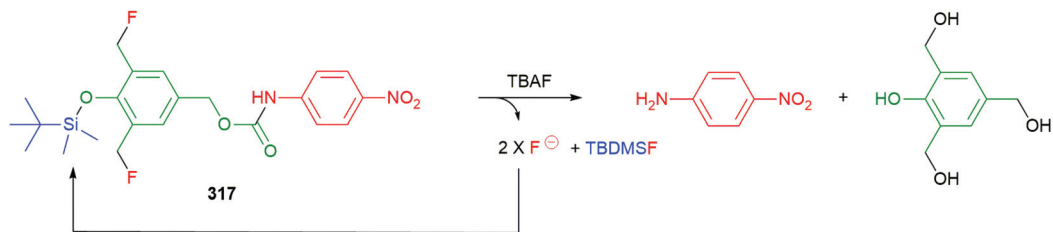
Scheme 73 The amplified colourimetric reporter system 314 developed by Phillips and co-workers.<sup>277</sup>

Scheme 75 for the likely identity of the coloured species. Once the fluoride is released, its high affinity for silicon triggers the amplifier 319. Trapping of the quinone methide from 319 by nucleophiles other than water, to afford 320 and 321, was also noted, again reinforcing this consideration in Katzenellenbogen's seminal paper. Thus, it can be seen that the self-immolative linkers in 318 and 319 serve as both linker and reporter, a feature frequently encountered with self-immolative polymers (*vide infra*).

Huang and co-workers have described<sup>282</sup> a self-immolative fluorometric probe 322 that uses autoinductive signal amplification for enhanced sensitivity and combines selectivity for fluoride with generation of a fluorogenic coumarin 323 ( $\lambda_{\text{em}} = 445$  nm), for the readout (Scheme 76). As seen above, the affinity of fluoride for silicon drives the selectivity whilst the generation of two fluorides from the disassembly of each molecule of 322 *via* intermediate 324 affords an exponential increase in the signal. Additionally, an alternative fluorometric probe 325, that fluoresces at longer wavelength ( $\lambda_{\text{em}} = 595$  nm), was shown to couple with this amplifier and is promising for applications with biological samples. Encouragingly, a limit of detection of 0.5 pM was reported.

In an interesting extension of their solution-phase methodology in which detection of an analyte signal with concomitant release of fluoride is coupled to triggering of an amplification cycle, Phillips has demonstrated that within a suitable copolymeric material, a fleeting signal can be converted to a macroscopic response (Scheme 77).<sup>283</sup> Exposure of a small section of copolymer 326 to 300 nm light gives cleavage of the *ortho*-nitrobenzyl moiety with release of a linker-reporter group unit that undergoes both 1,4 and 1,6-elimination to deliver four fluoride ions and copolymer 327. These fluoride ions then trigger an amplification unit on a separate side-





Scheme 74 Shabat's fluoride triggered autoinductive amplification system **317**.<sup>279</sup>



Scheme 75 The two-component difluoride specifier/amplifier **318/319** with colourimetric readout reported by Baker and Phillips.<sup>280,281</sup>

chain causing the effect to spread throughout the sample changing its physical properties from hydrophobic in **326** to hydrophilic in **328**. The idea has been further developed by Phillips and Sen to give a self-powered microsphere, based on a modified tentagel bead (**329**), that responds to a short stimulus of 365 nm light by pumping the surrounding fluid toward itself (Scheme 77).<sup>284</sup> A similar example of a macroscopic

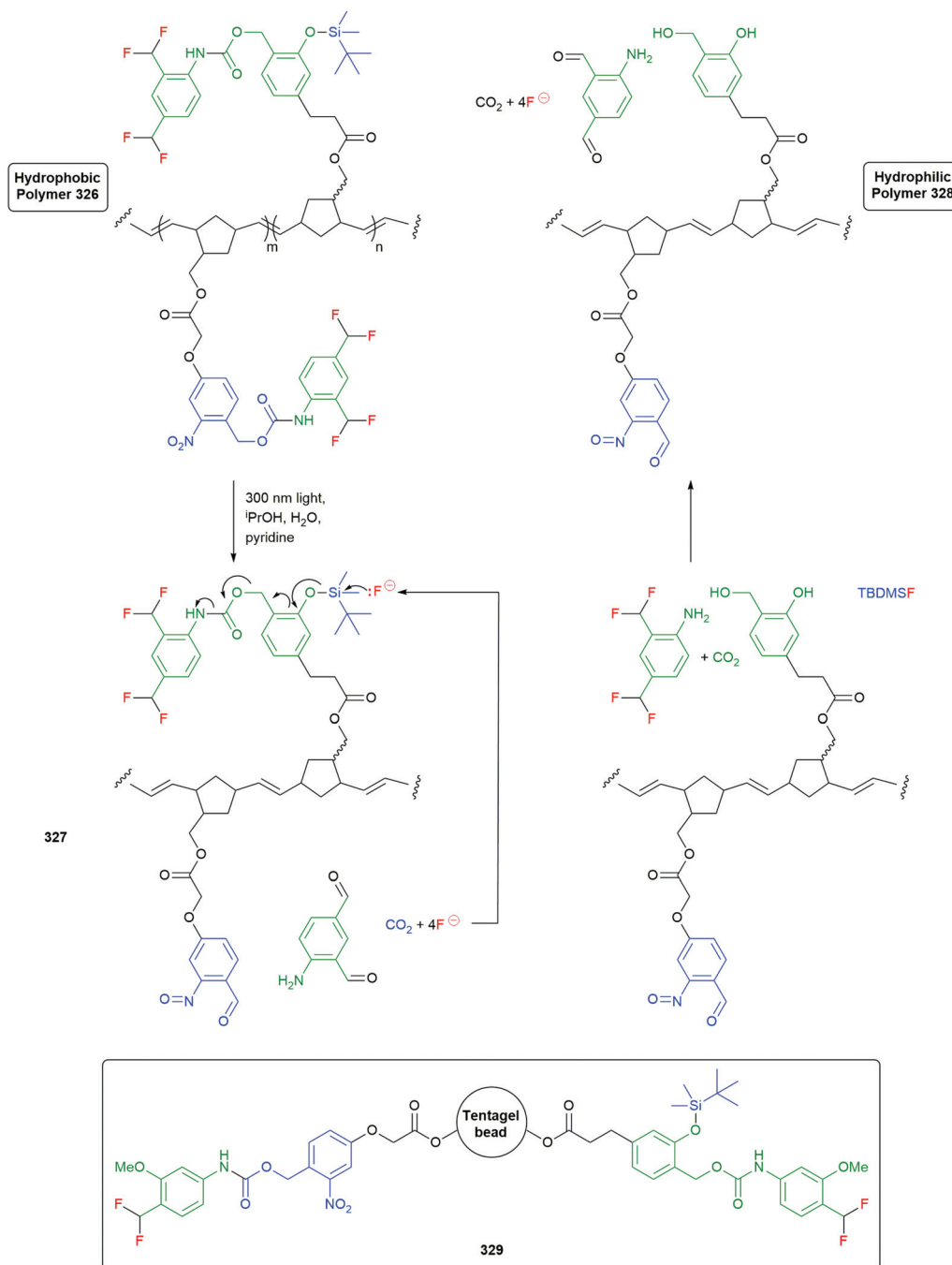
change to a polymer's properties, triggered by a fleeting thiol signal, has also been described.<sup>285</sup>

Anslyn and Phillips have applied the methodology set out above to the detection and quantification of G-class nerve agents. Taking the established reactivity of such compounds toward nucleophiles, G-series surrogate **330** was treated with benzaldoxime to give **331** and an initial fluoride signal





Scheme 76 Huang's fluoride triggered autoinductive signal amplification system **322**.<sup>282</sup>



Scheme 77 Polymeric species **326** and modified Tentagel beads **329** that undergo macroscopic responses to a fleeting signal.<sup>283</sup>





**Scheme 78** The detection and quantification system for G-series nerve agents reported by Anslyn and Phillips.<sup>10</sup>

(Scheme 78).<sup>10</sup> Transfer of this sample to a second vessel containing autoinductive amplifier molecule **332**, led to cleavage of the Si–O bond to afford phenolate **333** that disassembles by a series of 1,4- and 1,6-eliminations to give six fluoride ions and, initially, *para*-aminobenzaldehyde. Careful examination of the reaction products revealed that the colourimetric response was attributable to a group of short oligomers **334** (2–10 monomer units, monitored at  $\lambda = 425$  nm) derived from the first-formed *para*-aminobenzaldehyde; by inference, this is probably true in other systems that have used this indicator as readout. The fluoride ions produced during amplification can then be used in a third vessel to release fluorophore **91** from G1 dendron **335**, allowing readout by fluorescence methods ( $\lambda_{\text{max}} = 520$  nm).

The high effectiveness of readout from an assay by chemiluminescence has led a number of groups to explore this in the context of signal amplification; for example, in fluoride assays. Below is exemplified three approaches based around the Schaap dioxetane; first, Shabat has synthesised autoinductive molecule **336** wherein the cleavage of the O–Si bond to give phenolate **337** simultaneously promotes chemiluminescence and, by 1,6-elimination, release of a fluoride ion to restart the cycle (Scheme 79).<sup>286</sup> Second, Akkaya has developed their dendritic probe **277** (Scheme 61) to accommodate a third arm in the dendron that carries a self-immolative aniline (**338**).<sup>287</sup> This aniline moiety, by 1,6-elimination, releases two fluoride ions, facilitating a dendritic chain reaction. Third, Hisamatsu *et al.* used a two-component system (Scheme 79) where

dendron **339** upon triggering with fluoride releases two fluoride ions, leading to exponential amplification; once amplification is complete, **340** is added inducing its fragmentation with chemiluminescence from the excited state of **341**.<sup>288</sup> A straightforward system for fluoride amplification that works with particularly simple molecular components was reported by Gabrielli and Mancin in 2017.<sup>289</sup>

The fluoride dependent DCR systems noted above, proceed by cleavage of strong C(sp<sup>3</sup>)–F bonds. This release profile is inherently slow as fluoride is a poor nucleofuge; also, in the case of difluoromethyl groups, a high energy fluorinated quinomethide is formed. Anslyn and co-workers overcame this structural issue with the addition of benzoyl fluoride as a latent source of fluoride (Scheme 80).<sup>290</sup> Cleavage of the *tert*-butyldimethylsilyl ether trigger group of the dendron **342** led to the release of three equivalents of 4-amino-1,8-naphthalimide **91**, as the reporting fluorophore. The resultant dendritic core, 2,4,6-tris(hydroxymethyl)phenolate, was able to react with benzoyl fluoride (catalysed by 1,5-diazabicyclo[4.3.0]non-5-ene) to release up to four fluoride anions for subsequent triggering events.

Developing their work on an autoinductive cascade for sensing of thiols, to detect V-class nerve agents, Anslyn and Marcotte utilised a cyclisation–elimination, self-immolative linker to release a fluorescent 4-amino-1,8-naphthalimide **91** that can be the subject of ratiometric fluorescence sensing (Scheme 81).<sup>291,292</sup> Thus, a thiol is generated from the analyte *e.g.* VX nerve agent simulant demeton-*S*-methyl (DSM), and enters an amplification cycle by cleavage of 2-hydroxyethyl di-





Scheme 79 Autoinductive, DCR and two-component fluoride sensors with a chemiluminescent response.<sup>286–288</sup>

sulfide **343** to afford two equivalents of  $\beta$ -mercaptoethanol which then reacts with Meldrum's acid derivative **344** to liberate two equivalents of methylmercaptan for each molecule of  $\beta$ -mercaptoethanol consumed. Once the amplification has occurred, the sample may be analysed by addition of disulfide **345**. Upon cleavage of the disulfide to give, for example, **346** cyclisation–elimination occurs to afford **196** with concomitant decarboxylation and release of fluorophore **91**. A detailed explanation of a simple-to-apply method of data analysis, based upon chromaticity, using a cell phone was presented.

Recently, Milliron and Anslyn have incorporated Meldrum's acid derivatives related to **344** as a linker into hydrogel structures.<sup>293</sup> This has allowed their facile, self-propagating decomposition *via* a 'declick' reaction in response to the presence of thiols, with reporting by significant changes to their physical properties and release of dyes. These hydrogels have been applied to the detection of tabun mimics.

## 4 Self-immolative polymeric systems

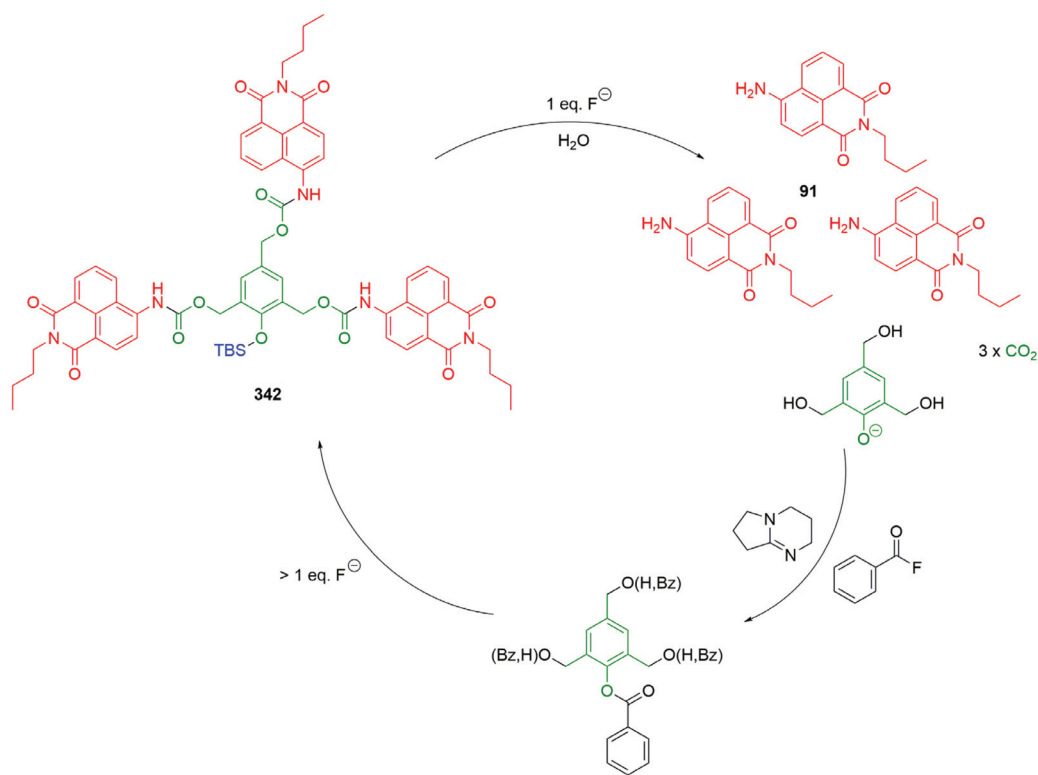
### 4.1 Self-immolative polycarbamates and polycarbonates

Shabat and co-workers reported the first example of a self-immolative linear polymer in 2008.<sup>294</sup> The polycarbamate **347**

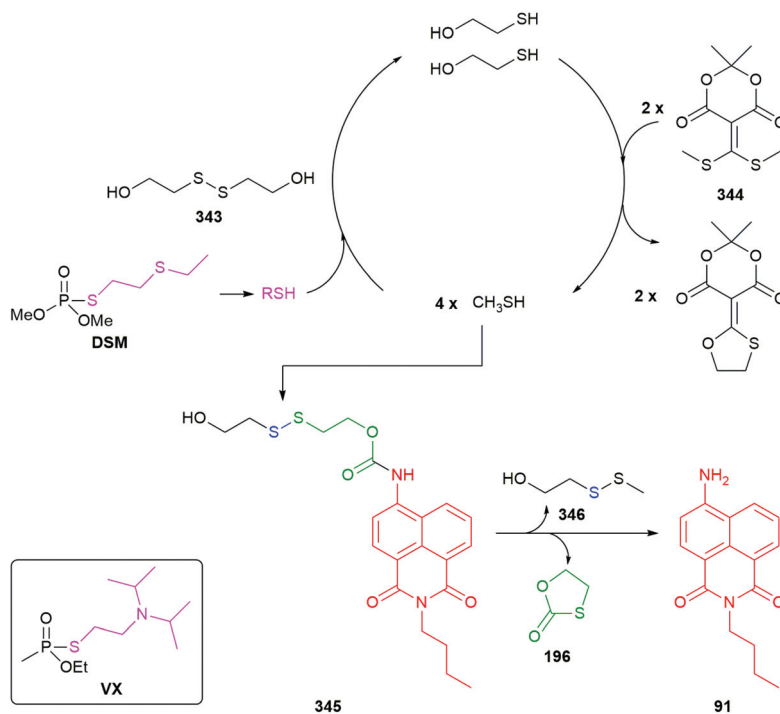
was based on a 4-aminobenzyl alcohol linker that had been used previously in prodrugs,<sup>295</sup> self-immolative dendritic systems,<sup>296</sup> and oligomers.<sup>297</sup> In this system, enzymatic action by BSA in PBS-buffered media promoted cleavage of the butanone trigger group and led to amplified release of fluorogenic aniline-acrylate monomers (Scheme 82). In the context of this self-immolative polymer system, the short oligomers of a 4-aminobenzyl alcohol linker prepared by Scheeren *et al.*,<sup>162</sup> to create extended linkers and activatable anticancer prodrugs plus the studies of Warnecke and Kratz<sup>297</sup> on structurally-related materials whereby elimination was triggered by reduction, are both worthy of mention as they laid out key principles in terms of the degradation process for linker units of this type. Trigger activation and cleavage allows for the aniline linker to undergo a head-to-tail disassembly *via* a series of sequential decarboxylation and 1,6-aza-quinone methide eliminations. Upon the depolymerisation the side product, aza-quinone methide, undergoes rapid conversion to the corresponding 4-aminobenzyl alcohol under the aqueous conditions used. The success of these initial studies on self-immolative polybenzylcarbamates have laid the foundation for extensive exploitation of this system as outlined in the following section.

The degradable 4-aminobenzyl alcohol linker unit has now been utilised successfully as the scaffold upon which to build





**Scheme 80** Silyl protected self-immolative dendron **342** capable of DCR with the addition of benzoyl fluoride as a latent source of fluoride to enhance the rate of disassembly, as described by Anslyn and co-workers.<sup>290</sup>

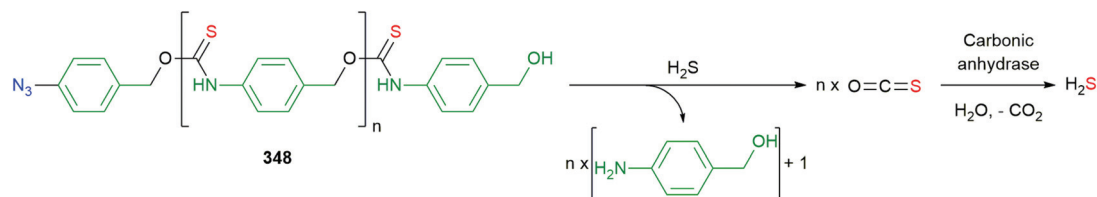


**Scheme 81** Anslyn and Marcotte's self-propagating chemical cascade for the detection and quantification of V-series nerve agents.<sup>291,292</sup>





**Scheme 82** Self-immolation linear polymer **347** capable of 1,6-elimination resulting in head-to-tail depolymerisation.<sup>294</sup>



**Scheme 83** A self-immolation linear polythiocarbamate **348** capable of 1,6-elimination resulting in amplification of an  $\text{H}_2\text{S}$  signal.<sup>110</sup>

complex polycarbamate drug delivery or detection systems whose degradation can be triggered by a diverse range of stimuli and in aqueous media.<sup>298–301</sup> For example, Matson and co-workers derivatised this linkage as a polythiocarbamate **348**, the trigger was activated by reduction with  $\text{Na}_2\text{S}$  forming an aniline, depolymerisation *via* aza-quinone methides resulted in the 4-aminobenzyl alcohol linker and carbonyl sulfide (COS) which was converted into  $\text{H}_2\text{S}$  in the presence of carbonic anhydrase, thus amplifying the release (Scheme 83).<sup>110</sup> In contrast to the example shown in Scheme 82, in this case, the linker serves just that function and reporting is done *via* the COS liberated from the thiocarbamate.

Systematic developments by the Phillips group on self-immolative oligocarbamates featuring a boronic ester trigger unit have led to the development of elegant microfluidic point of care colorimetric indicator devices for the quantification (at femtomole levels) of active enzymes.<sup>158,302,303</sup> Related studies using the same boronic ester trigger group have also led to the successful generation of colorimetric microfluidic multilayer devices capable of assessing the concentration of heavy metal salts ( $\text{Pb}^{2+}$  and  $\text{Hg}^{2+}$ ) in water.<sup>304</sup> Within discrete layers within the multilayer device are located a DNzyme, bead-bound glucose oxidase (GOX), glucose, the hydrophobic self-immolative polycarbamate, a food colouring and finally at the external viewing location in the assembly a layer of absorbent white paper. When the metal contaminated water sample is applied to the device, in the case of the  $\text{Pb}^{2+}$  metal ions, they activate the DNzyme which cleaves the GOX from its bound state enabling it to travel to the region of the device where it can react with the store of glucose, in turn generating hydrogen peroxide that then triggers the self-immolation of the polycarbamate. The hydrophobicity of this polymer layer decreases as the material degrades, enabling the aqueous phase to perme-

ate into the food dye and wet the external white paper layer affording a colorimetric response. Redy and Shabat have employed<sup>305</sup> an oligocarbamate featuring side chains to yield a modular prodrug system that generates a fluorescent signal through a FRET-activated self-immolative linker.

Following their earlier studies<sup>294</sup> wherein the function of linker and reporter are combined (Scheme 82), Gnaim and Shabat have adapted<sup>43</sup> the approach to allow chemiluminescent sensing of a range of analytes, according to the nature of the trigger group, **349a** (fluoride), **349b** ( $\text{H}_2\text{O}_2$ ) and **349c** Pd(0) (Fig. 22). The polymeric nature of the sensor offers significant sensitivity advantages over the equivalent small self-immolative molecules (for examples see section 2.1).

In 2014, Peterson *et al.* described<sup>306</sup> the site-specific thermal activation of a self-immolative polybenzylcarbamate-PDMA block copolymer **350**. In this block copolymer system, the two polymer blocks were joined by a temperature-sensitive oxazine linker unit (Scheme 84). At temperatures ranging between room temperature and  $85\text{ }^\circ\text{C}$ , the oxazine trigger unit was found to undergo thermal retro- $[4_\pi + 2_\pi]$  reaction followed by hydrolysis of the acyl nitroso moiety to permit depolymerisation of the block polymer in solution. These degradation temperatures are far lower than observed for poly(phthalaldehyde) block copolymers<sup>307</sup> ( $>150\text{ }^\circ\text{C}$ , however, the ceiling temperature of self-immolative poly(phthalaldehyde)s can be tuned to easily accessed conditions, see section 4.3). The oxazine unit degrades to the corresponding free amine *via* the unstable carbamoylnitroso and carbamic acid intermediates to permit depolymerisation of the polybenzylcarbamate block.

Trigger groups sensitive to UV irradiation such as perylene-3-yl units have been coupled to amphiphilic polybenzylcarbamates capable of self-assembling into polymersomes.<sup>300</sup> These stable polymersome assemblies can encapsulate photodynamic therapy agents such as eosin Y or other drug pay-



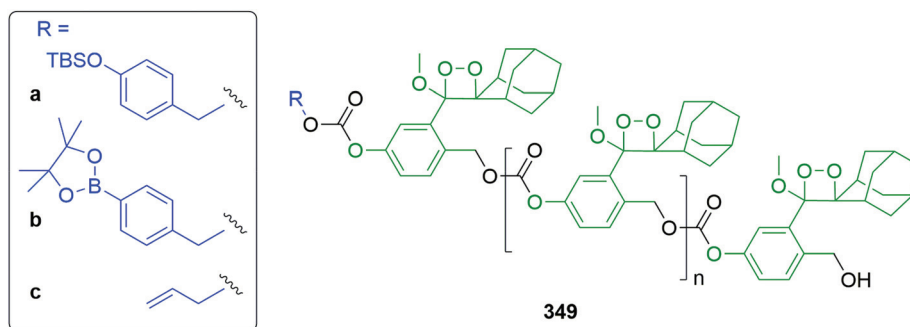
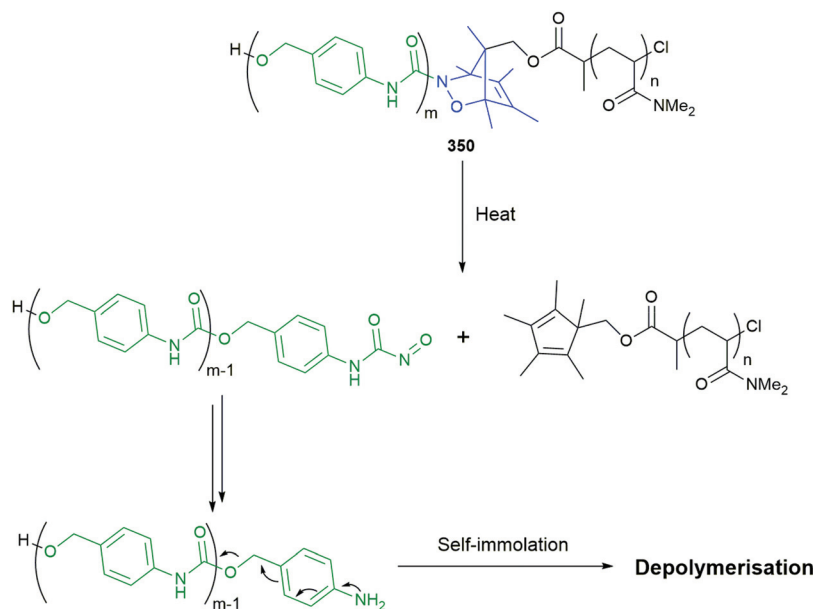


Fig. 22 Shabat's chemiluminescent self-immolative polymers **349a–c** equipped with various triggers.<sup>43</sup>



Scheme 84 The self-immolative polybenzylcarbamate-PDMA block copolymer **350** reported<sup>306</sup> by Peterson *et al.* featuring a temperature sensitive oxazine linker unit which can be degraded thermally to permit self-immolation of the polybenzylcarbamate block.

loads. Exposure of the photo-sensitive polymersomes to UV light (420 nm) for a period of thirty minutes leads to self-immolation of the carbamate blocks and results in disintegration of the polymersomes (so-called 'SIPsomes') and release of the reactive payload (Scheme 85). Liu *et al.* have also employed the perylene-3-yl trigger unit successfully in a hyper-branched polycarbamate functionalised with doxorubicin and hydrophilic PEG chains plus cell membrane targeting RGD units to facilitate spatiotemporal intracellular drug delivery in aqueous media.<sup>308</sup> Cornelissen and co-workers have reported an analogous photochemically initiated approach for the triggered degradation of polycarbamates and release of monomeric 4-aminobenzyl alcohol subunits from virus-like assemblies using 5-methoxy-2-nitro benzyl alcohol as the photolabile unit.<sup>309</sup> In 2020, Kumar *et al.* reported<sup>301</sup> the use of the photolabile 2-nitrobenzyl alcohol trigger system in conjunction with self-immolative amphiphilic polybenzylcarbamates to generate self-assembled vesicles that carry an enzyme payload. Upon

photochemical activation, the polybenzylcarbamate structure degrades leading to vesicle disassembly and ultimately payload release. The liberated enzyme promotes the formation of a stable hydrogel and thus triggered destruction of a polymer can be utilised to construct a different polymer-based material. The use of photolabile units in conjunction with degradable polycarbamates based on the 4-aminobenzyl alcohol repeat unit has also been utilised by Chujo *et al.* to yield highly efficient self-immolative hybrid colorimetric materials.<sup>310</sup>

Liu, Hu and co-workers have recently developed amphiphilic micellar polyurethane nanoparticles that can be degraded in a self-immolative fashion *via* exposure to only trace quantities of the appropriate stimulus.<sup>311</sup> The nanoparticles feature both external and internal 'built-in' triggers, activation of the external trigger liberates primary amine species capable of penetrating the micelle to react with and degrade the contents of the micelle in an amplified manner. This approach to highly efficient degradation of micellar systems (as demonstrated in this study using





**Scheme 85** The self-assembly of self-immolative polymersomes ('SIPsomes') from amphiphilic block copolymers capable of releasing an encapsulated payload of the photodynamic therapy agent Eosin Y as reported by Liu *et al.*<sup>300</sup>

a range of stimuli including enzymes or irradiation) offers an attractive route to the development of nanovectors to treat disease states<sup>312</sup> such as cancer *via* targeted means.

In contrast to the polymer degradation processes outlined above, Zhang *et al.* reported<sup>313</sup> in 2021 an alternative use of the quinone methide elimination cascade process whereby polycarbamates are produced *via* the controlled ring opening polymerisation<sup>314,315</sup> of macrocyclic monomers (Scheme 86). In this innovative study, a nucleophilic amine (such as *N*-hexylamine) was used to trigger the ring opening of a macrocyclic carbonate-benzylic carbamate **351** that then, in turn, degrades *via* the quinone methide elimination cascade process to yield a newly formed carbamate featuring a nucleophilic amine terminus that can then propagate chain growth. The lability of the carbonate unit in these carbonate-carbamate macrocycles was enhanced by the presence of an electron-withdrawing nitro group located on the phenyl ring *ortho*- to the carbonate and control of the polymerisation was improved by the addition of a nucleophilic trapping agent. In these studies, the relatively weak nucleophile, *N*-methylaniline, was employed to trap the reactive quinone methide generated in the self-immolative ring opening step. This aniline was insufficiently nucleophilic in nature to trigger ring opening and chain growth. Using this strategy, excellent control of the polymerisation was afforded with monomer conversions up to 97% and polydispersity (*D*) values as low as 1.06.

DeWit and Gillies developed the first self-immolative polymer containing alternating elimination and cyclization

spacers in 2009.<sup>316</sup> This system, **352**, was constructed using 4-hydroxybenzyl alcohol as the 1,6-elimination linker and *N,N'*-dimethylethylenediamine as the cyclization linker (Scheme 87). A self-immolative polycarbamate capped with a Boc protecting group was prepared and subsequent cleavage of the trigger group afforded self-immolative depolymerisation, yielding *N,N'*-dimethylimidazolidinone, 4-hydroxybenzyl alcohol, and CO<sub>2</sub>. In an extension of this study, Gillies and co-workers have been able to tune the rates of polymer degradation by replacing the cyclization linker, *N,N'*-dimethylethylenediamine, with *N*-methylaminoethanol **353** or 2-mercaptoethanol **354** (Scheme 87).<sup>317</sup> In 2013, McBride and Gillies described a detailed study of the effect of the chain length on the kinetics of self-immolative depolymerisation involving alternating elimination and cyclization; a proportional relationship between polymer chain length and the depolymerization time was established.<sup>318</sup> Further refinement of this elimination/cyclization approach by Gillies and co-workers involved<sup>319</sup> the use of an orange-coloured diazo trigger group to permit a colourimetric indicator for depolymerisation – in an approach related to the report of Hay and co-workers on the effect of leaving group effects in reductively triggered fragmentation of 4-nitrobenzyl carbamates,<sup>50</sup> reduction of the azo unit with hydrazine affords the corresponding electron rich hydrazine<sup>320</sup> that can then promote self-immolation and depolymerisation to yield a colourless solution.

Almutairi and co-workers have developed<sup>321</sup> a photochemically driven cyclization/elimination triggering process to





**Scheme 86** The controlled ring-opening polymerization of a macrocyclic monomer **351** employing the quinone methide elimination cascade reaction.<sup>313</sup>



**Scheme 87** Linear self-immolative polymers **352–354** containing alternating linkers as described by Gillies and co-workers.<sup>316,317</sup>

initiate the depolymerisation of polycarbamates (Fig. 23).<sup>322</sup> In this study, the trigger groups used on the polymer chain ends were either an *ortho*-nitrobenzyl residue **355** (for cleavage *via*

UV-irradiation) or 4-bromo-7-hydroxycoumarin **356** (sensitive to NIR light) that were coupled to the polycarbamate *via* a diamine cyclisation linker. Photo-irradiation cleaves the trigger

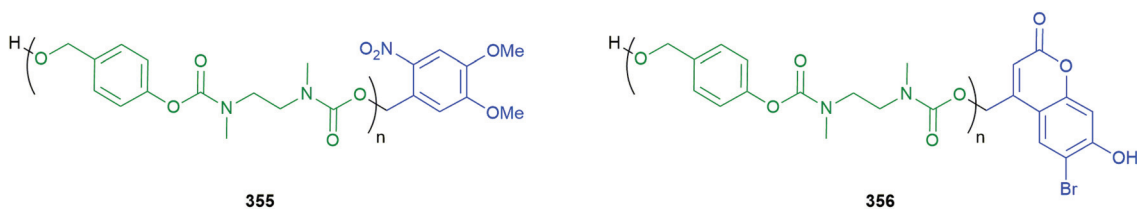


**Fig. 23** Example polycarbamate structures **355** and **356** reported by Almutairi and co-workers that undergo photochemically induced depolymerisation *via* a cyclisation/elimination process.<sup>322</sup>



group (*via* single photon and two photon absorption processes for UV and NIR exposure, respectively) permitting cyclization by the liberated amine end group that in turn promotes depolymerisation. Further work from these authors has studied photochemically triggered depolymerisation of polycaprolactone particles, with payload release.<sup>323</sup> Similarly, controlled degradation of poly(lactic-*co*-glycolic acid)-based and ornithine-based polymers were studied.<sup>324,325</sup>

UV-triggered self-immolative polycarbamate systems have also been reported by the Cheng research group that successfully demonstrate 2-directional polymer cleavage<sup>326</sup> and the ability to exhibit controlled delivery of the anti-cancer drug, 9-aminocamptothecin.<sup>2</sup>

Zimmerman and co-workers have demonstrated a new type of base-triggered self-amplifying self-immolating polycarbamate based on the Fmoc protecting group 357.<sup>327</sup> The polymer was obtained through polycondensation of the Fmoc-derivative, a diol, with hexamethylene diisocyanate and a catalytic amount of dibutyltin dilaurate. Several bases were screened to optimise the degradation of the polymer, hexylamine was selected as the appropriate base with which to initiate the E1cB elimination pathway. Deprotonation of the acidic methine proton of the fluorenylmethyl unit triggers the E1cB elimination and chain scission *via* a decarboxylation process leading to the production of two shorter polymer chains, one possessing a dormant fluorenyl end group and the other bearing a primary amine that is then capable of triggering further depolymerisation (Scheme 88). Evidence for the autocatalytic nature of this self-immolative depolymerisation process was provided by the sigmoidal shape of the plots of the <sup>1</sup>H NMR spectroscopic data *vs.* time for the degradation of the polycarbamate 357.

Zimmerman and co-workers advanced this further with the addition of the photo-cleavable trigger *ortho*-nitrobenzyl carbamate.<sup>328</sup> Exposure to UV irradiation (365 nm) promoted photo-lytic cleavage, activating the trigger through a Norrish-type II

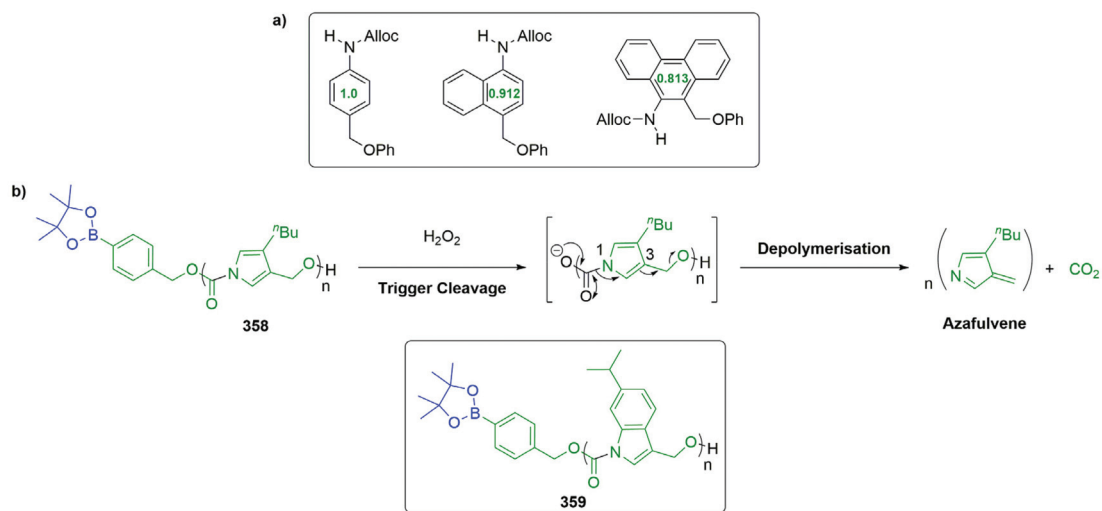
reaction mechanism, generating a nitrosobenzaldehyde and a primary aliphatic amine. The free amino groups can then act as a trigger to induce further self-immolation of the base sensitive Fmoc carbamate units in the polymer backbone. After irradiation at room temperature for 40 minutes and incubation at room temperature for 24 hours, only low molecular weight species were observed *via* GPC analysis. Zimmerman and co-workers noted that unlike the Fmoc containing polymer 357,<sup>327</sup> the degradation kinetics of the photo-triggered polymer did not show an exponential profile as expected for a self-amplifying system. This was attributed to quenching of the free amine *via* a Schiff base type reaction with the nitrosobenzaldehyde generated in the photocleavage of the trigger. More recently, Barner-Kowollik and co-workers have reported closely-related studies that involved the non-amplified photolysis of polyurethanes.<sup>329</sup>

Phillips and co-workers have developed recently a new class of self-immolative polymer, poly(carboxypyrrole)s, that are capable of undergoing complete head-to-tail depolymerisation in the solid state, offering a potential route to selectively depolymerisable adhesive and coating materials (Scheme 89).<sup>330</sup> Pyrrole was selected as the core for the repeat unit based upon observations in an earlier study by the Phillips group that reduction in the aromaticity of the central ring (using 1,4-disubstituted benzene, 1,4-disubstituted naphthalene and 9,10-disubstituted phenanthrene as the model substrates) provided an increase in the rate of triggered release of the pendant benzylic group.<sup>331</sup> Analogous calculations predicted that pyrrole would be 40% less aromatic than benzene,<sup>332,333</sup> hence it was anticipated that the depolymerisation rate would be faster. Polymerisation of bifunctional pyrrole monomers bearing phenyl carbamate at position 1 and a nucleophilic alcohol at position 3 of the heterocycle was achieved by heating at 60 °C using catalytic quantities of 1,8-diazabicycloundec-7-ene (DBU) in the presence of an alcohol functionalised end-capping unit equipped with a stimuli-responsive



**Scheme 88** The base-triggered Fmoc-derivative self-immolative polycarbamate 357 as described by Zimmerman and co-workers.<sup>327</sup>





**Scheme 89** (a) Calculated relative aromaticity values for three different aromatic systems (values shown in green correspond to rings without substituents);<sup>331</sup> (b) head-to-tail depolymerisation of poly(carboxypyrrole) **358** as described by Phillips and co-workers plus the analogous poly(carboxyindole) **359** assessed in this study.<sup>330</sup>

moiety. Depolymerisation of **358** that featured an aryl boronate trigger group ((4-(4,4,5,5-tetramethyl-1,3,2-dioxaborolan-2-yl)phenyl)methanol) *via* exposure to hydrogen peroxide resulted in rapid head-to-tail depolymerization to the corresponding azafulvene units within 40 minutes (Scheme 89). Within this study, Phillips and co-workers also reported the synthesis of an analogous poly(carboxyindole) **359** to strengthen the hypothesis that lower aromaticity affords more rapid depolymerization (see Table 1 for the resonance energy per  $\pi$ -electron).<sup>330,331</sup> Exposure of poly(carboxyindole) **359** to

hydrogen peroxide under the same degradation conditions as **358** revealed that poly(carboxyindole) depolymerizes twelve times slower than the poly(carboxypyrrole), thus supporting this hypothesis. Phillips and co-workers further demonstrated that **358** could undergo depolymerisation in the solid state within 9 hours when moulded into a disc with 40 wt% poly(ethylene glycol) ( $M_n = 400$ ) used as a plasticizer.

Almutairi and co-workers have also developed biocompatible polymeric capsules, prepared from polyesters that contain self-immolative dendron units; these capsules were able to carry cargo molecules, *e.g.* Nile Red or fluorescein diacetate. The dendron units are triggered by, and degrade in response to biologically relevant levels of  $H_2O_2$  (produced by cells in oxidative stress).<sup>334</sup> Capsules generated from polymers **360** and **361** (Fig. 24) were shown to undergo significant morphological changes on exposure to hydrogen peroxide, with release of Nile Red. Polymer **361** showed release of the cargo molecule fluorescein diacetate. Thus, these self-immolative materials are candidates for delivery of bioactive molecules.

**Table 1** Theoretical values of aromaticity for aromatic systems

Compound	Resonance energy per $\pi$ -electron (unit = $\beta$ )
Benzene	0.065
Pyrrole	0.039
Indole	0.047

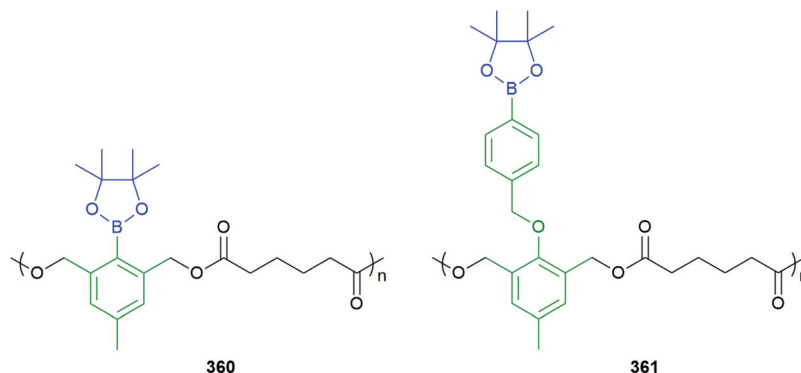
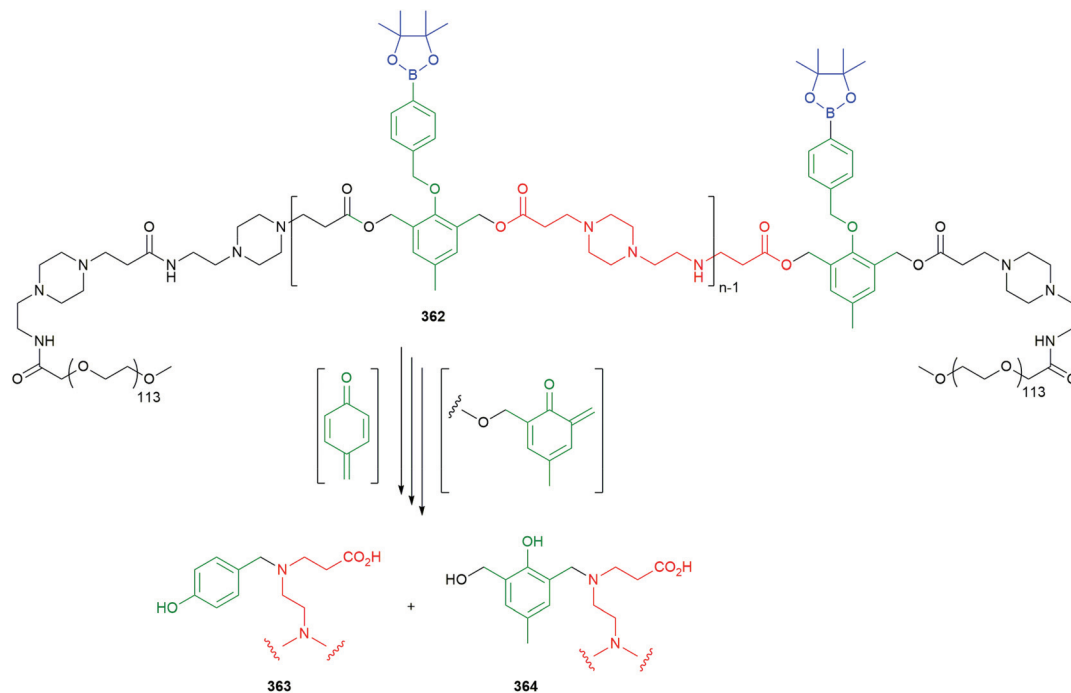


**Fig. 24** The repeat units used in self-immolative polymer-based capsules by Almutairi and co-workers.<sup>334</sup>





**Scheme 90** Du and Li's pH/H<sub>2</sub>O<sub>2</sub> sensitive self-immolative, amphiphilic poly(amino ester) **362**.<sup>51</sup>

In similar style, Du and Li have reported amphiphilic poly(amino ester)s that are degraded in the presence of hydrogen peroxide.<sup>51</sup> The copolymers represented by **362** in Scheme 90 had PEG chains attached, primarily at the primary terminal amines with limited attachment at the internal secondary amines. These amphiphilic copolymers self-assemble in aqueous media into nanoparticles and have proved responsive to both pH and hydrogen peroxide. Of general interest, is an extensive study of trapping of the quinone methides formed during self-immolation, with the amines (reporter groups) produced during the fragmentation process. These can give rise to compounds such as **363** and **364**.

Ansyn has introduced a fascinating and important set of sequence defined N-to-O repeating oligocarbamates such as **365** shown in Scheme 91 that have been shown to be readable using a single LC/MS trace as a result of their self-immolative nature.<sup>335</sup> Taking inspiration from Li's lactonization depolymerisation, Ansyn *et al.* established conditions for the controlled self-immolation of the oligocarbamates, initiated by reversible deprotonation of the primary alcohol as trigger (K<sub>3</sub>PO<sub>4</sub>, MeOH/H<sub>2</sub>O, 70 °C) and proceeding *via* a series of 5-*exo-trig* cyclisations (Scheme 91).<sup>336</sup> Excitingly, the potential in information storage has been addressed in a recent paper.<sup>337</sup> In addition to information storage, this system also has potential in areas such catalysis and self-assembly.

#### 4.2 Self-immolative poly(benzyl ether)s

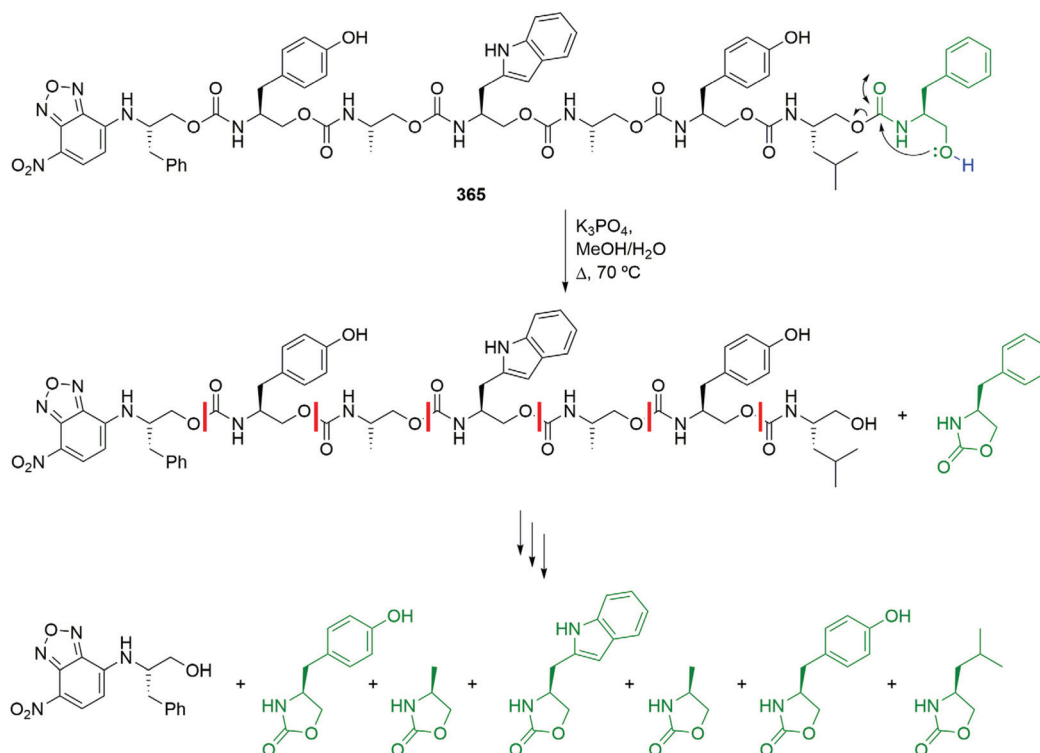
In 2003 McGrath and coworkers demonstrated the triggered degradation of branched polybenzyl ethers (PBEs) to permit both linear<sup>252</sup> and geometric dendrimer disassembly (so-called 'dendritic amplification') *via* a 1,6-elimination pathway analo-

gous to that observed in the self-immolation of materials featuring 4-aminobenzyl alcohol repeat units (*vide supra*).<sup>338</sup> Subsequent studies of the linear disassembly of dendritic oligomers<sup>339</sup> or oligomers involved structures that were based upon vanillin or *ortho*-vanillin as the cleavage vectors<sup>340</sup> in conjunction with either allyl or *ortho*-nitrobenzyl trigger groups (Fig. 25).

In the light of the above developments, in 2013 Phillips and co-workers reported the synthesis and degradation analysis of self-immolative linear PBEs (Scheme 92).<sup>341</sup> In this study, PBEs **366** were synthesised *via* anionic polymerisation of quinone methide monomers and capped with a range of stimulus-responsive (trigger) groups. Cleavage of the triggering group generates a phenolate which is capable of a 1,6-elimination cascade, releasing the quinone methide monomeric units and resulting in rapid depolymerisation within a few hours. The ether linkages of the PBEs offer a higher stability to acid, base, and heat which would cause unwanted degradation of a self-immolative polycarbamate or polycarbonate.

Subsequent evolution of this system led to the development of PBE-based materials (Fig. 26) that incorporated detection units onto each repeating unit and amplified depolymerisation in the solid-state was demonstrated in a colorimetric fashion.<sup>47</sup> Treatment of a rigid solid disk of PBE **367** with a solution of TBAF led to cleavage of the silyl ether trigger group and self-immolation of the polymer, with rapid reduction in the size of the polymer disk and release of the purple coloured, deprotonated quinone methide **368** (Fig. 26) into the solvent used (acetonitrile). In contrast, in the case of the analogous PBE where the trigger group was situated *only* at the polymer chain end, the degradation of cast disks proved to be negli-





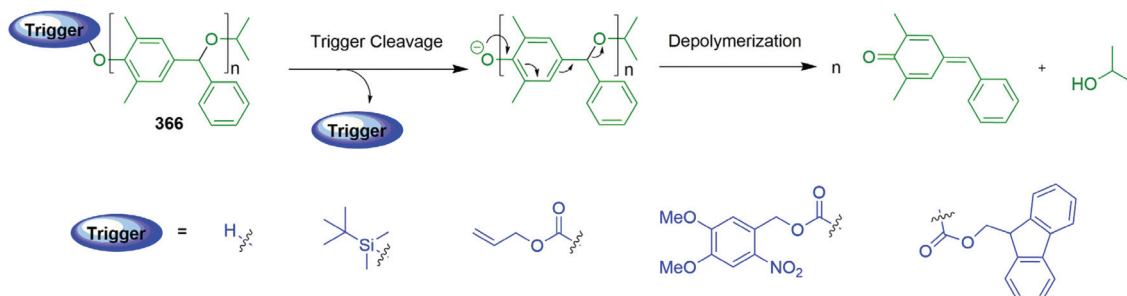
Scheme 91 Oligocarbamates information storage systems such as **365** reported by Anslyn and co-workers.<sup>335,337</sup>



Fig. 25 (a) Vanillin and (b) *ortho*-vanillin-based oligomers developed by McGrath and coworkers that degrade via the 1,6-elimination pathway upon activation of either the allyl or an *ortho*-nitrobenzyl trigger groups ( $n = 1-3$ ).<sup>340</sup>

gible, even after exposure to TBAF over more than seven days. A triggered degradative response of this type is extremely attractive in applications where dramatic changes in physical form of a polymer is needed (such as debond on demand) or where colorimetric disclosure of the presence a reactive agent on a surface may be needed. Indeed, the Phillips group extended the triggered decay of PBEs featuring silyl ethers using fluoride anion sources to demonstrate successful degradation of a cross-linked prototype adhesive.<sup>4</sup>

In an approach to demonstrate the applicability of self-immolative processes in polymer recycling, PBEs modified with tri(ethylene glycol) or fluoroalkyl groups to access desirable physical and mechanical properties of plastics were described in 2015 by Phillips and co-workers.<sup>342</sup> These modified PBEs featured a phenolic end group and thus were depoly-



Scheme 92 Disassembly pathway of a self-immolative poly(benzyl ether)-based polymer **366** with different triggers.<sup>341</sup>





**Fig. 26** The self-immolative PBE system **367** capable of revealing a colorimetric response (in the form of the purple coloured deprotonated quinone methide **368**) in the solid state.<sup>47</sup>

merised in a head-to-tail depolymerisation fashion at ambient temperatures upon exposure to the base, 1,8-diazabicycloundec-7-ene (DBU), and the recovered monomeric materials were of sufficient purity to permit repolymerisation, thus demonstrating end-of-life recycling capabilities.

Successful triggering of the self-immolation of PBEs bearing silyl ethers by fluoride anions is a strategy that has been employed by several other research groups to achieve materials with antimicrobial activity with reduced hemolytic toxicity<sup>343,344</sup> and degradable polymer brush architectures.<sup>345</sup> Bringing key aspects from these studies and those led by Phillips<sup>4,47,342</sup> (*vide supra*) have enabled Zhang and co-workers to develop so-called 'side chain-immolative polymers (ScIPs)'

based upon the PBE scaffold.<sup>346</sup> The ScIP PBEs in this case bear pendant pyridine disulfide units (Scheme 93), that, in the presence of thiols can undergo thiol-disulfide exchange reactions to prepare ScIP-*g*-PEG graft polymers and organogel networks. The self-immolative degradation of these ScIP PBE-based materials could, in theory, be triggered *via* two different approaches – (i) exposure to reductive cleavage conditions for the disulfide linkages in either the grafted side chains or organogel or (ii) treatment with a fluoride ion source to target reaction with the silyl ether chain end of the PBE backbone. On account of the higher density of the disulfide groups present in either of these ScIP PBE-based materials when compared to the chain end silyl ether trigger unit, it was found that treatment using reductive conditions in a basic environment (DTT in combination with DBU) led to rapid depolymerisation both in the solution and solid state. In stark contrast, when exposed to TBAF, a solid pellet of the parent ScIP PBE featuring the pendant pyridine disulfide units did not degrade over the same time frame (*ca.* 5 hours) demonstrating the advantage to rapid depolymerisation of solid-state materials that possess active side chains to permit self-immolation, in agreement with Phillips.

#### 4.3 Self-immolative poly(phthalaldehyde)s

Polyphthalaldehydes (PPAs), first reported in the late 1960s by Aso and Tagami,<sup>347,348</sup> are known to degrade under acidic



**Scheme 93** The side chain-immolative polybenzylether system (ScIP) reported by Zhang and co-workers.<sup>346</sup>





**Scheme 94** a) Head-to-tail depolymerisation of PPAs 369 as described by Phillips and co-workers; (b) selective degradation of a cylindrical region of a patterned film featuring a self-immolative PPA 370 reactive to fluoride ion sources such as TBAF.<sup>351</sup>

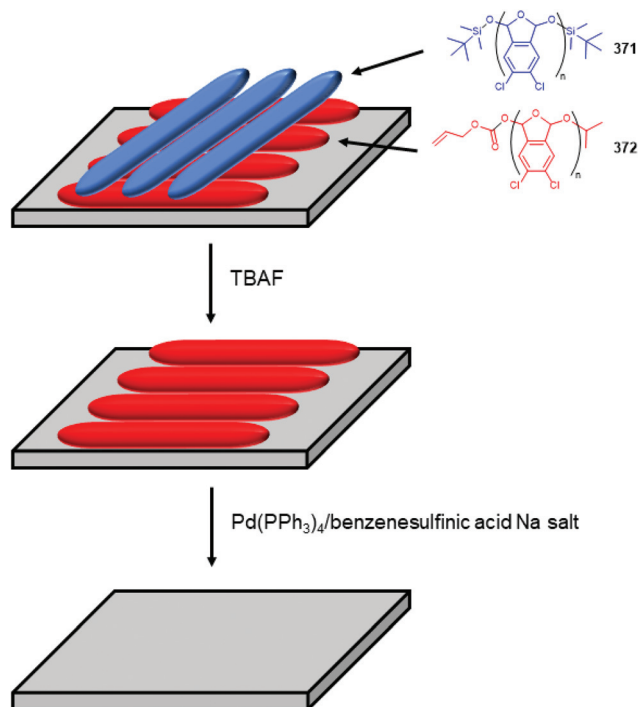
conditions.<sup>349,350</sup> They have now, however, been modified<sup>351</sup> with stimuli-responsive end-capping units by Seo and Phillips in order to introduce chemoselective self-immolative character to these materials. For example, the PPA 369 shown in Scheme 94a was generated from 1,2-benzenedicarboxaldehyde *via* anionic polymerisation and the reactive chain end capped with either an allyl or TBDMS group.<sup>351</sup> This approach to self-immolative materials was based upon a PPA which had been used successfully in photoresist technologies by Willson and Fréchet<sup>352</sup> and further refined for greater sensitivity by Ito and Willson.<sup>353,354</sup> In the case of the PPA bearing the TBDMS end capping group 370, exposure to a solution of TBAF resulted in the cleavage of the silyl trigger leading to formation of the hemiacetal and subsequent depolymerisation within 15 minutes. As part of this study, it was demonstrated that the self-immolative degradation of this type of polymer was very effective in the solid state. Patterned films (approximately 0.5 mm thick) were cast where defined regions of the film (a cylinder) were composed of the polyphthalaldehyde 370 and the rest of the film was a made from control polyphthalaldehyde that did not feature an end group sensitive to fluoride ions. When the patterned composite film was exposed to a buffered solution of TBAF for a period of only fifteen minutes and then washed with diethyl ether (to remove the 1,2-benzenedicarboxaldehyde) a cylindrical hole in the plastic film was revealed (Scheme 94b). In a manner similar to PBEs, PPAs are known to undergo rapid depolymerisation because of a significant lowering in ceiling temperature ( $T_C$ ) when the capping group is cleaved (the  $T_C$  of the hemiacetal is  $-40$  °C). Further studies by the Phillips group led to the development of PPAs with triggering groups located at both ends of the polymer chains in order to optimise the degradation rates.<sup>355,356</sup>

Sen, Phillips and co-workers reported further advances in self-immolative PPAs by reporting self-powered microscale

pumps which undergo depolymerisation with a fluoride stimulus.<sup>357</sup> The depolymerisation of an insoluble polymer causes the release of highly soluble monomers simulating a concentration gradient capable of moving fluids on a micrometer-scale. It was further demonstrated that the pump could be activated (or turned “on”) with the enzyme  $\beta$ -D-glucuronidase by synthesizing a separate self-immolative spacer capable of releasing fluoride ions upon activation by the enzyme. Phillips and co-workers also developed core-shell microcapsules which resulted in head-to-tail depolymerisation in an amplified response to fluoride.<sup>358</sup> The ability to employ PPAs in melt extrusion additive manufacturing processes is limited as a result of the thermal instability of linear PPAs. Phillips and co-workers proposed that polymer degradation may arise from non-specific cleavage of either the end-cap or the polymer backbone, or a combination of the two mechanisms.<sup>359,360</sup> To overcome the issue of instability, Phillips and co-workers synthesised polymers with the addition of electron-withdrawing chloride groups *para*- to the benzylic acetals (poly(4,5-dichlorophthalaldehyde (PCL<sub>2</sub>PA)); by doing so, the formation of the oxocarbenium ion intermediates would be disfavoured. This hypothesis was proved as variants of PCL<sub>2</sub>PA featuring different trigger groups (371 and 372) was shown to be suitable for selective laser sintering and selective layers of the resultant 3D image (that were doped with different coloured dyes to aid visualisation of the degradative processes) could be degraded *via* controlled exposure to the different chemical triggering agents (Scheme 95).<sup>359</sup>

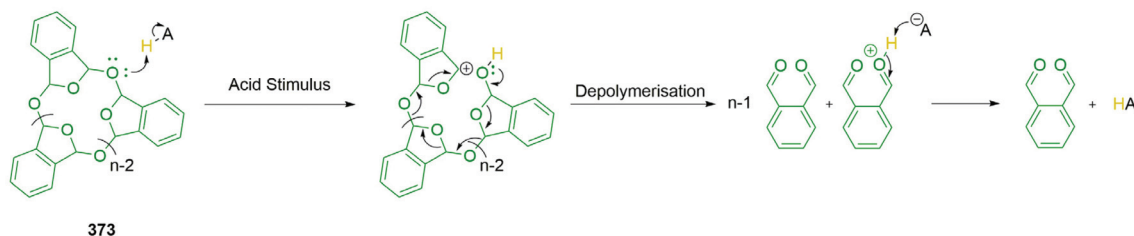
Moore and co-workers have reported the synthesis of PPAs, however, these systems did not include a stimuli-responsive end-cap but we include them here for contrast. These polymers could be depolymerised *via* acetal hydrolysis or mechanical degradation.<sup>361,362</sup> In 2013 their studies led to inadvertent synthesis of a cyclic PPA (cPPA) 373 *via* a cationic polymerization





**Scheme 95** Selective laser-sintered 3D gratings of two  $\text{PCl}_2\text{Pas}$  (**371** and **372**) that feature different triggering groups – exposure of the grating to a solution of TBAF leads to self-immolation and selective degradation of the blue coloured rods of the grating followed by the use of a Pd(0) source and the sodium salt of benzenesulfonic acid to trigger the conversion of the alloc-functionalised  $\text{PCl}_2\text{PA}$  into soluble products.<sup>359</sup>

using a Lewis acid to generate high-molecular-weight polymer with high purity.<sup>363</sup> They highlighted the increased stability of cPPA in comparison to PPA, noting that cPPAs are benchtop stable for several months whereas PPAs require diligent storage or risk untoward depolymerisation. Furthermore, it was demonstrated that the macrocycles could be opened with the addition of a Lewis acid and undergo ring expansion with the addition of more monomer. Interestingly, this phenomenon could be reversed resulting in ring contraction and was attributed to polymerization occurring close to the polymer ceiling temperature, rendering propagation and depropagation dependent on monomer concentration (Scheme 96). This interesting property was further explored by Moore and it was



**Scheme 96** cPPA **373** and self-immolation in the presence of an acidic stimulus as described by Moore and co-workers.<sup>363</sup>

demonstrated that the scrambling of distinct homopolymer mixtures to copolymers under cationic polymerisation conditions occurred.<sup>364</sup>

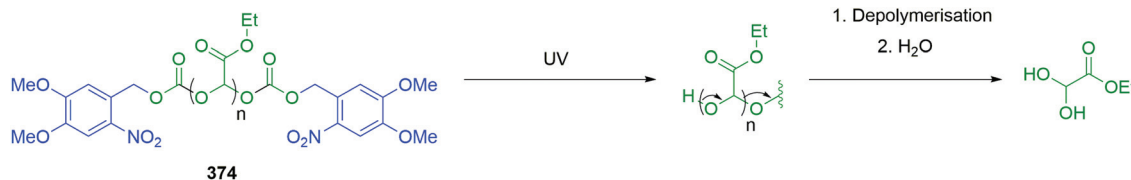
#### 4.4 Self-immolative polyglyoxylates

Polyglyoxylates (PGs) are another class of self-immolative polymers that were reported by Gillies and co-workers in 2014.<sup>365</sup> In a manner similar to PPHAs, without conjugation of an end-capping group, PGs undergo depolymerisation back to monomeric material *via* a hemiacetal mechanism. Gillies and co-workers reported the chain-growth polymerization of an ethyl glyoxylate followed by end-capping with the UV trigger, 4,5-dimethoxy-2-nitrobenzyl alcohol to afford poly(ethyl glyoxylate) (PetG) **374**. Irradiation with UV light (300–350 nm) resulted in cleavage of the trigger unit that, in turn, led to depolymerisation with 70% degradation to ethyl glyoxylate hydrate after 24 hours in the solution state (Scheme 97). Photo-triggered degradation of **374** in the solid state was further explored with polymer films exposed to UV irradiation, then immersed in pH 7.4 phosphate buffer. Solid state depolymerisation proceeded slower but after 17 days the films of **374** had undergone complete degradation. Gillies and co-workers have demonstrated subsequently that PGs are versatile self-immolative polymers *via* the incorporation of different end-capping groups that cleave upon exposure to heat, hydrogen peroxide or DTT.<sup>162,365,366</sup>

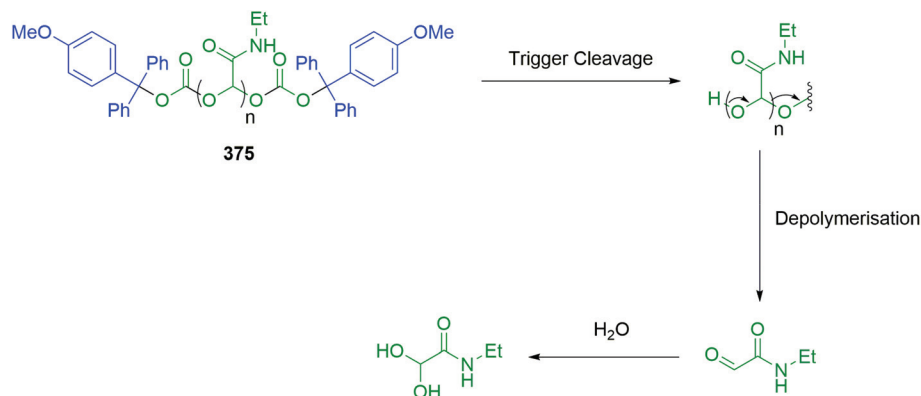
More recently, Gillies and co-workers have reported the preparation and synthesis of self-immolative polyglyoxylamides (PGAMs) **375**; whilst retaining the desirable stimuli-responsive depolymerisation (Scheme 98), they were able to obtain these materials through monomer polymerisation or post-polymerisation amidation of PetG under mild conditions without degradation of the polymers.<sup>367</sup> Furthermore, PGAMs exhibit very different properties to PGs with higher glass transition ( $T_g$ ) values as a result of hydrogen bonding from the amide motif (85 °C for PGAm-Net-MMT **375** *vs.* –10 °C for PetG-MMT) and higher water solubility at ambient temperature. This increased water solubility of PGAMs, compared to the predominantly hydrophobic PetG systems, allows for exploration of drug delivery applications. This work has also been reported with an application as kinetic hydrate inhibitors by Gillies and co-workers.<sup>368</sup>

In another innovative development of self-immolative PG-based systems, Fan and Gillies have conjugated poly(ethyl





**Scheme 97** Head-to-tail depolymerisation of PetG **374** upon exposure to UV radiation, as described by Gillies and co-workers.<sup>365</sup>



**Scheme 98** Head-to-tail depolymerisation of PGAm-Net-MMT **375** upon exposure to 0.9 M acetic acid as described by Gillies and co-workers.<sup>367</sup>

glyoxylate) (PEtG) with poly(ethylene oxide) (PEO) to generate amphiphilic block copolymers **376–379**. As a consequence of their amphiphilic nature, these block copolymers self-assemble to form nanoparticles in aqueous solution.<sup>369</sup> The apolar interior of these nanoparticles enables uptake of hydrophobic payloads such as dyes (*e.g.* Nile Red) or anti-cancer drugs (*e.g.* doxorubicin or curcumin). Several different self-immolative linker end caps were used to conjugate the two polymers so that each end of PEtG was coupled to a polar PEG unit. The chemistries of the linker end caps permitted triggering *via* exposure to UV light, thiols, hydrogen peroxide or importantly, combinations of these stimuli (Scheme 99). The trigger event leads to selective degradation of the linker end caps, thus fragmenting the amphiphilic block copolymer and initiating self-immolation of the PEtG block; the net result of this process is disassembly of the block copolymer-based nanoparticles and release of the payload.

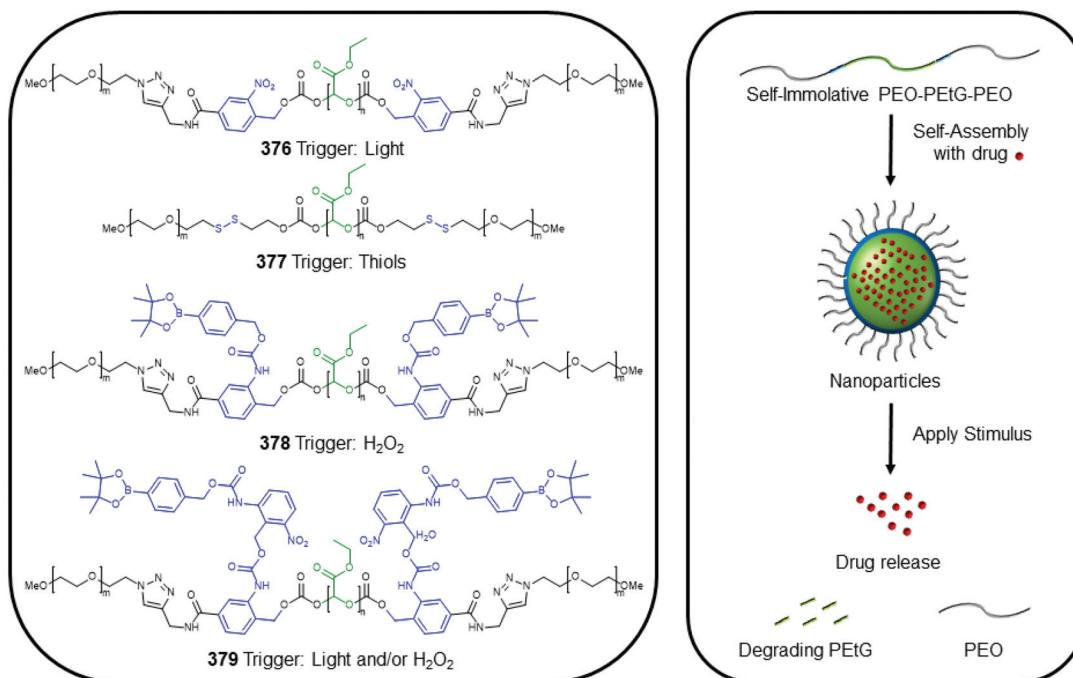
In a related approach, Gillies and co-workers have also developed<sup>175</sup> thermo-responsive micelles and vesicles utilising a poly(ethyl glyoxylate) block copolymer system **380** equipped with an end cap on the PEtG unit that is susceptible to a retro-[ $4\pi + 2\pi$ ] reaction, liberating a furan. This reaction fragments the hydrophilic and hydrophobic blocks of the copolymer; in addition, furans with this substitution pattern will cleave under the reaction conditions leading to end-to-end depolymerization (Scheme 100). Overall, the PEG-PEtG-PEG architecture with the thermally sensitive cycloadduct at the junction point between the different polymer blocks led to thermo-responsive micelles and vesicles that disassembled upon heating. In addition, stable assemblies could be generated that

incorporated iron oxide nanoparticles within the hydrophobic core – exposure to magnetic fields led to localised heating within the thus triggering disassembly.

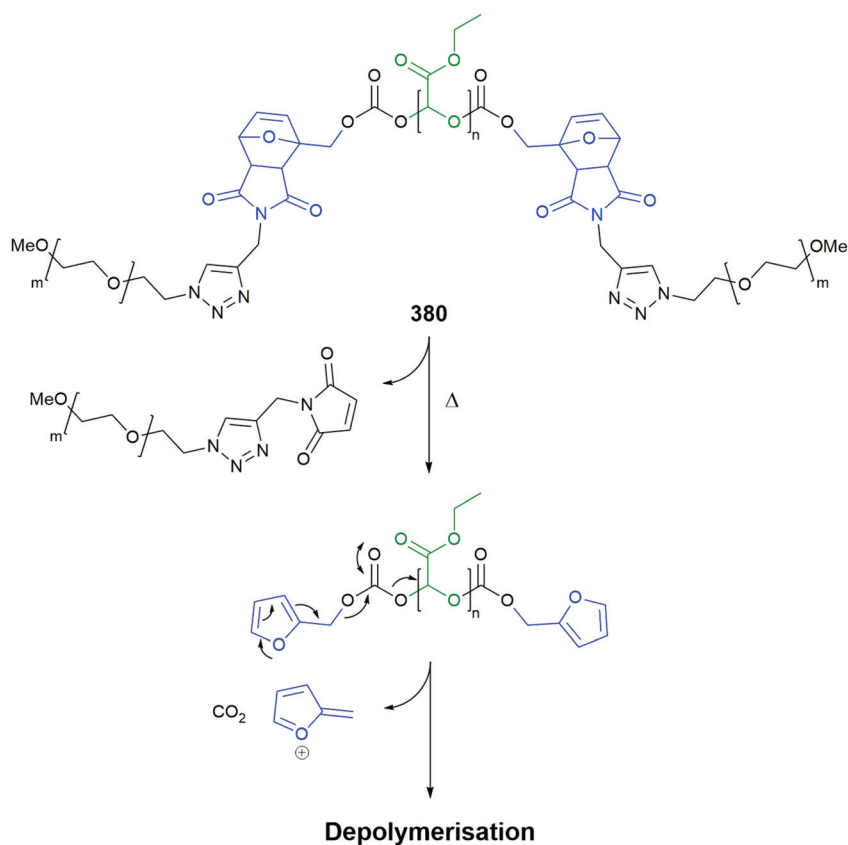
## 5 Self-immolative supramolecular systems

Developing their work on  $\beta$ -galactosidase triggered release of anticancer agents (Fig. 20), Papot *et al.* reported an inventive supramolecular drug delivery system based on a [2]-rotaxane.<sup>370</sup> In **381**, the taxol prodrug, with its esterase cleavable linker, is mechanically interlocked with a macrocyclic ring (Scheme 101). The macrocyclic ring has an in-built self-immolative linker triggered by  $\beta$ -galactosidase; on exposure to that enzyme, 1,6-elimination of the first, phenol-based linker is initiated to afford **382**. Following this, the 2,4-substituted aniline undergoes either 1,6 or 1,4-elimination to fragment the locking ring, exposing the scissile bond of prodrug **383**. Hence, this system falls into the category of SIEs that require two-trigger events to liberate the reporter group; with well-chosen triggering events, this has been shown to give improved targeting of the drug.<sup>40,217,229</sup> The galactosidase trigger unit was also employed by Leigh, Aucagne and Papot in rotaxane-based peptide delivery systems (*e.g.* Met-enkephalin) as part of the stopper.<sup>371,372</sup> The enhanced solubility of **381**, as compared the taxol, owes much to the inclusion of a hydrophilic stopper, attached through a ‘click’ reaction. The stopper features hydrophilic glucose units and was pioneered in earlier work toward a drug delivery system for cyclopamine.<sup>373</sup>





**Scheme 99** The structures of the PEG-PETG block copolymers 376–379 that could be triggered via exposure to light, thiols or hydrogen peroxide and a schematic illustrating the self-assembly of nanoparticles plus the mode of payload delivery post application of the key stimulus.<sup>369</sup>



**Scheme 100** The PEG-PETG-PEG block copolymer 380 reported by Gillies and co-workers that featured thermally degradable cycloadducts at the polymer block junctions.<sup>175</sup>





Scheme 101 Papot's [2]-rotaxane-based drug delivery system **381** for intracellular delivery of taxol.<sup>370</sup>

## 6 Perspectives and concluding remarks

This update assessment of the field of self-immolative linker systems and their implementation into polymeric materials has revealed a significant degree of progress over the past

decade – the number of publications has burgeoned with innovative uses of self-immolative linkers that undergo either an electronic cascade or a cyclisation event (or indeed a combination of both processes) following triggering events. There has been a natural progression from studies that targeted establishment of fundamentals of the self-immolative pathways to the application of these degradable materials. It is



notable that self-immolative linkers have now found use within small molecular and macromolecular drug delivery or sensor systems that, with further development, can transition to commercially viable systems. The fate of the by-products of the self-immolative process have also been considered and an overview of their role in the reactive milieu is being gained – this aspect of these degradable systems has particular relevance in the context of the ability to recycle and re-use materials. However, more in-depth studies are needed to comprehensively understand the reactive pathway of these potentially reactive by-products to permit use of self-immolative polymers, especially in biological applications such as drug delivery systems or biosensors. Practical challenges to the commercial uptake of these materials still exist (especially relating to the synthetic complexity of many of the systems reported in this review) but it is not unreasonable to expect that within the next decade we will see the introduction into modern society of self-immolative materials in the form of ‘smart’ medicines, highly sensitive/selective sensor and security devices, or adhesives or coatings that can be debonded on demand to permit recycling of valuable components.

## Conflicts of interest

There are no conflicts to declare.

## Acknowledgements

This study was supported by Dstl (contract DSTLX1000116213R) for A. G. G.

## References

- 1 R. C. Elgersma, R. G. E. Coumans, T. Huijbregts, W. M. P. B. Menge, J. A. F. Joosten, H. J. Spijker, F. M. H. de Groot, M. M. C. van der Lee, R. Ubink, D. J. van den Dobbelsteen, D. F. Egging, W. H. A. Dokter, G. F. M. Verheijden, J. M. Lemmens, C. M. Timmers and P. H. Beusker, *Mol. Pharmaceutics*, 2015, **12**, 1813–1835.
- 2 Y. Zhang, Q. Yin, L. Yin, L. Ma, L. Tang and J. Cheng, *Angew. Chem., Int. Ed.*, 2013, **52**, 6435–6439.
- 3 J. A. Sáez, B. Escuder and J. F. Miravet, *Tetrahedron*, 2010, **66**, 2614–2618.
- 4 H. Kim, H. Mohapatra and S. T. Phillips, *Angew. Chem., Int. Ed.*, 2015, **54**, 13063–13067.
- 5 T. S. Babra, A. Trivedi, C. N. Warriner, N. Bazin, D. Castiglione, C. Siviour, W. Hayes and B. W. Greenland, *Polym. Chem.*, 2017, **8**, 7207–7216.
- 6 T. S. Babra, M. Wood, J. S. Godleman, S. Salimi, C. Warriner, N. Bazin, C. R. Siviour, I. W. Hamley, W. Hayes and B. W. Greenland, *Eur. Polym. J.*, 2019, **119**, 260–271.
- 7 J. Yan, S. Lee, A. Zhang and J. Yoon, *Chem. Soc. Rev.*, 2018, **47**, 6900–6916.
- 8 A. L. Acton, F. Leroux, A. Feula, K. Melia, M. R. Sambrook, W. Hayes and A. T. Russell, *Chem. Commun.*, 2019, **55**, 5219–5222.
- 9 W. Tuo, J. Bouquet, F. Taran and T. Le Gall, *Chem. Commun.*, 2019, **55**, 8655–8658.
- 10 X. Sun, J. F. Reuther, S. T. Phillips and E. V. Anslyn, *Chem. – Eur. J.*, 2017, **23**, 3903–3909.
- 11 P. L. Carl, P. K. Chakravarty and J. A. Katzenellenbogen, *J. Med. Chem.*, 1981, **24**, 479–480.
- 12 C. A. Blencowe, A. T. Russell, F. Greco, W. Hayes and D. W. Thornthwaite, *Polym. Chem.*, 2011, **2**, 773–790.
- 13 A. P. Esser-Kahn, S. A. Odom, N. R. Sottos, S. R. White and J. S. Moore, *Macromolecules*, 2011, **44**, 5539–5553.
- 14 G. I. Peterson, M. B. Larsen and A. J. Boydston, *Macromolecules*, 2012, **45**, 7317–7328.
- 15 A. D. Wong, M. A. DeWit and E. R. Gillies, *Adv. Drug Delivery Rev.*, 2012, **64**, 1031–1045.
- 16 N. Krall, J. Scheuermann and D. Neri, *Angew. Chem., Int. Ed.*, 2013, **52**, 1384–1402.
- 17 S. T. Phillips and A. M. Dilauro, *ACS Macro Lett.*, 2014, **3**, 298–304.
- 18 S. T. Phillips, J. S. Robbins, A. M. Dilauro and M. G. Olah, *J. Appl. Polym. Sci.*, 2014, **131**, 40992.
- 19 S. Gnaim and D. Shabat, *Acc. Chem. Res.*, 2014, **47**, 2970–2984.
- 20 R. E. Wang, F. Costanza, Y. Niu, H. Wu, Y. Hu, W. Hang, Y. Sun and J. Cai, *J. Controlled Release*, 2012, **159**, 154–163.
- 21 A. Alouane, R. Labruère, T. Le Saux, F. Schmidt and L. Jullien, *Angew. Chem., Int. Ed.*, 2015, **54**, 7492–7509.
- 22 J. A. Kaitz, O. P. Lee and J. S. Moore, *MRS Commun.*, 2015, **5**, 191–204.
- 23 M. E. Roth, O. Green, S. Gnaim and D. Shabat, *Chem. Rev.*, 2016, **116**, 1309–1352.
- 24 S. Goggins and C. G. Frost, *Analyst*, 2016, **141**, 3157–3218.
- 25 Y. J. Wang, Y. Y. Li, X. Y. Liu, X. L. Lu, X. Cao and B. H. Jiao, *Mar. Drugs*, 2017, **15**, 18.
- 26 M. Gisbert-Garzarán, M. Manzano and M. Vallet-Regí, *Chem. Eng. J.*, 2018, **340**, 24–31.
- 27 X. Sun, D. Shabat, S. T. Phillips and E. V. Anslyn, *J. Phys. Org. Chem.*, 2018, **31**, e3827.
- 28 S. Gnaim, O. Green and D. Shabat, *Chem. Commun.*, 2018, **54**, 2073–2085.
- 29 R. E. Yardley, A. R. Kenaree and E. R. Gillies, *Macromolecules*, 2019, **52**, 6342–6360.
- 30 A. Dal Corso, L. Pignataro, L. Belvisi and C. Gennari, *Chem. – Eur. J.*, 2019, **25**, 14740–14757.
- 31 V. Saluja, A. Mankoo, G. K. Saraogi, M. M. Tambuwala and V. Mishra, *J. Drug Delivery Sci. Technol.*, 2019, **52**, 15–26.
- 32 N. Hananya and D. Shabat, *ACS Cent. Sci.*, 2019, **5**, 949–959.
- 33 S. Gnaim and D. Shabat, *Acc. Chem. Res.*, 2019, **52**, 2806–2817.
- 34 Q. E. A. Sirianni and E. R. Gillies, *Polymer*, 2020, **202**, 122638.



- 35 Y. Xiao, X. Tan, Z. Li and K. Zhang, *J. Mater. Chem. B*, 2020, **8**, 6697–6709.
- 36 O. Shelef, S. Gnaim and D. Shabat, *J. Am. Chem. Soc.*, 2021, **143**, 21177–21188.
- 37 Y. Xue, H. Bai, B. Peng, B. Fang, J. Baell, L. Li, W. Huang and N. H. Voelcker, *Chem. Soc. Rev.*, 2021, **50**, 4872–4931.
- 38 C. M. Geiselhart, H. Mutlu and C. Barner-Kowollik, *Angew. Chem., Int. Ed.*, 2021, **60**, 17290–17313.
- 39 A. Dal Corso, S. Arosio, N. Arrighetti, P. Perego, L. Belvisi, L. Pignataro and C. Gennari, *Chem. Commun.*, 2021, **57**, 7778–7781.
- 40 P. K. Chakravarty, P. L. Carl, M. J. Weber and J. A. Katzenellenbogen, *J. Med. Chem.*, 1983, **26**, 638–644.
- 41 F. M. H. De Groot, L. W. A. Van Berkomp and H. W. Scheeren, *J. Med. Chem.*, 1999, **42**, 5277–5283.
- 42 A. Kastrati and C. G. Bochet, *J. Org. Chem.*, 2019, **84**, 7776–7785.
- 43 S. Gnaim and D. Shabat, *J. Am. Chem. Soc.*, 2017, **139**, 10002–10008.
- 44 L. Peles-Strahl, R. Sasson, G. Slor, N. Edelstein-Pardo, A. Dahan and R. J. Amir, *Macromolecules*, 2019, **52**, 3268–3277.
- 45 N. Karton-Lifshin and D. Shabat, *New J. Chem.*, 2012, **36**, 386–393.
- 46 E. M. Lloyd, H. Lopez Hernandez, E. C. Feinberg, M. Yourdkhani, E. K. Zen, E. B. Mejia, N. R. Sottos, J. S. Moore and S. R. White, *Chem. Mater.*, 2019, **31**, 398–406.
- 47 K. Yeung, H. Kim, H. Mohapatra and S. T. Phillips, *J. Am. Chem. Soc.*, 2015, **137**, 5324–5327.
- 48 D. A. Roberts, B. S. Pilgrim, T. N. Dell and M. M. Stevens, *Chem. Sci.*, 2020, **11**, 3713–3718.
- 49 K. M. Schmid, L. Jensen and S. T. Phillips, *J. Org. Chem.*, 2012, **77**, 4363–4374.
- 50 B. M. Sykes, M. P. Hay, D. Bohinc-Herceg, N. A. Helsby, C. J. O'Connor and W. A. Denny, *J. Chem. Soc., Perkin Trans. 1*, 2000, 1601–1608.
- 51 C. C. Song, R. Ji, F. S. Du and Z. C. Li, *Macromolecules*, 2013, **46**, 8416–8425.
- 52 S. A. Nuñez, K. Yeung, N. S. Fox and S. T. Phillips, *J. Org. Chem.*, 2011, **76**, 10099–10113.
- 53 F. Fakhari and S. E. Rokita, *Nat. Commun.*, 2014, **5**, 5591.
- 54 Y. S. Cho, S. W. Chung, H. R. Kim, T. H. Won, J. U. Choi, I. S. Kim, S. Y. Kim and Y. Byun, *J. Controlled Release*, 2019, **296**, 241–249.
- 55 S. W. Chung, Y. S. Cho, J. U. Choi, H. R. Kim, T. H. Won, S. Y. Kim and Y. Byun, *Biomaterials*, 2019, **192**, 109–117.
- 56 Y. Anami, C. M. Yamazaki, W. Xiong, X. Gui, N. Zhang, Z. An and K. Tsuchikama, *Nat. Commun.*, 2018, **9**, 2512.
- 57 B. Q. Wei, J. Gunzner-Toste, H. Yao, T. Wang, J. Wang, Z. Xu, J. Chen, J. Wai, J. Nonomiya, S. P. Tsai, J. Chuh, K. R. Kozak, Y. Liu, S.-F. Yu, J. Lau, G. Li, G. D. Phillips, D. Leipold, A. Kamath, D. Su, K. Xu, C. Eigenbrot, S. Steinbacher, R. Ohri, H. Raab, L. R. Staben, G. Zhao, J. A. Flygare, T. H. Pillow, V. Verma, L. A. Masterson, P. W. Howard and B. Safina, *J. Med. Chem.*, 2018, **61**, 989–1000.
- 58 A. R. M. Dias, L. Bodero, A. Martins, D. Arosio, S. Gazzola, L. Belvisi, L. Pignataro, C. Steinkühler, A. Dal Corso, C. Gennari and U. Piarulli, *ChemMedChem*, 2019, **14**, 938–942.
- 59 P. D. Senter, W. E. Pearce and R. S. Greenfield, *J. Org. Chem.*, 1990, **55**, 2975–2978.
- 60 F. Groot, E. Damen and H. Scheeren, *Curr. Med. Chem.*, 2012, **8**, 1093–1122.
- 61 R. Erez and D. Shabat, *Org. Biomol. Chem.*, 2008, **6**, 2669.
- 62 I. Niculescu-Duvaz, D. Niculescu-Duvaz, F. Friedlos, R. Spooner, J. Martin, R. Marais and C. J. Springer, *J. Med. Chem.*, 1999, **42**, 2485–2489.
- 63 R. Perry, R. J. Amir and D. Shabat, *New J. Chem.*, 2007, **31**, 1307.
- 64 E. Bouvier, S. Thiroit, F. Schmidt and C. Monneret, *Org. Biomol. Chem.*, 2003, **1**, 3343–3352.
- 65 J. C. Florent, X. Dong, G. Gaudel, S. Mitaku, C. Monneret, J. P. Gesson, J. C. Jacquesy, M. Mondon, B. Renoux, S. Andrianomenjanahary, S. Michel, M. Koch, F. Tillequin, M. Gerken, J. Czech, R. Straub and K. Bosslet, *J. Med. Chem.*, 1998, **41**, 3572–3581.
- 66 R. Perry-Feigenbaum, P. S. Baran and D. Shabat, *Org. Biomol. Chem.*, 2009, **7**, 4825–4828.
- 67 M. P. Hay, B. M. Sykes, W. A. Denny and C. J. O'Connor, *J. Chem. Soc., Perkin Trans. 1*, 1999, 2759–2770.
- 68 K. Matsuo, R. Kamada, K. Mizusawa, H. Imai, Y. Takayama, M. Narazaki, T. Matsuda, Y. Takaoka and I. Hamachi, *Chem. – Eur. J.*, 2013, **19**, 12875–12883.
- 69 J. Zhao, B. Zhang, Q. Mao, K. Ping, P. Zhang, F. Lin, D. Liu, Y. Feng, M. Sun, Y. Zhang, Q. H. Li, T. Zhang, Y. Mou and S. Wang, *J. Med. Chem.*, 2022, **65**, 4926–4948.
- 70 X.-b. Zhao, W. Ha, K. Gao and Y.-p. Shi, *Anal. Chem.*, 2020, **92**, 9039–9047.
- 71 B. E. Toki, C. G. Cervený, A. F. Wahl and P. D. Senter, *J. Org. Chem.*, 2002, **67**, 1866–1872.
- 72 C. J. M. Stirling, *Acc. Chem. Res.*, 1979, **12**, 198–203.
- 73 P. J. Burke, P. D. Senter, D. W. Meyer, J. B. Miyamoto, M. Anderson, B. E. Toki, G. Manikumar, M. C. Wani, D. J. Kroll and S. C. Jeffrey, *Bioconjugate Chem.*, 2009, **20**, 1242–1250.
- 74 Y. L. Leu, C. S. Chen, Y. J. Wu and J. W. Chern, *J. Med. Chem.*, 2008, **51**, 1740–1746.
- 75 G. P. Yan, C. W. Ai, L. Li, R. F. Zong and F. Liu, *Chin. Sci. Bull.*, 2010, **55**, 3085–3093.
- 76 Y. L. Leu, S. R. Roffler and J. W. Chern, *J. Med. Chem.*, 1999, **42**, 3623–3628.
- 77 D. Zhang, H. Le, J. D. Cruz-Chuh, S. Bobba, J. Guo, L. Staben, C. Zhang, Y. Ma, K. R. Kozak, G. D. Lewis Phillips, B. S. Vollmar, J. D. Sadowsky, R. Vandlen, B. Wei, D. Su, P. Fan, P. S. Dragovich, S. C. Khojasteh, C. E. C. A. Hop and T. H. Pillow, *Bioconjugate Chem.*, 2018, **29**, 267–274.
- 78 R. Weinstain, P. S. Baran and D. Shabat, *Bioconjugate Chem.*, 2009, **20**, 1783–1791.
- 79 D. A. Rose, J. W. Treacy, Z. J. Yang, J. H. Ko, K. N. Houk and H. D. Maynard, *J. Am. Chem. Soc.*, 2022, **144**, 6050–6058.



- 80 G. C. Van De Bittner, E. A. Dubikovskaya, C. R. Bertozzi and C. J. Chang, *Proc. Natl. Acad. Sci. U. S. A.*, 2010, **107**, 21316–21321.
- 81 D. Srikun, E. W. Miller, D. W. Domaille and C. J. Chang, *J. Am. Chem. Soc.*, 2008, **130**, 4596–4597.
- 82 J. L. M. Jourden, K. B. Daniel and S. M. Cohen, *Chem. Commun.*, 2011, **47**, 7968–7970.
- 83 R. A. Mosey and P. E. Floreancig, *Org. Biomol. Chem.*, 2012, **10**, 7980–7985.
- 84 R. A. J. Smith, C. M. Porteous, C. V. Coulter and M. P. Murphy, *Eur. J. Biochem.*, 1999, **263**, 709–716.
- 85 A. Muratovska, R. N. Lightowers, R. W. Taylor, J. A. Wilce and M. P. Murphy, *Adv. Drug Delivery Rev.*, 2001, **49**, 189–198.
- 86 D. V. Santi, E. L. Schneider and G. W. Ashley, *J. Med. Chem.*, 2014, **57**, 2303–2314.
- 87 R. V. Kolakowski, K. T. Haelsig, K. K. Emmerton, C. I. Leiske, J. B. Miyamoto, J. H. Cochran, R. P. Lyon, P. D. Senter and S. C. Jeffrey, *Angew. Chem., Int. Ed.*, 2016, **55**, 7948–7951.
- 88 Y. Zheng, B. Yu, Z. Li, Z. Yuan, C. L. Organ, R. K. Trivedi, S. Wang, D. J. Lefer and B. Wang, *Angew. Chem., Int. Ed.*, 2017, **56**, 11749–11753.
- 89 J. Kang, S. Xu, M. N. Radford, W. Zhang, S. S. Kelly, J. J. Day and M. Xian, *Angew. Chem., Int. Ed.*, 2018, **57**, 5893–5897.
- 90 R. D. Hanna, Y. Naro, A. Deiters and P. E. Floreancig, *J. Am. Chem. Soc.*, 2016, **138**, 13353–13360.
- 91 Y. Kuang, K. Balakrishnan, V. Gandhi and X. Peng, *J. Am. Chem. Soc.*, 2011, **133**, 19278–19281.
- 92 W. Chen, Y. Han and X. Peng, *Chem. – Eur. J.*, 2014, **20**, 7410–7418.
- 93 S. Cao, R. Christiansen and X. Peng, *Chem. – Eur. J.*, 2013, **19**, 9050–9058.
- 94 L. R. Staben, S. G. Koenig, S. M. Lehar, R. Vandlen, D. Zhang, J. Chuh, S. F. Yu, C. Ng, J. Guo, Y. Liu, A. Fourie-O'Donohue, M. Go, X. Linghu, N. L. Segraves, T. Wang, J. Chen, B. Wei, G. D. L. Phillips, K. Xu, K. R. Kozak, S. Mariathan, J. A. Flygare and T. H. Pillow, *Nat. Chem.*, 2016, **8**, 1112–1119.
- 95 F. M. F. Santos, A. I. Matos, A. E. Ventura, J. Gonçalves, L. F. Veiros, H. F. Florindo and P. M. P. P. Gois, *Angew. Chem.*, 2017, **129**, 9474–9478.
- 96 K. E. Broaders, S. Grandhe and J. M. J. Fréchet, *J. Am. Chem. Soc.*, 2011, **133**, 756–758.
- 97 A. K. Steiger, S. Pardue, C. G. Kevil and M. D. Pluth, *J. Am. Chem. Soc.*, 2016, **138**, 7256–7259.
- 98 Y. Zhao and M. D. Pluth, *Angew. Chem.*, 2016, **128**, 14638–14642.
- 99 Y. Zhao, H. A. Henthorn and M. D. Pluth, *J. Am. Chem. Soc.*, 2017, **139**, 16365–16376.
- 100 V. S. Khodade, B. M. Pharoah, N. Paolucci and J. P. Toscano, *J. Am. Chem. Soc.*, 2020, **142**, 4309–4316.
- 101 P. Chauhan, S. Jos and H. Chakrapani, *Org. Lett.*, 2018, **20**, 3766–3770.
- 102 A. K. Sharma, M. Nair, P. Chauhan, K. Gupta, D. K. Saini and H. Chakrapani, *Org. Lett.*, 2017, **19**, 4822–4825.
- 103 P. Štacko, L. Muchová, L. Vitek and P. Klán, *Org. Lett.*, 2018, **20**, 4907–4911.
- 104 A. T. Dharmaraja, G. Ravikumar and H. Chakrapani, *Org. Lett.*, 2014, **16**, 2610–2613.
- 105 L. Yuan, W. Lin, Y. Xie, B. Chen and S. Zhu, *J. Am. Chem. Soc.*, 2012, **134**, 1305–1315.
- 106 P. Chauhan, P. Bora, G. Ravikumar, S. Jos and H. Chakrapani, *Org. Lett.*, 2017, **19**, 62–65.
- 107 A. K. Steiger, M. Marcatti, C. Szabo, B. Szczesny and M. D. Pluth, *ACS Chem. Biol.*, 2017, **12**, 2117–2123.
- 108 Y. Zhao, A. K. Steiger and M. D. Pluth, *Chem. Commun.*, 2018, **54**, 4951–4954.
- 109 P. Shukla, V. S. Khodade, M. Sharathchandra, P. Chauhan, S. Mishra, S. Siddaramappa, B. E. Pradeep, A. Singh and H. Chakrapani, *Chem. Sci.*, 2017, **8**, 4967–4972.
- 110 C. R. Powell, J. C. Foster, S. N. Swilley, K. Kaur, S. J. Scannelli, D. Troya and J. B. Matson, *Polym. Chem.*, 2019, **10**, 2991–2995.
- 111 A. K. Steiger, Y. Yang, M. Royzen and M. D. Pluth, *Chem. Commun.*, 2017, **53**, 1378–1380.
- 112 K. A. Pardeshi, G. Ravikumar and H. Chakrapani, *Org. Lett.*, 2018, **20**, 4–7.
- 113 C. R. Powell, K. M. Dillon, Y. Wang, R. J. Carrazzone and J. B. Matson, *Angew. Chem., Int. Ed.*, 2018, **57**, 6324–6328.
- 114 P. Bora, P. Chauhan, K. A. Pardeshi and H. Chakrapani, *RSC Adv.*, 2018, **8**, 27359–27374.
- 115 A. P. Schaap, T. Chen, R. S. Handley, R. DeSilva and B. P. Giri, *Tetrahedron Lett.*, 1987, **28**, 1155–1158.
- 116 A. P. Schaap, R. S. Handley and B. P. Giri, *Tetrahedron Lett.*, 1987, **28**, 935–938.
- 117 A. P. Schaap, M. D. Sandison and R. S. Handley, *Tetrahedron Lett.*, 1987, **28**, 1159–1162.
- 118 O. Green, T. Eilon, N. Hananya, S. Gutkin, C. R. Bauer and D. Shabat, *ACS Cent. Sci.*, 2017, **3**, 349–358.
- 119 T. Eilon-Shaffer, M. Roth-Konforti, A. Eldar-Boock, R. Satchi-Fainaro and D. Shabat, *Org. Biomol. Chem.*, 2018, **16**, 1708–1712.
- 120 S. Gnaim, A. Scomparin, A. Eldar-Boock, C. R. Bauer, R. Satchi-Fainaro and D. Shabat, *Chem. Sci.*, 2019, **10**, 2945–2955.
- 121 S. P. Gholap, C. Yao, O. Green, M. Babjak, P. Jakubec, T. Malatinský, J. Ihssen, L. Wick, U. Spitz and D. Shabat, *Bioconjugate Chem.*, 2021, **32**, 991–1000.
- 122 Z. Wang, H. Wu, P. Liu, F. Zeng and S. Wu, *Biomaterials*, 2017, **139**, 139–150.
- 123 S. Gnaim, A. Scomparin, S. Das, R. Blau, R. Satchi-Fainaro and D. Shabat, *Angew. Chem., Int. Ed.*, 2018, **57**, 9033–9037.
- 124 M. Roth-Konforti, O. Green, M. Hupfeld, L. Fieseler, N. Heinrich, J. Ihssen, R. Vorberg, L. Wick, U. Spitz and D. Shabat, *Angew. Chem., Int. Ed.*, 2019, **58**, 10361–10367.
- 125 J. A. Richard, L. Jean, A. Romieu, M. Massonneau, P. Noack-Fraissignes and P. Y. Renard, *Org. Lett.*, 2007, **9**, 4853–4855.
- 126 J. A. Richard, L. Jean, C. Schenkels, M. Massonneau, A. Romieu and P. Y. Renard, *Org. Biomol. Chem.*, 2009, **7**, 2941–2957.



- 127 S. Gutkin, S. Gandhesiri, A. Brik and D. Shabat, *Bioconjugate Chem.*, 2021, **32**, 2141–2147.
- 128 J. I. Scott, S. Gutkin, O. Green, E. J. Thompson, T. Kitamura, D. Shabat and M. Vendrell, *Angew. Chem., Int. Ed.*, 2021, **60**, 5699–5703.
- 129 S. Gutkin, O. Green, G. Raviv, D. Shabat and O. Portnoy, *Bioconjugate Chem.*, 2020, **31**, 2488–2493.
- 130 B. M. Babin, G. Fernandez-Cuervo, J. Sheng, O. Green, A. A. Ordonez, M. L. Turner, L. J. Keller, S. K. Jain, D. Shabat and M. Bogoy, *ACS Cent. Sci.*, 2021, **7**, 803–814.
- 131 M. Ponomariov, D. Shabat and O. Green, *Bioconjugate Chem.*, 2021, **32**, 2134–2140.
- 132 O. Shelef, A. C. Sedgwick, S. Pozzi, O. Green, R. Satchi-Fainaro, D. Shabat and J. L. Sessler, *Chem. Commun.*, 2021, **57**, 11386–11389.
- 133 M. J. Lobba, C. Fellmann, A. M. Marmelstein, J. C. Maza, E. N. Kissman, S. A. Robinson, B. T. Staahl, C. Urnes, R. J. Lew, C. S. Mogilevsky, J. A. Doudna and M. B. Francis, *ACS Cent. Sci.*, 2020, **6**, 1564–1571.
- 134 X. Wu, L. Li, W. Shi, Q. Gong and H. Ma, *Angew. Chem., Int. Ed.*, 2016, **55**, 14728–14732.
- 135 H. Li, W. Liu, F. Zhang, X. Zhu, L. Huang and H. Zhang, *Anal. Chem.*, 2018, **90**, 855–858.
- 136 X. Chen, X. Ma, Y. Zhang, G. Gao, J. Liu, X. Zhang, M. Wang and S. Hou, *Anal. Chim. Acta*, 2018, **1033**, 193–198.
- 137 S. Ye, J. J. Hu and D. Yang, *Angew. Chem., Int. Ed.*, 2018, **57**, 10173–10177.
- 138 S. Ye, N. Hananya, O. Green, H. Chen, A. Q. Zhao, J. Shen, D. Shabat and D. Yang, *Angew. Chem., Int. Ed.*, 2020, **59**, 14326–14330.
- 139 S. Ye, B. Yang, M. Wu, Z. Chen, J. Shen, D. Shabat and D. Yang, *CCS Chem.*, 2021, **3**, 2181–2188.
- 140 S. Das, J. Ihssen, L. Wick, U. Spitz and D. Shabat, *Chem. – Eur. J.*, 2020, **26**, 3647–3652.
- 141 K. J. Bruemmer, R. R. Walvoord, T. F. Brewer, G. Burgos-Barragan, N. Wit, L. B. Pontel, K. J. Patel and C. J. Chang, *J. Am. Chem. Soc.*, 2017, **139**, 5338–5350.
- 142 T. F. Brewer, G. Burgos-Barragan, N. Wit, K. J. Patel and C. J. Chang, *Chem. Sci.*, 2017, **8**, 4073–4081.
- 143 W. Liu, C. Truillet, R. R. Flavell, T. F. Brewer, M. J. Evans, D. M. Wilson and C. J. Chang, *Chem. Sci.*, 2016, **7**, 5503–5507.
- 144 K. J. Bruemmer, O. Green, T. A. Su, D. Shabat and C. J. Chang, *Angew. Chem., Int. Ed.*, 2018, **57**, 7508–7512.
- 145 X. Wu, W. Shi, X. Li and H. Ma, *Angew. Chem., Int. Ed.*, 2017, **56**, 15319–15323.
- 146 K. Gorska and N. Winssinger, *Angew. Chem., Int. Ed.*, 2013, **52**, 6820–6843.
- 147 T. N. Grossmann, A. Strohbach and O. Seitz, *ChemBioChem*, 2008, **9**, 2185–2192.
- 148 A. P. Silverman and E. T. Kool, *Chem. Rev.*, 2006, **106**, 3775–3789.
- 149 K. Gorska, A. Manicardi, S. Barluenga and N. Winssinger, *Chem. Commun.*, 2011, **47**, 4364–4366.
- 150 A. Shibata, Y. Ito and H. Abe, *Chem. Commun.*, 2013, **49**, 270–272.
- 151 A. Alouane, R. Labruère, T. Le Saux, I. Aujard, S. Dubruille, F. Schmidt and L. Jullien, *Chem. – Eur. J.*, 2013, **19**, 11717–11724.
- 152 K. K. Sadhu and N. Winssinger, *Chem. – Eur. J.*, 2013, **19**, 8182–8189.
- 153 M. Roth and O. Seitz, *Chem. – Eur. J.*, 2021, **27**, 14189–14194.
- 154 R. Labruère, A. Alouane, T. Le Saux, I. Aujard, P. Pelupessy, A. Gautier, S. Dubruille, F. Schmidt and L. Jullien, *Angew. Chem., Int. Ed.*, 2012, **51**, 9344–9347.
- 155 M. Staderini, A. Gambardella, A. Lilienkampff and M. Bradley, *Org. Lett.*, 2018, **20**, 3170–3173.
- 156 C. Zang, H. Wang, T. Li, Y. Zhang, J. Li, M. Shang, J. Du, Z. Xi and C. Zhou, *Chem. Sci.*, 2019, **10**, 8973–8980.
- 157 B. A. Hess and L. J. Schaad, *Tetrahedron Lett.*, 1977, **18**, 535–538.
- 158 J. S. Robbins, K. M. Schmid and S. T. Phillips, *J. Org. Chem.*, 2013, **78**, 3159–3169.
- 159 S. Goggins, B. J. Marsh, A. T. Lubben and C. G. Frost, *Chem. Sci.*, 2015, **6**, 4978–4985.
- 160 H. Wang, M. B. Cleary, L. C. Lewis, J. W. Bacon, P. Caravan, H. S. Shafaat and E. M. Gale, *Angew. Chem.*, 2022, **61**, e202114019.
- 161 R. Weinstain, E. Segal, R. Satchi-Fainaro and D. Shabat, *Chem. Commun.*, 2010, **46**, 553–555.
- 162 E. W. P. Damen, T. J. Nevalainen, T. J. M. Van den Bergh, F. M. H. De Groot and H. W. Scheeren, *Bioorg. Med. Chem.*, 2002, **10**, 71–77.
- 163 F. M. H. De Groot, W. J. Loos, R. Koekkoek, L. W. A. Van Berkomp, G. F. Busscher, A. E. Seelen, C. Albrecht, P. De Bruijn and H. W. Scheeren, *J. Org. Chem.*, 2001, **66**, 8815–8830.
- 164 P. Bertrand and J. P. Gesson, *J. Org. Chem.*, 2007, **72**, 3596–3599.
- 165 C. A. Blencowe, D. W. Thornthwaite, W. Hayes and A. T. Russell, *Org. Biomol. Chem.*, 2015, **13**, 8703–8707.
- 166 C. A. Blencowe, PhD Thesis, University of Reading, UK, 2012.
- 167 T. N. Forder, P. G. Maschmeyer, H. Zeng and D. A. Roberts, *Chem. – Asian J.*, 2021, **16**, 287–291.
- 168 P. G. Maschmeyer, X. Liang, A. Hung, O. Ahmadzai, A. L. Kenny, Y. C. Luong, T. N. Forder, H. Zeng, E. R. Gillies and D. A. Roberts, *Polym. Chem.*, 2021, **12**, 6824–6831.
- 169 H. Kunz, *Chem. Ber.*, 1976, **109**, 2670–2683.
- 170 D. Chantreux, J. P. Gamet, R. Jacquier and J. Verducci, *Tetrahedron*, 1984, **40**, 3087–3094.
- 171 A. G. Gavriel, F. Leroux, G. S. Khurana, V. G. Lewis, A. M. Chippindale, M. R. Sambrook, W. Hayes and A. T. Russell, *J. Org. Chem.*, 2021, **86**, 10263–10279.
- 172 B. L. Oliveira, Z. Guo and G. J. L. Bernardes, *Chem. Soc. Rev.*, 2017, **46**, 4895–4950.
- 173 A. C. Knall and C. Slugovc, *Chem. Soc. Rev.*, 2013, **42**, 5131–5142.
- 174 K. Neumann, A. Gambardella, A. Lilienkampff and M. Bradley, *Chem. Sci.*, 2018, **9**, 7198–7203.



- 175 B. Fan, J. F. Trant, G. Hemery, O. Sandre and E. R. Gillies, *Chem. Commun.*, 2017, **53**, 12068–12071.
- 176 K. Neumann, S. Jain, A. Gambardella, S. E. Walker, E. Valero, A. Lilienkamp and M. Bradley, *ChemBioChem*, 2017, **18**, 91–95.
- 177 M. L. Blackman, M. Royzen and J. M. Fox, *J. Am. Chem. Soc.*, 2008, **130**, 13518–13519.
- 178 N. K. Devaraj, R. Upadhyay, J. B. Haun, S. A. Hilderbrand and R. Weissleder, *Angew. Chem., Int. Ed.*, 2009, **48**, 7013–7016.
- 179 J. Li, S. Jia and P. R. Chen, *Nat. Chem. Biol.*, 2014, **10**, 1003–1005.
- 180 R. M. Versteegen, R. Rossin, W. Ten Hoeve, H. M. Janssen and M. S. Robillard, *Angew. Chem., Int. Ed.*, 2013, **52**, 14112–14116.
- 181 S. Davies, B. L. Oliveira and G. J. L. Bernardes, *Org. Biomol. Chem.*, 2019, **17**, 5725–5730.
- 182 J. M. Mejia Oneto, I. Khan, L. Seebald and M. Royzen, *ACS Cent. Sci.*, 2016, **2**, 476–482.
- 183 R. Rossin, R. M. Versteegen, J. Wu, A. Khasanov, H. J. Wessels, E. J. Steenbergen, W. Ten Hoeve, H. M. Janssen, A. H. A. M. van Onzen, P. J. Hudson and M. S. Robillard, *Nat. Commun.*, 2018, **9**, 1484.
- 184 Q. Yao, F. Lin, X. Fan, Y. Wang, Y. Liu, Z. Liu, X. Jiang, P. R. Chen and Y. Gao, *Nat. Commun.*, 2018, **9**, 5032.
- 185 W. S. C. Ngai, S. Yang, X. Zeng, Y. Liu, F. Lin, X. Wang, H. Zhang, X. Fan and P. R. Chen, *J. Am. Chem. Soc.*, 2022, **144**, 5411–5417.
- 186 S. Dadhwal, J. M. Fairhall, S. K. Goswami, S. Hook and A. B. Gamble, *Chem. – Asian J.*, 2019, **14**, 1143–1150.
- 187 S. S. Matikonda, D. L. Orsi, V. Staudacher, I. A. Jenkins, F. Fiedler, J. Chen and A. B. Gamble, *Chem. Sci.*, 2015, **6**, 1212–1218.
- 188 S. S. Matikonda, J. M. Fairhall, F. Fiedler, S. Sanhajariya, R. A. J. Tucker, S. Hook, A. L. Garden and A. B. Gamble, *Bioconjugate Chem.*, 2018, **29**, 324–334.
- 189 R. van Brakel, R. C. M. Vulders, R. J. Bokdam, H. Grüll and M. S. Robillard, *Bioconjugate Chem.*, 2008, **19**, 714–718.
- 190 A. S. Cohen, E. A. Dubikovskaya, J. S. Rush and C. R. Bertozzi, *J. Am. Chem. Soc.*, 2010, **132**, 8563–8565.
- 191 M. Xu, J. Tu and R. M. Franzini, *Chem. Commun.*, 2017, **53**, 6271–6274.
- 192 M. Xu, R. Galindo-Murillo, T. E. Cheatham, III and R. M. Franzini, *Org. Biomol. Chem.*, 2017, **15**, 9855–9865.
- 193 J. Tu, D. Svatunek, S. Parvez, H. J. Eckvahl, M. Xu, R. T. Peterson, K. N. Houk and R. M. Franzini, *Chem. Sci.*, 2020, **11**, 169–179.
- 194 J. Tu, M. Xu, S. Parvez, R. T. Peterson and R. M. Franzini, *J. Am. Chem. Soc.*, 2018, **140**, 8410–8414.
- 195 H. Stöckmann, A. A. Neves, S. Stairs, K. M. Brindle and F. J. Leeper, *Org. Biomol. Chem.*, 2011, **9**, 7303–7305.
- 196 B. P. Imming, R. Mohr, E. Müller, W. Overheu and G. Seitz, *Angew. Chem., Int. Ed. Engl.*, 1982, **21**, 284.
- 197 Z. Shao, W. Liu, H. Tao, F. Liu, R. Zeng, P. A. Champagne, Y. Cao, K. N. Houk and Y. Liang, *Chem. Commun.*, 2018, **54**, 14089–14092.
- 198 K. Haba, M. Popkov, M. Shamis, R. A. Lerner, C. F. Barbas and D. Shabat, *Angew. Chem., Int. Ed.*, 2005, **44**, 716–720.
- 199 S. Huvelle, A. Alouane, T. Le Saux, L. Jullien and F. Schmidt, *Org. Biomol. Chem.*, 2017, **15**, 3435–3443.
- 200 Y. Meyer, J. A. Richard, M. Massonneau, P. Y. Renard and A. Romieu, *Org. Lett.*, 2008, **10**, 1517–1520.
- 201 Y. Meyer, J. A. Richard, B. Delest, P. Noack, P. Y. Renard and A. Romieu, *Org. Biomol. Chem.*, 2010, **8**, 1777–1780.
- 202 R. J. Amir and D. Shabat, *Chem. Commun.*, 2004, **4**, 1614–1615.
- 203 I. Artaud and E. Galardon, *ChemBioChem*, 2014, **15**, 2361–2364.
- 204 J. Tang, Z. Zeng, J. Yan, C. Chen, J. Liu and X. Feng, *J. Controlled Release*, 2019, **307**, 90–97.
- 205 W. A. Henne, D. D. Doorneweerd, A. R. Hilgenbrink, S. A. Kularatne and P. S. Low, *Bioorg. Med. Chem. Lett.*, 2006, **16**, 5350–5355.
- 206 S. Santra, C. Kaittanis, O. J. Santiesteban and J. M. Perez, *J. Am. Chem. Soc.*, 2011, **133**, 16680–16688.
- 207 A. R. M. Dias, A. Pina, A. Dean, H.-G. Lerchen, M. Caruso, F. Gasparri, I. Fraietta, S. Troiani, D. Arosio, L. Belvisi, L. Pignataro, A. Dal Corso and C. Gennari, *Chem. – Eur. J.*, 2019, **25**, 1696–1700.
- 208 R. J. Amir, N. Pessah, M. Shamis and D. Shabat, *Angew. Chem., Int. Ed.*, 2003, **42**, 4494–4499.
- 209 N. Fomina, C. L. Mc Fearin and A. Almutairi, *Chem. Commun.*, 2012, **48**, 9138–9140.
- 210 A. Dal Corso, V. Borlandelli, C. Corno, P. Perego, L. Belvisi, L. Pignataro and C. Gennari, *Angew. Chem., Int. Ed.*, 2020, **59**, 4176–4181.
- 211 M. A. Dewit and E. R. Gillies, *Org. Biomol. Chem.*, 2011, **9**, 1846–1854.
- 212 T. Yamamoto, D. R. Caldwell, A. Gandioso and M. J. Schnermann, *Photochem. Photobiol.*, 2019, **95**, 951–958.
- 213 R. R. Nani, A. P. Gorka, T. Nagaya, T. Yamamoto, J. Ivanic, H. Kobayashi and M. J. Schnermann, *ACS Cent. Sci.*, 2017, **3**, 329–337.
- 214 R. R. Nani, A. P. Gorka, T. Nagaya, H. Kobayashi and M. J. Schnermann, *Angew. Chem., Int. Ed.*, 2015, **54**, 13635–13638.
- 215 R. R. Nani, J. A. Kelley, J. Ivanic and M. J. Schnermann, *Chem. Sci.*, 2015, **6**, 6556–6563.
- 216 A. P. Gorka, R. R. Nani, J. Zhu, S. Mackem and M. J. Schnermann, *J. Am. Chem. Soc.*, 2014, **136**, 14153–14159.
- 217 W. Feng, C. Gao, W. Liu, H. Ren, C. Wang, K. Ge, S. Li, G. Zhou, H. Li, S. Wang, G. Jia, Z. Li and J. Zhang, *Chem. Commun.*, 2016, **52**, 9434–9437.
- 218 N. Singh, A. Gupta, P. Prasad, R. K. Sah, A. Singh, S. Kumar, S. Singh, S. Gupta and P. K. Sasmal, *J. Med. Chem.*, 2021, **64**, 17813–17823.
- 219 N. Gagey, P. Neveu, C. Benbrahim, B. Goetz, I. Aujard, J.-B. Baudin and L. Jullien, *J. Am. Chem. Soc.*, 2007, **129**, 9986–9998.
- 220 S. Chen, X. Zhao, J. Chen, J. Chen, L. Kuznetsova, S. S. Wong and I. Ojima, *Bioconjugate Chem.*, 2010, **21**, 979–987.



- 221 D. Shan, M. G. Nicolaou, R. T. Borchardt and B. Wang, *J. Pharm. Sci.*, 1997, **86**, 765–767.
- 222 P. B. Carvalho and M. A. Avery, *J. Med. Chem.*, 2001, **14**, 369–378.
- 223 O. A. Okoh and P. Klahn, *ChemBioChem*, 2018, **19**, 1668–1694.
- 224 Y. Zheng, B. Yu, K. Ji, Z. Pan, V. Chittavong and B. Wang, *Angew. Chem., Int. Ed.*, 2016, **55**, 4514–4518.
- 225 B. Yu, Y. Zheng, Z. Yuan, S. Li, H. Zhu, L. K. De La Cruz, J. Zhang, K. Ji, S. Wang and B. Wang, *J. Am. Chem. Soc.*, 2018, **140**, 30–33.
- 226 R. Wang, K. Cai, H. Wang, C. Yin and J. Cheng, *Chem. Commun.*, 2018, **54**, 4878–4881.
- 227 P. Liu, J. Xu, D. Yan, P. Zhang, F. Zeng, B. Li and S. Wu, *Chem. Commun.*, 2015, **51**, 9567–9570.
- 228 B. Li, P. Liu, D. Yan, F. Zeng and S. Wu, *J. Mater. Chem. B*, 2017, **5**, 2635–2643.
- 229 Z. Chen, B. Li, X. Xie, F. Zeng and S. Wu, *J. Mater. Chem. B*, 2018, **6**, 2547–2556.
- 230 S. Son, M. Won, O. Green, N. Hananya, A. Sharma, Y. Jeon, J. H. Kwak, J. L. Sessler, D. Shabat and J. S. Kim, *Angew. Chem., Int. Ed.*, 2019, **58**, 1739–1743.
- 231 N. Hananya, J. P. Reid, O. Green, M. S. Sigman and D. Shabat, *Chem. Sci.*, 2019, **10**, 1380–1385.
- 232 B. Prasai, W. C. Silvers and R. L. McCarley, *Anal. Chem.*, 2015, **87**, 6411–6418.
- 233 S. U. Hettiarachchi, B. Prasai and R. L. McCarley, *J. Am. Chem. Soc.*, 2014, **136**, 7575–7578.
- 234 C. Ji and M. J. Miller, *Bioorg. Med. Chem.*, 2012, **20**, 3828–3836.
- 235 W. Wang and B. Wang, *Chem. Commun.*, 2017, **53**, 10124–10127.
- 236 J. C. Kern, D. Dooney, R. Zhang, L. Liang, P. E. Brandish, M. Cheng, G. Feng, A. Beck, D. Bresson, J. Firdos, D. Gately, N. Knudsen, A. Manibusan, Y. Sun and R. M. Garbaccio, *Bioconjugate Chem.*, 2016, **27**, 2081–2088.
- 237 M. W. Becker, H. H. Chapman, T. Cihlar, E. J. Eisenberg, G. X. He, M. R. Kernan, W. A. Lee, E. J. Prisbe, J. C. Rohloff and M. L. Sparacino, WO2002008241, 2002.
- 238 Y. Wei, G. Qiu, B. Lei, L. Qin, H. Chu, Y. Lu, G. Zhu, Q. Gao, Q. Huang, G. Qian, P. Liao, X. Luo, X. Zhang, C. Zhang, Y. Li, S. Zheng, Y. Yu, P. Tang, J. Ni, P. Yan, Y. Zhou, P. Li, X. Huang, A. Gong and J. Liu, *J. Med. Chem.*, 2017, **60**, 8580–8590.
- 239 C. McGuigan, R. N. Pathirana, N. Mahmood, K. G. Devine and A. J. Hay, *Antiviral Res.*, 1992, **17**, 311–321.
- 240 C. McGuigan, R. N. Pathirana, N. Mahmood and A. J. Hay, *Bioorg. Med. Chem. Lett.*, 1992, **2**, 701–704.
- 241 C. McGuigan, R. N. Pathirana, S. S. M. Choi, D. Kinchington and T. J. O'Connor, *Antiviral Chem. Chemother.*, 1993, **4**, 97–101.
- 242 D. Cahard, C. McGuigan and J. Balzarini, *Mini-Rev. Med. Chem.*, 2004, **4**, 371–381.
- 243 Y. Mehellou, J. Balzarini and C. McGuigan, *ChemMedChem*, 2009, **4**, 1779–1791.
- 244 C. J. Choy, J. J. Geruntho, A. L. Davis and C. E. Berkman, *Bioconjugate Chem.*, 2016, **27**, 824–830.
- 245 B. S. Backer, C. J. Choy, A. L. Davis, Z. S. Browne and C. E. Berkman, *Tetrahedron Lett.*, 2020, **61**, 151650.
- 246 C. J. Choy, C. R. Ley, A. L. Davis, B. S. Backer, J. J. Geruntho, B. H. Clowers and C. E. Berkman, *Bioconjugate Chem.*, 2016, **27**, 2206–2213.
- 247 F. P. Olatunji, J. W. Herman, B. N. Kesic, D. Olabode and C. E. Berkman, *Tetrahedron Lett.*, 2020, **61**, 152398.
- 248 F. P. Olatunji, B. N. Kesic, C. J. Choy and C. E. Berkman, *Bioorg. Med. Chem. Lett.*, 2019, **29**, 2571–2574.
- 249 P. Šimon, M. Tichotová, M. García Gallardo, E. Procházková and O. Baszczyński, *Chem. – Eur. J.*, 2021, **27**, 12763–12775.
- 250 M. Ximenis, A. Sampedro, L. Martínez-Crespo, G. Ramis, F. Orvay, A. Costa and C. Rotger, *Chem. Commun.*, 2021, **57**, 2736–2739.
- 251 F. M. H. De Groot, C. Albrecht, R. Koekkoek, P. H. Beusker and H. W. Scheeren, *Angew. Chem., Int. Ed.*, 2003, **42**, 4490–4494.
- 252 S. Li, M. L. Szalai, R. M. Kevitch and D. V. McGrath, *J. Am. Chem. Soc.*, 2003, **125**, 10516–10517.
- 253 M. Shamis, H. N. Lode and D. Shabat, *J. Am. Chem. Soc.*, 2004, **126**, 1726–1731.
- 254 M. Shamis and D. Shabat, *Chem. – Eur. J.*, 2007, **13**, 4523–4528.
- 255 M. Avital-Shmilovici and D. Shabat, *Bioorg. Med. Chem. Lett.*, 2009, **19**, 3959–3962.
- 256 N. Pessah, M. Reznik, M. Shamis, F. Yantiri, H. Xin, K. Bowdish, N. Shomron, G. Ast and D. Shabat, *Bioorg. Med. Chem.*, 2004, **12**, 1859–1866.
- 257 O. Redy, E. Kisin-Finifer, E. Sella and D. Shabat, *Org. Biomol. Chem.*, 2012, **10**, 710–715.
- 258 I. S. Turan and E. U. Akkaya, *Org. Lett.*, 2014, **16**, 1680–1683.
- 259 J. Sloniec, U. Resch-Genger and A. Hennig, *J. Phys. Chem. B*, 2013, **117**, 14336–14344.
- 260 K. Gill, X. Mei and E. R. Gillies, *Chem. Commun.*, 2021, **57**, 11072–11075.
- 261 X. Tan, B. B. Li, X. Lu, F. Jia, C. Santori, P. Menon, H. Li, B. Zhang, J. J. Zhao and K. Zhang, *J. Am. Chem. Soc.*, 2015, **137**, 6112–6115.
- 262 W. S. Shin, J. Han, P. Verwilt, R. Kumar, J. H. Kim and J. S. Kim, *Bioconjugate Chem.*, 2016, **27**, 1419–1426.
- 263 M. Grinda, J. Clarhaut, I. Tranoy-Opalinski, B. Renoux, A. Monvoisin, L. Cronier and S. Papot, *ChemMedChem*, 2011, **6**, 2137–2141.
- 264 M. Grinda, J. Clarhaut, B. Renoux, I. Tranoy-Opalinski and S. Papot, *MedChemComm*, 2012, **3**, 68–70.
- 265 M. Grinda, T. Legigan, J. Clarhaut, E. Peraudeau, I. Tranoy-Opalinski, B. Renoux, M. Thomas, F. Guillhot and S. Papot, *Org. Biomol. Chem.*, 2013, **11**, 7129–7133.
- 266 T. Legigan, J. Clarhaut, I. Tranoy-Opalinski, A. Monvoisin, B. Renoux, M. Thomas, A. Le Pape, S. Lerondel and S. Papot, *Angew. Chem., Int. Ed.*, 2012, **51**, 11606–11610.
- 267 B. Renoux, F. Raes, T. Legigan, E. Péraudeau, B. Eddhif, P. Pointot, I. Tranoy-Opalinski, J. Alsarraf, O. Koniev, S. Kolodych, S. Lerondel, A. Le Pape, J. Clarhaut and S. Papot, *Chem. Sci.*, 2017, **8**, 3427–3433.



- 268 T. Legigan, J. Clarhaut, B. Renoux, I. Tranoy-Opalinski, A. Monvoisin, J.-M. Berjeaud, F. Guilhot and S. Papot, *J. Med. Chem.*, 2012, **55**, 4516–4520.
- 269 R. Châtre, J. Lange, E. Péraudeau, P. Poinot, S. Lerondel, A. Le Pape, J. Clarhaut, B. Renoux and S. Papot, *J. Controlled Release*, 2020, **327**, 19–25.
- 270 E. Sella and D. Shabat, *J. Am. Chem. Soc.*, 2009, **131**, 9934–9936.
- 271 C. M. Niemeyer, M. Adler and R. Wacker, *Trends Biotechnol.*, 2005, **23**, 208–216.
- 272 J. Y. Hyo and C. A. Mirkin, *J. Am. Chem. Soc.*, 2008, **130**, 11590–11591.
- 273 T. Yoshii, S. Onogi, H. Shigemitsu and I. Hamachi, *J. Am. Chem. Soc.*, 2015, **137**, 3360–3365.
- 274 K. Porte, B. Renoux, E. Péraudeau, J. Clarhaut, B. Eddhif, P. Poinot, E. Gravel, E. Doris, A. Wijkhuisen, D. Audisio, S. Papot and F. Taran, *Angew. Chem., Int. Ed.*, 2019, **58**, 6366–6370.
- 275 H. Mohapatra, K. M. Schmid and S. T. Phillips, *Chem. Commun.*, 2012, **48**, 3018–3020.
- 276 K. Yeung, K. M. Schmid and S. T. Phillips, *Chem. Commun.*, 2013, **49**, 394–396.
- 277 A. D. Brooks, K. Yeung, G. G. Lewis and S. T. Phillips, *Anal. Methods*, 2015, **7**, 7186–7192.
- 278 H. Mohapatra and S. T. Phillips, *Chem. Commun.*, 2013, **49**, 6134–6136.
- 279 R. Perry-Feigenbaum, E. Sella and D. Shabat, *Chem. – Eur. J.*, 2011, **17**, 12123–12128.
- 280 M. S. Baker and S. T. Phillips, *J. Am. Chem. Soc.*, 2011, **133**, 5170–5173.
- 281 M. S. Baker and S. T. Phillips, *Org. Biomol. Chem.*, 2012, **10**, 3595–3599.
- 282 J. A. Gu, V. Mani and S. T. Huang, *Analyst*, 2015, **140**, 346–352.
- 283 H. Kim, M. S. Baker and S. T. Phillips, *Chem. Sci.*, 2015, **6**, 3388–3392.
- 284 M. S. Baker, V. Yadav, A. Sen and S. T. Phillips, *Angew. Chem., Int. Ed.*, 2013, **52**, 10295–10299.
- 285 H. Mohapatra, H. Kim and S. T. Phillips, *J. Am. Chem. Soc.*, 2015, **137**, 12498–12501.
- 286 S. Gnaim and D. Shabat, *Chem. Commun.*, 2018, **54**, 2655–2658.
- 287 I. S. Turan, O. Seven, S. Ayan and E. U. Akkaya, *ACS Omega*, 2017, **2**, 3291–3295.
- 288 S. Hisamatsu, S. Suzuki, S. Kohmoto, K. Kishikawa, Y. Yamamoto, R. Motokawa and T. Yaita, *Tetrahedron*, 2017, **73**, 3993–3998.
- 289 L. Gabrielli and F. Mancin, *J. Org. Chem.*, 2016, **81**, 10715–10720.
- 290 X. Sun, S. D. Dahlhauser and E. V. Anslyn, *J. Am. Chem. Soc.*, 2017, **139**, 4635–4638.
- 291 X. Sun and E. V. Anslyn, *Angew. Chem., Int. Ed.*, 2017, **56**, 9522–9526.
- 292 X. Sun, A. A. Boulgakov, L. N. Smith, P. Metola, E. M. Marcotte and E. V. Anslyn, *ACS Cent. Sci.*, 2018, **4**, 854–861.
- 293 D. H. Lee, S. A. Valenzuela, M. N. Dominguez, M. Otsuka, D. J. Milliron and E. V. Anslyn, *Cell Rep. Phys. Sci.*, 2021, **2**, 100552.
- 294 A. Sagi, R. Weinstain, N. Karton and D. Shabat, *J. Am. Chem. Soc.*, 2008, **8**, 5434–5435.
- 295 F. Kratz, I. A. Müller, C. Rypa and A. Warnecke, *ChemMedChem*, 2008, **3**, 20–53.
- 296 E. Sella and D. Shabat, *Chem. Commun.*, 2008, 5701.
- 297 A. Warnecke and F. Kratz, *J. Org. Chem.*, 2008, **73**, 1546–1552.
- 298 M. F. Nichol, K. D. Clark, N. D. Dolinski and J. R. de Alaniz, *Polym. Chem.*, 2019, **10**, 4914–4919.
- 299 A. P. Esser-Kahn, N. R. Sottos, S. R. White and J. S. Moore, *J. Am. Chem. Soc.*, 2010, **132**, 10266–10268.
- 300 G. Liu, X. Wang, J. Hu, G. Zhang and S. Liu, *J. Am. Chem. Soc.*, 2014, **136**, 7492–7497.
- 301 V. Kumar, J. T. Harris, A. Ribbe, M. Franc, Y. Bae, A. J. McNeil and S. Thayumanavan, *ACS Macro Lett.*, 2020, **9**, 377–381.
- 302 G. G. Lewis, J. S. Robbins and S. T. Phillips, *Macromolecules*, 2013, **46**, 5177–5183.
- 303 G. G. Lewis, J. S. Robbins and S. T. Phillips, *Anal. Chem.*, 2013, **85**, 10432–10439.
- 304 G. G. Lewis, J. S. Robbins and S. T. Phillips, *Chem. Commun.*, 2014, **50**, 5352–5354.
- 305 O. Redy and D. Shabat, *J. Controlled Release*, 2012, **164**, 276–282.
- 306 G. I. Peterson, D. C. Church, N. A. Yakelis and A. J. Boydston, *Polymer*, 2014, **55**, 5980–5985.
- 307 S. Kostler, B. Zechne, B. Trathnigg, H. Fasl, W. Kern and V. Ribitsch, *J. Polym. Sci., Part A: Polym. Chem.*, 2009, **47**, 1499–1509.
- 308 G. Liu, G. Zhang, J. Hu, X. Wang, M. Zhu and S. Liu, *J. Am. Chem. Soc.*, 2015, **137**, 11645–11655.
- 309 M. Brasch, I. K. Voets, M. S. T. Koay and J. L. M. Cornelissen, *Faraday Discuss.*, 2013, **166**, 47–57.
- 310 H. Okada, K. Tanaka, W. Ohashi and Y. Chujo, *Bioorg. Med. Chem.*, 2014, **22**, 3435–3440.
- 311 J. Tan, Z. Deng, C. Song, J. Xu, Y. Zhang, Y. Yu, J. Hu and S. Liu, *J. Am. Chem. Soc.*, 2021, **143**, 13738–13748.
- 312 J. Huang, X. Chen, Y. Jiang, C. Zhang, S. He, H. Wang and K. Pu, *Nat. Mater.*, 2022, **21**, 598–607.
- 313 Y. He, Y. Wu, M. Zhang, Y. Zhang, H. Ding and K. Zhang, *Macromolecules*, 2021, **54**, 5797–5805.
- 314 P. Hodge, *Chem. Rev.*, 2014, **114**, 2278–2312.
- 315 P. Hodge and H. M. Colquhoun, *Polym. Adv. Technol.*, 2005, **16**, 84–94.
- 316 M. A. DeWit and E. R. Gillies, *J. Am. Chem. Soc.*, 2009, **131**, 18327–18334.
- 317 E. K. Y. Chen, R. A. McBride and E. R. Gillies, *Macromolecules*, 2012, **45**, 7364–7374.
- 318 R. A. McBride and E. R. Gillies, *Macromolecules*, 2013, **46**, 5157–5166.
- 319 A. D. Wong, T. M. Güngör and E. R. Gillies, *ACS Macro Lett.*, 2014, **3**, 1191–1195.



- 320 H. Mutlu, C. M. Geiselhart and C. Barner-Kowollik, *Mater. Horiz.*, 2018, **5**, 162–183.
- 321 N. Fomina, C. L. McFearn, M. Sermsakdi, J. M. Morachis and A. Almutairi, *Macromolecules*, 2011, **44**, 8590–8597.
- 322 C. de Gracia Lux, C. L. McFearn, S. Joshi-Barr, J. Sankaranarayanan, N. Fomina and A. Almutairi, *ACS Macro Lett.*, 2012, **1**, 922–926.
- 323 C. de Gracia Lux and A. Almutairi, *ACS Macro Lett.*, 2013, **2**, 432–435.
- 324 J. Olejniczak, M. Chan and A. Almutairi, *Macromolecules*, 2015, **48**, 3166–3172.
- 325 C. de Gracia Lux, J. Olejniczak, N. Fomina, M. L. Viger and A. Almutairi, *J. Polym. Sci., Part A: Polym. Chem.*, 2013, **51**, 3783–3790.
- 326 Y. Zhang, L. Ma, X. Deng and J. Cheng, *Polym. Chem.*, 2013, **4**, 224–228.
- 327 Y. Xu, S. Sen, Q. Wu, X. Zhong, R. H. Ewoldt and S. C. Zimmerman, *Chem. Sci.*, 2020, **11**, 3326–3331.
- 328 Y. Xu, E. G. Morado and S. C. Zimmerman, *Polym. Chem.*, 2020, **11**, 6215–6220.
- 329 C. Petit, J. Bachmann, L. Michalek, Y. Catel, E. Blasco, J. P. Blinco, A. N. Unterreiner and C. Barner-Kowollik, *Chem. Commun.*, 2021, **57**, 2911–2914.
- 330 H. Kim, A. D. Brooks, A. M. Dilauro and S. T. Phillips, *J. Am. Chem. Soc.*, 2020, **142**, 9447–9452.
- 331 K. M. Schmid and S. T. Phillips, *J. Phys. Org. Chem.*, 2013, **26**, 608–610.
- 332 Z. Zhou and R. G. Parr, *J. Am. Chem. Soc.*, 1989, **111**, 7371–7379.
- 333 B. A. Hess, L. J. Schaad and C. W. Holyoke, *Tetrahedron*, 1972, **28**, 3657–3667.
- 334 C. de Gracia Lux, S. Joshi-Barr, T. Nguyen, E. Mahmoud, E. Schopf, N. Fomina and A. Almutairi, *J. Am. Chem. Soc.*, 2012, **134**, 15758–15764.
- 335 S. D. Dahlhauser, P. R. Escamilla, A. N. Vandewalle, J. T. York, R. M. Rapagnani, J. S. Shei, S. A. Glass, J. N. Coronado, S. R. Moor, D. P. Saunders and E. V. Anslyn, *J. Am. Chem. Soc.*, 2020, **142**, 2744–2749.
- 336 L. J. Zhang, X. X. Deng, F. S. Du and Z. C. Li, *Macromolecules*, 2013, **46**, 9554–9562.
- 337 S. D. Dahlhauser, S. R. Moor, M. S. Vera, J. T. York, P. Ngo, A. J. Boley, J. N. Coronado, Z. B. Simpson and E. V. Anslyn, *Cell Rep. Phys. Sci.*, 2021, **2**, 100393.
- 338 M. L. Szalai, R. M. Kevitch and D. V. McGrath, *J. Am. Chem. Soc.*, 2003, **125**, 15688–15689.
- 339 A. Ortiz, C. S. Shanahan, D. T. Sisk, S. C. Perera, P. Rao and D. V. McGrath, *J. Org. Chem.*, 2010, **75**, 6154–6162.
- 340 R. M. Kevitch, C. S. Shanahan and D. V. McGrath, *New J. Chem.*, 2012, **36**, 492–505.
- 341 M. G. Olah, J. S. Robbins, M. S. Baker and S. T. Phillips, *Macromolecules*, 2013, **46**, 5924–5928.
- 342 M. S. Baker, H. Kim, M. G. Olah, G. G. Lewis and S. T. Phillips, *Green Chem.*, 2015, **17**, 4541–4545.
- 343 C. Ergene and E. F. Palermo, *Biomacromolecules*, 2017, **18**, 3400–3409.
- 344 C. Ergene and E. F. Palermo, *J. Mater. Chem. B*, 2018, **6**, 7217–7229.
- 345 Y. Xiao, H. Li, B. Zhang, Z. Cheng, Y. Li, X. Tan and K. Zhang, *Macromolecules*, 2018, **51**, 2899–2905.
- 346 Y. Xiao, Y. Li, B. Zhang, H. Li, Z. Cheng, J. Shi, J. Xiong, Y. Bai and K. Zhang, *ACS Macro Lett.*, 2019, **8**, 399–402.
- 347 C. Aso and S. Tagami, *Macromolecules*, 1969, **2**, 414–419.
- 348 C. Aso, S. Tagami and T. Kunitake, *J. Polym. Sci., Part A-1: Polym. Chem.*, 1969, **7**, 497–511.
- 349 H. Lopez Hernandez, S. K. Kang, O. P. Lee, S. W. Hwang, J. A. Kaitz, B. Inci, C. W. Park, S. Chung, N. R. Sottos, J. S. Moore, J. A. Rogers and S. R. White, *Adv. Mater.*, 2014, **26**, 7637–7642.
- 350 K. M. Lee, O. Phillips, A. Engler, P. A. Kohl and B. P. Rand, *ACS Appl. Mater. Interfaces*, 2018, **10**, 28062–28068.
- 351 W. Seo and S. T. Phillips, *J. Am. Chem. Soc.*, 2010, **132**, 9234–9235.
- 352 S. A. MacDonald, C. G. Willson and J. M. J. Fréchet, *Acc. Chem. Res.*, 1994, **27**, 151–158.
- 353 H. Ito, *J. Polym. Sci., Part A: Polym. Chem.*, 2003, **41**, 3863–3870.
- 354 H. Ito and C. G. Willson, *Polym. Eng. Sci.*, 1983, **23**, 1012–1018.
- 355 A. M. Dilauro, J. S. Robbins and S. T. Phillips, *Macromolecules*, 2013, **46**, 2963–2968.
- 356 A. M. Dilauro, H. Zhang, M. S. Baker, F. Wong, A. Sen and S. T. Phillips, *Macromolecules*, 2013, **46**, 7257–7265.
- 357 H. Zhang, K. Yeung, J. S. Robbins, R. A. Pavlick, M. Wu, R. Liu, A. Sen and S. T. Phillips, *Angew. Chem., Int. Ed.*, 2012, **51**, 2400–2404.
- 358 A. M. Dilauro, A. Abbaspourrad, D. A. Weitz and S. T. Phillips, *Macromolecules*, 2013, **46**, 3309–3313.
- 359 A. M. Dilauro, G. G. Lewis and S. T. Phillips, *Angew. Chem., Int. Ed.*, 2015, **54**, 6200–6205.
- 360 A. M. Dilauro and S. T. Phillips, *Polym. Chem.*, 2015, **6**, 3252–3258.
- 361 J. A. Kaitz and J. S. Moore, *Macromolecules*, 2013, **46**, 608–612.
- 362 J. A. Kaitz, C. M. Possanza, Y. Song, C. E. Diesendruck, A. J. H. Spiering, E. W. Meijer and J. S. Moore, *Polym. Chem.*, 2014, **5**, 3788–3794.
- 363 J. A. Kaitz, C. E. Diesendruck and J. S. Moore, *J. Am. Chem. Soc.*, 2013, **135**, 12755–12761.
- 364 J. A. Kaitz, C. E. Diesendruck and J. S. Moore, *Macromolecules*, 2013, **46**, 8121–8128.
- 365 B. Fan, J. F. Trant, A. D. Wong and E. R. Gillies, *J. Am. Chem. Soc.*, 2014, **136**, 10116–10123.
- 366 B. Fan, J. F. Trant and E. R. Gillies, *Macromolecules*, 2016, **49**, 9309–9319.
- 367 Q. E. A. Sirianni, A. R. Kenaree and E. R. Gillies, *Macromolecules*, 2019, **52**, 262–270.



- 368 L. H. S. Ree, Q. E. A. Sirianni, E. R. Gillies and M. A. Kelland, *Energy Fuels*, 2019, **33**, 2067–2075.
- 369 B. Fan and E. R. Gillies, *Mol. Pharmaceutics*, 2017, **14**, 2548–2559.
- 370 R. Barat, T. Legigan, I. Tranoy-Opalinski, B. Renoux, E. Péraudeau, J. Clarhaut, P. Poinot, A. E. Fernandes, V. Aucagne, D. A. Leigh and S. Papot, *Chem. Sci.*, 2015, **6**, 2608–2613.
- 371 A. Fernandes, A. Viterisi, F. Coutrot, S. Potok, D. A. Leigh, V. Aucagne and S. Papot, *Angew. Chem., Int. Ed.*, 2009, **48**, 6443–6447.
- 372 A. Fernandes, A. Viterisi, V. Aucagne, D. A. Leigh and S. Papot, *Chem. Commun.*, 2012, **48**, 2083–2085.
- 373 B. Renoux, T. Legigan, S. Bensalma, C. Chadéneau, J.-M. Muller and S. Papot, *Org. Biomol. Chem.*, 2011, **9**, 8459–8464.

